ACUTE RESPONSE OF PRIMARY GLIAL CELLS TO METHYLMERCURY EXPOSURE

By

MINGWEI NI

Dissertation

Submitted to the faculty of the

Graduate School of Vanderbilt University

in partial fulfillment of requirements

for the degree of

DOCTOR OF PHILOSOPHY

in

Pharmacology

December 2011

Nashville, Tennessee

Approved:

Ariel Deutch

Michael Aschner

Eugenia Gurevich

Ronald Wiley

Aaron Bowman

ABSTRACT

Mercury accumulates in fish-eating populations. Glial cells have diverse functions including providing nutrition[1], maintaining CNS homeostasis, removing pathogens, inducing neuronal differentiation and mediating CNS immune responsiveness. Dysfunction of glial cells is contributed to MeHg-induced brain damage. We hypothesized that 1) the cellular responses to MeHg are cell-type specific; 2) differences exist in the uptake of MeHg between astrocytes and microglia, leading to differential temporal cellular responses. I tested the unique response of primary glial cells to MeHg exposure at physiologically relevant concentration. The results are presented in this dissertation.

Firstly, I established the methodology to separate a large amount of rat primary microglial cells with high purity (>95%) from mixed glial cell culture. Secondly, I investigated the toxic effects of MeHg on primary glial cells as well as their cellular response to acute MeHg exposure at environmentally relevant concentrations (0.1μM~ 5μM). The results showed MeHg treatment caused a concentration- and time- dependent microglial cell death, intracellular ROS generation and GSH depletion. I analyzed the dynamic changes of nuclear factor erythroid- derived 2- like 2 (NFE2L2) in both cytosolic fraction and nuclear fraction. My results suggested that the increase in Nrf2 protein level and the subsequent nuclear translocation are regulated by ROS in both glial cell types. However, Nrf2 changes in astrocytes occurred on a protracted time scale. Thirdly, the effects of Nrf2 on its downstream gene expression and cell viability post MeHg exposure were further studied, using short hairpin RNA (shRNA) approach. Finally the responses of rat primary

microglial cells post MeHg treatment were compared with those of rat primary astrocytes. In conclusion, our study has demonstrated that microglial cells are more sensitive than astrocytes to MeHg. Their regulation kinetics differ, therefore allowing astrocytes and microglial cells to play different roles in mediating MeHg toxicity.

To my father, Jianlin Ni, missing you forever

To my wife, Xin Li,

and my mother, Meizhen Cai, for their infinite support

and

To my wonderful daughter, Ailin, happy everyday

ACKNOWLEDGEMENTS

This study was supported by the National Institute of Environment Health Sciences NIEHS 10563 to Dr. Michael Aschner. This work would not have been possible without the superior guidance of Dr. Aschner, who accepted me as a graduate student during the most difficult time of my life, and kindly provided me extensive personal and professional guidance. He has taught me more than I could ever ask for. Being my role model, Dr. Aschner, has exhibited what an outstanding scientist should be.

I am indebted to my committee members, Dr. Aerial Deutch, Dr. Michael Aschner, Dr. Aaron Bowman, Dr. Eugenia Gurevich and Dr. Ronald Wiley, who have been working actively to help me through my PhD training and teach me the values of scientific research. I especially appreciate Dr. Joey Barnett, Director of Graduate Studies in Pharmacology and Dr. Heidi Hamm, Chairman of Pharmacology Department, who are always supportive of my career goals and help me to pursue those goals. It is great to have the opportunities to work with many good scientists and researchers during my PhD training at Vanderbilt University and I am grateful to all of them for their kindness, supportiveness and considerations.

Last but not least, I would like to thank my wife, Xin Li and my parents, whose love helps me to conquer whatever difficulties I met. This thesis is in memorial of my father, Jianlin Ni, who taught me to always dream high. Most importantly, I am blessed to have my beautiful baby girl, Ailin, who makes me realize the true value of my life.

TABLE OF CONTENTS

LIST OF TABLES

LIST OF FIGURES

LIST OF ABBREVBIATIONS

Abbreviation	Meaning
As	arsenic
Cd	cadnium
CNS	Central Nervous System
Co	cobalt
Cr	Chromium
Cu	Copper
DCF	Dichlorodihydrofluorescein
GSH	reduced glutathione
GSSG	oxidized glutathione
Hg	mercury
HO-1	hemeoxygenase-1
HPLC	High-performance liquid chromatography
Keap 1	Kelch-like ECH-associating protein 1
LDH	Lactate Dehydrogenase
MeHg	methylmercury
Mn	Manganese
MTT	3-(4,5-Dimethylthiazol-2-yl)-2,5-diphenyltetrazolium bromide
Ni	nickel
Nqo1	NADPH:quinone oxidoreductase-1

Nrf2	erythroid-derived 2-like 2
Pb	Lead
PCR	polymerase chain reaction
ROS	Reactive oxygen species
Sn	Tin
Ti	Titanium
xCT	cysteine/glutamate transporter

CHAPTER I

INTRODUCTION

Heavy Metal Pollution

Toxic heavy metals in air, soil and water are growing global threats to human beings. Heavy metal pollution comes from various sources, including coal, natural gas, chlor-alkali industries and volcanic eruptions [3], but the most common source arises from the purification of metals, e.g., the smelting of copper and the preparation of nuclear fuels [4]. Currently, the thirteen elements of highest concern worldwide are As, Cd, Co, Cr, Cu, Hg, Mn, Ni, Pb, Sn and Ti [4], of which the emission is tightly regulated in waste incinerators. Some of these heavy metals are actually essential for humans in minute amounts (Co, Cu, Cr, Mn and Ni), but others are highly toxic (e.g. Hg, Pb and As). Notably, different heavy metals have different target organs. For example, Hg, Mn and Pb mainly cause damage to the central nervous system (CNS), especially during developmental stages. Kidneys and livers are susceptible to Cr and Cu, while hard tissues such as bones and teeth are mainly affected by Ni, Cd and Pb.

Once released into environment, heavy metal pollutants can localize and do not decay. As the result, their toxicity may last for generations. Coastal fish and seabirds are often monitored for the presence of heavy metal contamination based on the fact the accumulative capability of sea animals presents the major concern of bioaccumulation and biomagnification of several heavy metals that have been linked to human diseases. Among them, the most notorious one is Minamata disease caused by organic mercury, MeHg poisoning [5-7]. Besides Minamata disease

caused by organic mercury, other heavy metals also cause human diseases. For example, Cd poisoning in Toyama Prefecture, Japan in 1912 caused Itai- itai disease, which led to weak and brittle bones, spinal and leg pain and waddling gait [8, 9]. Lead (Pb) poisoning can cause a variety of symptoms and signs, depending on the individual and the duration of lead exposure, and individuals with elevated lead levels may exhibit no symptoms [10]. In general, the symptoms of heavy metal poisoning are different between inorganic and its organic forms. And symptoms appear in children at lower blood level than in adults [11].

Mercury and MeHg Pollution

There are multiple natural sources of mercury. For example, cinnabar ore has high concentration of mercury. Volcanic eruptions release large amount of mercury to environment, especially to water system. Once in the water system, bacteria in oceans convert inorganic mercury into the organic form, methylmercury (MeHg), which is the most prevalent and one of the most toxic forms. Human exposure to mercury is predominantly from the consumption of fish [12-14] and mainly in the form of MeHg. MeHg enrichment in the aquatic food chain is not uniform and is dependent upon water Hg content, bottom sediments, water pH and redox potential, the species, age and the size of a particular fish. The micro-environment conditions, especially anoxia, favors the growth of micro-organisms and further increases the methylation rate of Hg [15].

Japan [5, 6] and Sweden [16] have reported catastrophic epidemics caused by environmental MeHg poisoning. Analogous to sensitivity to other heavy metal pollution, children are more vulnerable to MeHg toxicity and have been found to exhibit diskinesia and intellectual disturbances [17]. In the general population, symptoms of MeHg poisoning are clinically

significant once the Hg exposure level exceeds the U.S. EPA RfD of 0.1 μg/kg body weight/day. These symptoms include mental retardation, primitive reflexes, coordination disturbance, dysarthria, limb deformation, growth disorder, chorea-athetose and hypersalivation[18].

Once in the human body, MeHg redistributed from gastrointestinal tract to almost all organ systems. *Figure 1* summarizes the kinetics of MeHg distribution in the human body. As shown in Figure 1, MeHg derived from food or occupational exposure is efficiently absorbed (90%) and has a long retention time (half-life of ~70 days). After ingestion, the distribution to the blood compartment is complete within 30 hours, and the blood level accounts for about 7% of the ingested dose [19]. Circulating MeHg accumulates predominantly in red cells where it binds to cysteinyl residues (-SH) on the hemoglobin beta-chain [20], and is then slowly distributed, reaching an equilibrium with other tissues at ~4 days [19].

The MeHg concentration in blood and hair reflects the body burden, with a blood/hair concentration in humans approximating 1/250 under steady-state conditions [21]. The net mercury excretion rate in humans is approximately 1% of the body content at non-symptomatic body burden level [22]. Most of the MeHg is eliminated through the liver into the bile and through the kidney into the urine. But most MeHg undergoes enterohepatic circulation by reabsorption from the bile in the gut. Slower urine excretion of MeHg in female versus male rats has been reported to result in higher toxicity in female rats [23]. Diet can affect the MeHg excretion rate, since certain dietary components can interfere with MeHg reabsorption in the lower part of the intestines, thus breaking up the enterohepatic circulation [24].

Fig 1

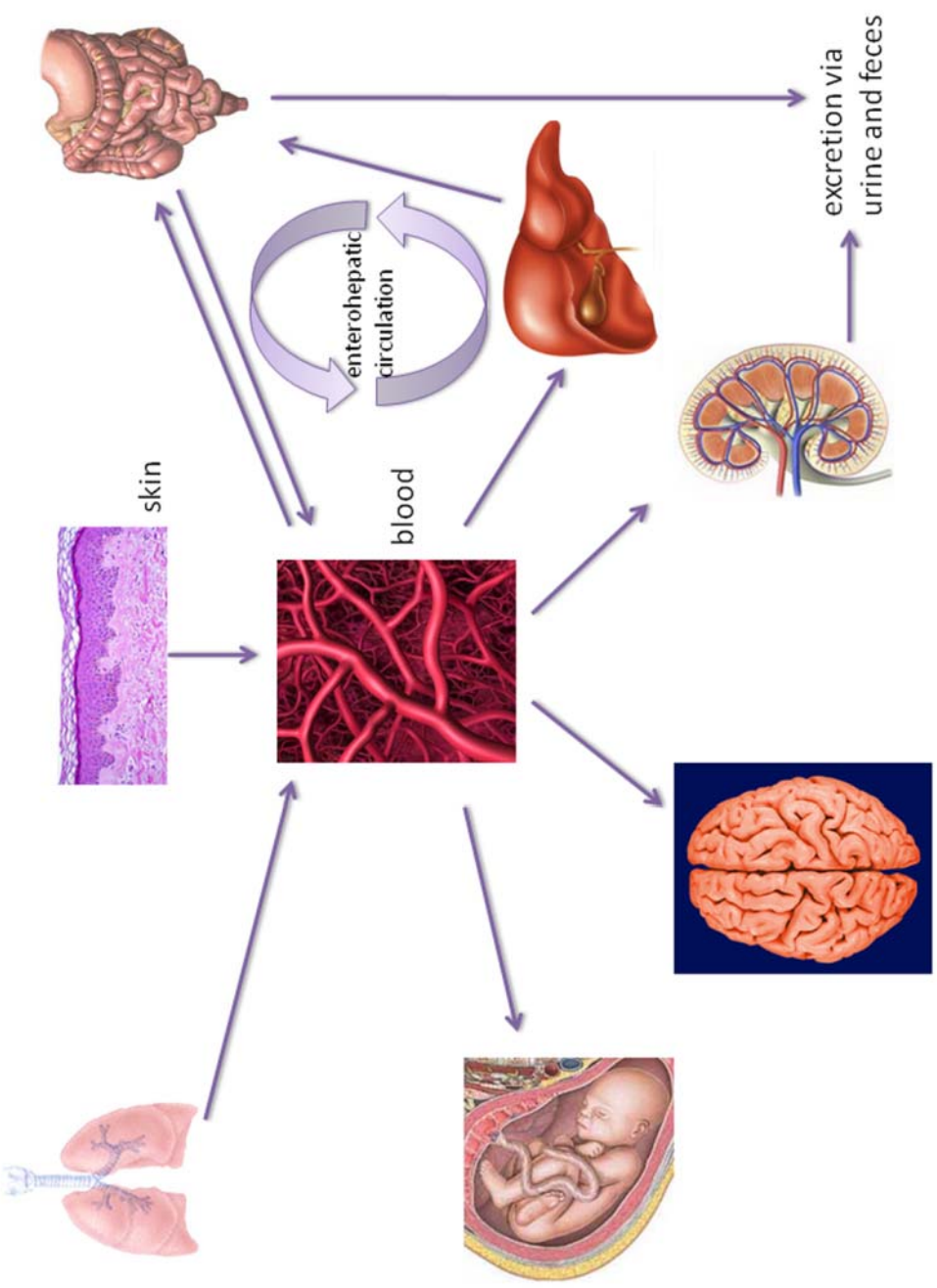

Fig 1. The distribution of MeHg in the human body. MeHg is readily absorbed by the lung, skin and gastrointestinal tract. Once in the circulation, MeHg predominantly accumulates in red blood cells and is slowly re-distributed to other organ systems, including the CNS (major), kidneys and liver. MeHg can cross the placental-blood barrier and it accumulates in the fetus at a higher concentrations compared to the mother. (Mingwei Ni, et al. Chapter 35, Mercury, Reproductive and Developmental Toxicology, 2011)

Notably, MeHg can cross the placenta and accumulate in the fetus at concentration higher than that in the mother. For example, MeHg level in the neonatal cord blood is more than twice as high as that in maternal blood at delivery. And approximately 5% of the total MeHg in the maternal blood is found in breast milk [25]. However, infant blood MeHg level decreases significantly during the first 13 weeks of the infant's life, and, at three months, maternal MeHg concentrations are higher than those of the infant, in contrast to those seen at parturition [26]. The rapid decline in infant MeHg concentrations postpartum can be explained by lower mercury transfer through breast milk and rapid infant growth after birth [26]. Furthermore, the systems for excretion develop as the children mature. For example, in experiment feeding young chickens with mercury contained water, the authors found an increase in relative kidney weight, which could indicate the increase in the excretion capability [27]. Mercury exposure also increases the urinary flow rate, which is suggested by the increase in the creatinine excretion rate in children [28].

The mechanism of MeHg uptake has been extensively investigated and it has been shown that MeHg has a remarkably high affinity for the anionic form of –SH groups [29] and subsequently, MeHg form a complex with the –SH containing amino acid cysteine [30]. The MeHg-SH bond is highly thermodynamically stable, but the very rapid exchange of MeHg between –SH groups is known to occur [31]. Our laboratory has successfully shown that the MeHg-S-Cys complex closely mimics the structure of the neutral amino acid, methionine, and is therefore is a substrate of the L type large neutral amino acid transporter system (LAT1) [32]. Over-expression of LAT1 in CHO-k1 cells is associated with enhanced uptake of [^{14}C]-MeHg when the cells are treated with L-cysteine. On the other hand, L-methionine, the substrate for LAT1, significantly

decreases the uptake of L-cysteine-conjugated [^{14}C]-MeHg [32]. Kajiwara [33] also reported that MeHg crosses the placenta via a similar neutral amino acid carrier, accumulating in fetal blood in a time- and dose-dependent manner.

Glial Cells

I. Astrocytes

Astrocytes, also known as astroglia, are characteristic star shaped glial cells in the brain and spinal cord. Astrocytes carry out many important functions to maintain CNS homeostasis, including supporting endothelial cells, participating in the formation of blood-brain barrier (BBB), providing nutrients to neuronal cells, playing principle role in the repair of brain and spinal cord after trauma. Astrocytes can be easily identified by glial fibrillary acidic protein (GFAP) staining. Histologically, astrocytes can be classified as three major types: fibrous, protoplasmic and radial glial cells. Fibrous glial cells have vascular feet, the long unbranched celluluar processes, wrapping the capillary wall. Protoplasmic glia are mainly found in grey matter tissue with large amount of intracellular organelles and this type of glial cells have short highly branched processes, which participating in the maintenance of extracellular ion balance. Radial glial cells are mostly present during development and guarding the developing neuron migration. Pathologically, astrocytes are the major cell type in the scarring process of CNS after traumatic injury, infection and inflammation. Astrocytes also have many more functions including 1) glutamate uptake; For example, Bechtholt-Gompf [34] reported that the blockage of the central astrocytic glutamate uptake with the astrocytic glutamate transporter (GLT-1) inhibitor, dihydrokainic acid (DHK), induces signs of anhedonia and impaired spatial memory. 2) astrocytes also function as the doorkeepers of GABA receptor functions; Beenhakker and his

colleagues [35] reported that astrocytic GABA transporters, GAT1 and GAT3 have different regulatory functions of GABA-mediated inhibitory postsynaptic currents (IPSCs), which are critical for the generation of generalized thalamocortical seizures. They further discovered that the perisynaptic expression of GAT1 enables it to regulate GABA levels near synapses and selectively modulate peak IPSC amplitude, which is largely dependent on perisynaptic receptor occupancy. GAT3 expression, on the other hand, is broader and includes distal extrasynaptic regions. 3) Astrocytes also participate in potassium (K+) spatial buffering; The depolarization of neurons tends to raise potassium concentration in the extracellular fluid. If a significant rise occurs, it will interfere with neuronal signaling by depolarizing neurons. Astrocytes have large numbers of potassium ion channels facilitating removal of potassium ions from the extracellular fluid and the uptaken potassium are then distributed to its neighbors via gap junctions. This keeps extracellular potassium at levels that prevent interference with normal propagation of an action potential [36]. 4) astrocytes are also involved in the control pH. Carbonic anhydrase is found to be located in astrocytes at the blood brain barrier [37, 38], involving the transport of HCO3- linked to the acceleration of intra-astrocytic CO2 hydration. Subsequent studies also showed Na+/H+ and Cl-/HCO3- exchangers in primary astrocyte culture [39].

II. Microglia

Mcroglia are the resident macrophages of brain and spinal cord, acting as the main form of active immune defense in CNS. Microglia are distributed in large non-overlapping regions throughout the CNS and they are constantly excavating the CNS for damaged neurons, plaques and infectious agents. Microglia recognize foreign bodies and act as antigen-presenting cells

activating T helper cells. Since this unique proper of microglia, microglia are extremely sensitive to even small pathological changes in CNS to prevent potentially fatal damage happening [40]. Microglia have multiple functions, including scavenging and phagocytosis: each microglial cell surveys its own domain on a regular basis and it will be activated and phagocytose any foreign material, damages cells, apoptotic cells, DNA fragments or plagues. Thus, microglial cells act as "housekeeping" cells in CNS [41]. In addition to destroying infectious organisms through direct cell-to-cell contact via phagocytosis, microglia are also able to release numerous cytotoxic substrances. For example, Zhang [42] reported that cultured microglia secrete large amount of hydrogen peroxide. Ryu further [43] reported that activated microglia release NO after thrombin treatment via protein kinase C, mitogen-activated protein kinase and NF-κB signal pathway. Both these chemicals can directly damage cells and lead to neuronal cell death. Microglial cells also participate in the formation of complex extracellular signaling system which allows them to communicate with other cell types in the CNS including astrocytes, neurons, T cells and oligodentratic cells. For example, microglial cells release INF-γ into the extracellular space, which activates more microglial cells and astrocytes. Microglia also release TNF-α causing neuronal apoptosis and increasing inflammation. Another cytokine, IL-8, promotes B cells differentiation allowing it to assist microglia in cleaning infections. Additional dendritic cells and T cells are further recruited to the injured site via IL-8. Microglial activation leads to neuronal damage via NMDA receptor- mediated processes by secreting glutamate and aspartate. Takeuchi [44] reported that microglia have high concentration of glutaminase, which generates glutamate. When glutaminase was inhibited in vitro by adding glutamase inhibitor, 6-diazo-5-oxo-l-norleucine (DON), to cultured microglia, the ability of the activated microglia to make glutamate and subsequently to kill neurons was decreased. It is noteworthy that the blockage of

glutamate receptor has been proven to have therapeutic functions. For example, Riluzole, the first drug approved for treatment of amyotrophic lateral sclerosis (ALS) works in part through suppressing the interaction of glumate with its receptor, as well as upregulating activity of glutamate transporters that clear glutamate. Furthermore, Riluzole has actually been demonstrated to inhibit MS-like disease in the EAE (experimental allergic encephalomyelitis) model [45].

Pathologically, microglia play critical role in neuroinflammation by expanding the neurodestructive effects via releasing cytokines (IL-1α, IL-1β and TNF-α), chemokines (monocyte chemoattractant protein-1, chemokine C-C motif receptor3, 5 and fractalkine receptor), release of proteases (cathepsins B, L, and S, the matrix metalloproteinases MMP-1, MMP-2, MMP-3, and MMP-9). Microglia are also involved in numerous neurodegenerative diseases, such as Alzheimer's disease, Parkinson's disease, HIV- associated dementia and etc. For example, in brain samples of Alzheimer's disease patient, microglia are often found near damaged tissue and previous studies revealed that microglia play opposing roles in Alzheimer's disease pathogenesis: on one hand, they eliminate β-amyloid aggregates via phagocytosis, on the other hand, they also kill nearby neurons by causing inflammation and the release of neurotoxic proteases.[46-48]. Microglia also play a significant role in dopaminergic cell injury. Le [49] developed an in vitro model of nigral injury, in which lipopolysaccharide (LPS)- induced microglial activation leads to injury of a dopaminergic cell line and dopaminergic neurons in primary messencephalic cell cultures. Microglia are also activated in Parkinson's disease IgGs in the presence of low-dose dopa-quinone- or H_2O_2-modified dopaminergic cell membranes but not cholinergic cell membrane. Furthermore, this activation requires the microglial FcγR receptor as

demonstrated by the lack of activation with PD IgG Fab fragments or microglia from FcγR−/− mice. Human immunodeficiency virus type 1 (HIV-1) infection of the central nervous system (CNS) can result in neurological dysfunction with devastating consequences. Interestingly, HIV-1 does not infect neurons directly but induces damage indirectly through the accumulation of activated microglia. The infected microglia release neurotoxic mediators including both cellular activation products and viral proteins [50]. These viral proteins and cellular products have neurotoxic properties as well, both directly and through induction of astrocyte dysfunction, which ultimately lead to neuronal injury and death [50].

On the other hand, microglia also play critical role in the neuroprotection. For example, in vertebrates, several lines of evidence demonstrate that microglia are also involved in neuroprotection by t\secretiing IL-4 which triggers neural repair and contributes to the creation of an environment conductive for regeneration. Microglial IL-4 also induces neurogenesis and oligodendrogenesis *in vitro* [51]. In addition, microglia are principally the first cell type engaged in phagocytosis, removing neuronal debris [51]. Given the complexity of microglial functions, further studies are warranted to better understand their role in CNS diseases and repair processes.

MeHg-induced Brain Injury

MeHg caused brain injury is pathologically characterized by atrophy of cerebral cortex and white matter [52]. Eto further reported the thinning of the corpus callosum [53]. Microscopically, calcarine, postcentral and precentral cortices of cerebrum were found to be atrophic with a slightly decreased number of neurons and gliosis[53]. Calcification can also be detected in the globus pallidus. In the basal ganglia, there is loss in neurons. Interestingly, ventral nerve roots of

the spinal cord generally remain intact, but the connective tissue is increased. Furthermore, segmental demyelination in the dorsal nerve fibers is also observed [53]. Electron microscopy of human autopsy specimen clearly shows that nerve cells are shrunken with an increase in nuclear chromatin. Ribosome aggregation and loss of rough endoplasmic reticula (Nissl bodies) are also noted [52],

MeHg causes severe brain injury, which is reflected by behavior changes in both human beings and animals. Among all neurodeficits, the motor impairment is an important behavioral sign observed in MeHg-poisoned animals, Kitamura[54] reported that cats fed a diet that primarily consisted of fish in Minamata district presented a severe movement disorders, convulsions and death. Takeuchi [55] also reported that fish-feeding cats that lived on Indian Reserves in Northwestern Ontario, Canada, developed acute neurological symptoms characterized by ataxic gait, abnormal movements, uncontrolled howling, and seizures. Similar symptoms have been observed in numerous experimental animals including dogs [56], mice [57, 58]; rats [59, 60], monkeys [61] and zebrafish (Danio rerio) [62]. Notably, other CNS symptoms such as visual dysfunction (measured by visual contrast sensitivity task) [63], cognitive impairment (tested by passive avoidance task) [64] and emotional dysfunction (depression-like behavior evaluated in the forced swimming test) [65] have also been reported.

The neurotoxicity of MeHg is also dependent on the stage of development. Compared to the adult CNS, the developing CNS is more susceptible to MeHg [66]. Mansour [67] showed that MeHg is transferred across the placenta from pregnant rats to their fetuses. Olson [68] further conducted a study on the pharmacokinetics of MeHg using murine maternal-fetal unit which

showed that the fetal accumulation of mercury increased with fetal age and peak fetal mercury was reached 3 days post MeHg administration. Another interesting experimental study using pregnant mice showed significant changes in biochemical parameters in the fetuses' brain and absent changes in the mothers' brain [69], which suggested that the transfer of MeHg from the pregnant animals to their fetuses via the placenta led to neurotoxicity in the offspring with no evident neurotoxic signs in their respective mothers. Interestingly, epidemiological studies corroborated this observation in humans as well [70]. Taken together, all the literatures support the notion that the developing CNS is most susceptible to the deleterious effects of MeHg than adult CNS.

Toxicity of MeHg in Neurons

The neuron is the primary target for MeHg [71], but the vulnerability of neurons decreases as the CNS matures [72, 73]. In general, MeHg poisoning results in focal damage in adults and widespread and diffuse damage in the fetal and neonatal brain [74]. In adult patient, the brain areas most vulnerable to MeHg include the primary sensory and motor cortices, pre- and post-central gyri, the temporal transverse gyrus and the cerebellum (but not Purkinje cells) [75]. In contrast, congenital exposure to MeHg leads to widespread neuron injury. Pathologically, it results in cortical atrophy, thinning of the corpus collosum, white matter shrinkage and diffuse spongiosus [75, 76].

The mechanisms of MeHg-induced neuronal death have been studied in the past decades, which points to several critical features, namely: **1) inhibition of neuronal macromolecule synthesis (DNA, RNA and protein);** The binding of MeHg with neuronal DNA and RNA results in

changes in the secondary structure of these molecules [77, 78]. Furthermore, MeHg inhibits DNA repair by directly binding to the "zinc finger" core of DNA repair enzymes, deforming the structural integrity and activity of these enzymes and consequently affecting their activity [79]. **2) MeHg disrupts microtubules;** Sager [80] reported that MeHg inhibits the polymerization of tubulin. Castoldi [81] reported that MeHg at concentration of 0.5–1 μM leads to microtubular fragmentation formation in cultured primary rat cerebellar granular neurons. Given the fact that microtubules participate in cell division, their fragmentation by MeHg results in antimitotic effects, as well as the inhibition of neuronal migration and the degeneration of neuritis [82]. Furthermore, Leong [83] reported that mercury inhibits tubulin polymerization into microtubules using large pedal A (PeA) neurons from the central ring ganglia of snails. The tubulin/microtubule structure of growth cones was found to be disintegrated after mercury exposure using immunohistochemistry. He demonstrated that mercury markedly disrupted membrane structure and linear growth rates of neurites in 77% of all nerve growth cones [83]. Interestingly, Vendrell [84] proposed that mercury may affect neuronal polarity formation. She reported methylmercury disrupts the balance between phosphorylated and non-phosphorylated cofilin in primary mice cerebellar granule cells culture using MALDI-TOF PMF and MALDI-TOF/TOF sequencing. As the result of the disruption of cofilin phosphorylation, the actin dynamics were changed, which may disrupt cellular polarity formation [84]. However, more studies are warranted in order to fully understand the effects of mercury on neuronal polarity change. **3) MeHg leads to an increase in intracellular Ca^{2+};** MeHg increases Na^{2+} and decreases K^{+} ion concentration in synaptic spaces, which leads to increased intracellular Ca^{2+} concentration [85, 86]. Ca^{2+} is the key molecule in the regulating neurotransmitter release and the change in intracellular Ca^{2+} leads to the disruption of cell signaling cascade. For example,

the increased release of dopamine, glutamate, γ-amino butyric acid (GABA), glycine, choline [87] and acetylcholine [88] have been reported. Furthermore, the inhibition of the uptake of glutamate and aspartate, has also been implicated as a major mechanism of MeHg-induced neurotoxicity [89, 90]. **4) MeHg alters neuronal energy metabolism;** MeHg stimulates the ubiquinol: cytochrome C reductase complex (complex III) on the mitochondrial membrane [91], while inhibiting glutathione peroxidase (GPx) [92], which leads to lipid peroxidation. MeHg also inhibits tri-carboxylic-acid (TCA) cycle activity and decreasing ATP utilization in neurons [93, 94]. Since the neuron is strictly dependent upon glucose for its energy production, high oxygen utilization and excitability renders it especially susceptible to MeHg; and **5) MeHg causes oxidative stress in neurons.** MeHg is known to induce oxidative stress both *in vitro* and *in vivo* [95-97]. The production of ROS by MeHg exacerbates toxicity by facilitating cell death via apoptotic pathways. Inhibition of glutathione peroxidase (GPx) by MeHg further potentiates lipid peroxidation. Conversely, several studies have demonstrated partial amelioration of MeHg neurotoxicity in the presence of antioxidants For example, Li [98] reported that antioxidant vitamins (vitamin A, E and C) have protective effects on the early neurodevelopment of children against mercury toxicity. Shichiri [99] also reported that fat-soluble antioxidant tocopherols and tocotrienols ameliorate MeHg-induced neurotoxicity using cultured cerebellar granule cells (CGCs). Zhang [100] further reported that pyrroloquinoline quinone (PQQ), a novel redox cofactor, exhibits the neuroprotective effects on cultured PC12 cells.

MeHg Toxicity in Glia

After MeHg exposure, approximately 10% mercury is retained in the brain. However, Hg is not universally distributed and is preferably deposited in certain CNS cell types. Charleston [101]

reported that tissue staining following six months of exposure to MeHg reveals the largest Hg deposits in glia including astrocytes and microglia. The total mercury accumulation in neurons is significantly lower than those present in the glial cells and increase with the length of exposure; virtually all neurons are labeled following 18 months of exposure. In contrast, endothelial cells and pericytes do not contain notable mercury deposits, and deposits in oligodendrocytes are rarely observed. These data are consistent with the hypothesis that the neurotoxicity of MeHg is mediated, at least in part, by glial cells and that glia-neuron interactions play important roles in the process. Notably, staining of mercury deposits in inorganic Hg-exposed animals is lower compared to MeHg-exposed animals, supporting the observation that it is the organic form of mercury that more readily crosses the blood-brain barrier (BBB) [102].

I. MeHg Toxicity in Astrocytes

Astrocytes are the major glial cell type, which provide support and nutrition [1], maintain CNS homeostasis [103], form myelin [103], participate in signal transmission [104, 105], secret growth factors, release of cytokines and modulate synaptic transmission by removal of neurotransmitters such as glutamate from the synaptic cleft [104, 105].

MeHg inhibits the astrocytic uptake of cystiene, a crucial precursor for glutathione (GSH) synthesis, leading to decreased GSH levels [106]. GSH has been shown to be the key molecule to reduce reactive oxygen species. Therefore, intracellular ROS increases after MeHg exposure [107]. MeHg also leads to oxidative stress by directly disrupt mitochondrial functions as demonstrated by decreased mitochondrial TMRE fluorescence [107]. Astrocytes dysfunction also affect nearby neurons. Because astrocytes provide GSH precursors to neurons, MeHg-

induced decrease in cystiene uptake in astrocytes contributes to neuronal oxidative damage [108]. Furthermore, MeHg also inhibits astrocytic glutamate uptake, while stimulating glutamate efflux [90, 107], which results in excessive glutamate concentrations in the synapse and, consequently, neuronal excitotoxicity. Moreover, a number of previous studies have shown that MeHg exposure led to astrocytic dysfunction associated with increased Na^+ [109] and aspartate uptake [110, 111] and excessive production of excitatory neurotransmitter, affecting the glia-neuron interaction [112].

II. MeHg Toxicity in Microglia

Microglia, derived from myeloid lineage [113], are the second largest glial cell type (typically 8-12 um in diameter). The major functions of microglia include phagocytosis and surveillance of parenchyma. Microglia also function as antigen presenting cells (APC) by expressing low level of Major Histocompatibility Complex (MHC-II) [113]. Physiologically, microglia are not isolated from other cell types in the brain; instead, they participate in the formation of cell-network by close contacting with astrocytes, which mediates and synergizes responses. Notably, microglia are the first cell type to become activated in the presence of inflammation, infection, and brain trauma [113]. Microglia also play important role in the numerous neurodegenerative diseases, such as Alzheimer's disease [114], Parkinson's disease [115] and HIV dementia [116]. Once activated, microglia produce soluble proinflammatory cytokines, prostaglandins and interleukins, such as tumor necrosis factor-α (TNF-α), PGE2, interleukin-1 (IL-1) and interleukin-6 (IL-6), which not only contribute to the neighboring neuronal damage, but also recruit immune cells into the CNS. Previous literature showed that microglia are more sensitive than other CNS cell types to adverse stimuli. For example, Monnet showed that microglial cells

respond to adverse stimuli at lower concentrations [117, 118] and such reactions occur prior to astrocytic dysfunction and neuronal death [119, 120]. After MeHg exposure, microglia accumulate the largest concentration of mercury in non-human primates, which limits the amount of free Hg in the CNS [102]. However, the majority of previous studies are focused on the MeHg toxicity on neurons and astrocytes [107, 121, 122], but little on microglia. Therefore, my thesis project is carried out to answer this question.

Protective Effects of NF-E2-related factor 2 (Nrf2) and its Downstream Genes

Nrf2 is the primary transcription factor that controls the antioxidant response essential for maintaining cellular redox homeostasis in numerous cells, including vascular smooth muscle cells [123], mononuclear cells [124] and liver cells [125] etc. Nrf2 also maintains redox balance in glia after exposure to the murine leukemia virus [126] and a variety of environmental toxicants, such as lipopolysaccharides **(**LPS) [127] and kainic acid [128]. Under physiological conditions, inactive Nrf2 is bound to the Kelch-like ECH-associating protein 1 (Keap1) in the cytoplasm [129]. Keap1 functions both as an Nrf2 cytosolic repressor [130] and as an adaptor for cullin 3-based E3 ubiquitin ligase, leading to rapid proteasomal degradation of Nrf2 [131, 132]. Upon oxidative stress, the interaction between Nrf2 and Keap1 is disrupted, which decreases the rate of proteasomal degradation of Nrf2. This causes *de novo* Nrf2 to build up within the cells, leading to increased translocation of Nrf2 into nuclei [133]. In the nucleus, Nrf2 forms heterodimers with small Maf proteins, such as FosB, C- Jun, JunD, ATF2 and ATF4 [132, 134, 135]. These heterodimers interact with the antioxidant response element (ARE) to initiate the transcription of target genes including the light chain of the cysteine/glutamate transporter (*xCT*), γ-glutamyl cysteine synthase, hemeoxygenase-1 (*Ho-1*) and NADPH:quinone oxidoreductase-1

(*Nqo1*), in order to detoxify xenobiotics and endogenous reactive electrophiles [136-138]. Furthermore, *Nrf2* knockout mice show increased sensitivity to a variety of pharmacological and environmental toxicants, such as carcinogens and oxidative stressors such as acetaminophen [139, 140]. For example, Das [141] reported that acetaminophen induces cellular injury mainly through reducing glutathione level, increasing lipid peroxidation and causing hepatic DNA fragmentation which ultimately leads to cellular necrosis. Chan [142] clearly demonstrated the importance of Nrf2 in the detoxification of acetaminophen in their recent paper entitled 'An important function of Nrf2 in combating oxidative stress: detoxification of acetaminophen'.1 They showed that the toxicity of acetaminophen is markedly augmented in Nrf2 knock out mice. The most striking data are that the Nrf2 knock out mice died rapidly between 6 and 12 h after injection, whereas the wild-type mice died over a more extended period, with the last deaths occurring between 36 and 48 h post injection. The LD50 was 235 and 320 mg kg−1 for male and female Nrf2 knock out mice, respectively, and 400 and 540 mg kg−1 for the male and female wild-type mice, respectively.

As stated above, MeHg causes oxidative stress in glia, therefore, it is reasonable to hypothesize that Nrf2-mediated antioxidant machinery is likely to be used in both astrocytes and microglia to detoxify the free radicals post MeHg exposure.

Hypotheses and Specific Aims

Given the fact that in the past several decades, the majority of studies on MeHg-induced CNS damage have been focused on its effects on neurons and astrocytes [107, 121, 122] and little

work has been done on microglial cells, my thesis project was carried out in order to better understand mechanisms of MeHg toxicity in glial cells and cellular response after acute MeHg exposure. Although previous studies have assessed the effects of high concentrations of MeHg after long term of exposure on immortalized microglial cell lines [143, 144], these results may not represent the acute response of primary microglial cells to lower concentrations of MeHg as detected in the early stage of Minamata disease patients. More importantly, the immortalized microglia cell lines derived from cancers may not represent the natural response of primary microglia. Given these limitations, it is necessary to characterize primary microglial response to MeHg and to test the role of microglial cells in exhibiting an acute response to low concentrations of MeHg after short term of exposure. We hypothesized that 1) the cellular responses to MeHg are cell-type specific; 2) there are differences in the uptake of MeHg between astrocytes and microglia, leading to differential temporal cellular responses associated with oxidative stress.

The aims of my thesis project are 1) assess the acute responses of primary microglia after short period of MeHg exposure; 2) investigate and compare the kinetics of microglial activation with that of astrocytes; 3) study the function of Nrf2 and its downstream genes including *Ho-1, xCT* and *Nqo1* after MeHg exposure in astrocytes and microglia, respectively; 4) determine the differences in the kinetics of Nrf2 activation in glial cell subtypes in order to better understand their respective roles in mediating adaptive responses to MeHg treatment.

CHAPTER II

ACUTE RESPONSE OF RAT PRIMARY MICROGLIAL CELLS TO METHYLMERCURY (MeHg) EXPOSURE

This chapter has been published as an article under the title as

"Methylmercury Induces Acute Oxidative Stress, Altering Nrf2 Protein Level in Primary Microglial Cells"

In Toxicol Sci. 2010 Aug; 116(2):590-603.

Summary

The neurotoxicity of methylmercury (MeHg) is well documented in both humans and animals. MeHg causes acute and chronic damage to multiple organs, most profoundly the central nervous system (CNS). Microglial cells are derived from macrophage cell linage, making up ~12% of cells in the CNS, yet their role in MeHg-induced neurotoxicity is not well defined. The purpose of present study was to characterize microglial vulnerability to MeHg and their potential adaptive response to acute MeHg exposure. We examined the effects of MeHg on microglial viability, reactive oxygen species (ROS) generation, glutathione (GSH) level, redox homeostasis and Nrf2 protein expression. Our data showed that MeHg (1-5 μM) treatment caused a rapid (within 1 min) concentration- and time-dependent increase in ROS generation, accompanied by a statistically significant decrease in the ratio of GSH and its' oxidized form glutathione disulfide (GSSG) (GSH/GSSG ratio). MeHg increased the cytosolic Nrf2 protein level within 1 min of exposure, followed by its nuclear translocation after 10 min of treatment. Consistent with the

nuclear translocation of Nrf2, quantitative real-time PCR revealed a concentration-dependent increase in the mRNA level of Ho-1, Nqo1 and xCT 30 min post MeHg exposure, while Nrf2 knockdown greatly reduced the upregulation of these genes. Furthermore, we observed increased microglial death upon Nrf2 knockdown by the shRNA approach. Taken together, our study has demonstrated that microglial cells are exquisitely sensitive to MeHg and respond rapidly to MeHg by upregulating the Nrf2-mediated antioxidant response.

Introduction

Except neurons, the majority non-electrically excitable cells in the CNS are glial cells, including astrocytes, microglial cells and small amount of oligodendrocytes. Glial cells have diverse functions, such as providing support and nutrition [1], maintaining CNS homeostasis [103], forming myelin [103] and participating in signal transmission [104, 105], just to name a few. The majority of glial cells are astrocytes, which are intimately involved in maintaining the extracellular milieu. Some selected functions of astrocytes include secretion of growth factors, release of cytokines and modulation of synaptic transmission by removal of neurotransmitters such as glutamate from the synaptic cleft. Oligodendrocytes are the myelin-forming cells in the CNS and are analogues to Schwann cells of the peripheral nervous system.

Microglial cells comprise approximately 12% of total cell population in the brain and are the second largest glial cell type. Microglia are derived from myeloid lineage [113]. In postnatal rodents, immunocytochemical studies using antibodies to F4/80 (ERM1), CR3 and FcγRII/III establish that the microglia enter the brain from the circulation and are derived from circulating monocytes [113]. In the brain, they possess phagocytic activity and survey the parenchyma.

Microglia express low level of Major Histocompatibility Complex (MHC-II) and function as antigen presenting cells (APC) of the CNS [113]. They are in close contact with other cells in the brain, mainly astrocytes, thus establishing cross-talk that mediates and synergizes responses both in physiological and pathological conditions. Under optimal conditions microglial surface receptors, such as TREM2 and Siglecs, maintain the microglia in an inactivated state [113]. In the presence of inflammation, infection, trauma and degenerative diseases, microglial cells are the first cell type to become activated. Their activation is inherent to Alzheimer's disease [114], Parkinson's disease [115], HIV dementia [116] as well as numerous other pathological conditions. Once activated, microglia produce soluble proinflammatory cytokines, prostaglandins and interleukins, such as tumor necrosis factor-α (TNF-α), PGE2, interleukin-1 (IL-1) and interleukin-6 (IL-6), which not only contribute to the neighboring neuronal damage, but also recruit immune cells into the CNS.

MeHg affects neurons and glial cells in the CNS both acutely and chronically. In the past several decades, the majority of studies on MeHg-induced CNS damage have focused on its effects on neurons and astrocytes [107, 121, 122]. It has been reported that MeHg disrupts cellular redox homeostasis through excessive ROS generation. The interaction of MeHg with the mitochondrial electron transport chain (ETC) represents a major mechanism of MeHg-induced ROS generation [91]. It causes a concentration-dependent reduction of the inner mitochondrial membrane potential [107] by altering Ca^{2+} homeostasis [145]. MeHg also decreases ATP synthesis in neurons by inhibiting both glycolysis and the Krebs cycle [146], thereby contributing to neuronal dysfunction and death. Furthermore, MeHg inhibits astrocytic glutamate uptake, while

stimulating glutamate efflux [90], consequently resulting in an excessive concentration of synaptic glutamate, which ultimately leads to neuronal excitotoxicity and cell death [147].

Until recently, the toxicity of MeHg on primary microglial cells has not been fully investigated. More and more evidences suggesting the import role of microglial cells in mediating MeHg induced brain toxicity. For example, comparative studies carried out in animals treated with neurotoxins have shown that microglial cells react at lower concentrations [117, 118] and that such reactions occur prior to astrocytic dysfunction and neuronal death [119, 120]. Monnet reported that the earliest sign of MeHg-induced neurotoxicity was inherent to microglial cells by using three-dimensional brain cell cultures [148]. Consistently, Charleston et al. reported that microglial cells accumulated the largest concentration of mercury following MeHg exposure in non-human primates [102]. Although some studies have assessed the effects of high concentrations of MeHg after long times of exposure on immortalized microglial cell lines [143, 144], these results may not represent the acute response of primary microglial cells to lower concentrations of MeHg as detected in the early stage of Minamata disease patients. Given existing limitations, it is necessary to characterize microglial vulnerability to MeHg and to test the role of microglial cells in exhibiting an acute response to low concentrations of MeHg after short times of exposure.

Here, for the first time, we assessed microglial functional changes after short-term exposure to MeHg concentrations, which failed to elicit detrimental effects in other cell types. For example, MeHg treatment at concentrations lower than 5 μM did not cause decrease in formazan production (MTT assay) or oxidative stress in rat striatal synaptosomes [149]. Similar results

were also observed in primary rat astrocytes where MeHg at concentrations lower than 5 μM failed to elicit ROS production [150].

Analogous to other cell types, the generation of ROS in microglial cells by MeHg plays a critical role in its toxicity [144]. The Nrf2-mediated antioxidant machinery is likely used in microglial cells to detoxify free radicals. Nrf2 maintains redox balance in microglial cells after exposure to the murine leukemia virus [126] and a variety of environmental toxicants, such as lipopolysaccharides (LPS) [127] and kainic acid [128]. Under physiological conditions, inactive Nrf2 is bound to the Kelch-like ECH-associating protein 1 (Keap1) in the cytoplasm [129]. Keap1 functions both as an Nrf2 cytosolic repressor [130] and as an adaptor for cullin 3-based E3 ubiquitin ligase, leading to rapid proteasomal degradation of Nrf2 [131, 132]. Upon oxidative stress, the interaction between Nrf2 and Keap1 is disrupted, decreasing the rate of proteasomal degradation of Nrf2. This causes de novo Nrf2 to build-up within the cells, leading to increased translocation of Nrf2 into the nuclei [133]. In the nucleus, Nrf2 forms heterodimers with small Maf proteins, such as FosB, C- Jun, JunD, ATF2 and ATF4 [132, 134, 135]. These heterodimers interact with the antioxidant response element (ARE) to initiate the transcription of target genes including the light chain of the cysteine/glutamate transporter (xCT), γ-glutamyl cysteine synthase, hemeoxygenase-1 (Ho-1) and NADPH:quinone oxidoreductase-1 (Nqo1), in order to detoxify xenobiotics and endogenous reactive electrophiles [136-138]. Furthermore, Nrf2 knockout mice show increased sensitivity to a variety of pharmacological and environmental toxicants, such as carcinogens and acetaminophen [139, 140]. Therefore, it is important to explore the role of Nrf2 in MeHg toxicity in microglial cells.

The present study was carried out to test the hypothesis that microglial cells are exquisitely sensitive to MeHg and that they undergo rapid activation upon being treated with low concentrations of MeHg (0.1~ 5μM), representative of common environmental exposure levels [151]. We found that acute MeHg treatment immediately resulted in ROS generation, GSH depletion and, consequently, the upregulation of both Nrf2 protein and the expression of Ho-1, Nqo1 and xCT in primary microglial cells. Nrf2 knockdown attenuated the upregulation of such genes, resulting in increased microglial death upon MeHg exposure.

Experimental Procedures

Primary Microglial Culture

Primary microglial cells were isolated and cultured according to a published protocol [152]. Briefly, the cerebral hemispheres of postnatal day-1 neonatal Sprague-Dawley rats were removed and the meninges were dissected off. The cortical tissue was digested with dispase (BD Biosciences, Two Oak Park Dr. Bedford, MA, USA). The mixed glial cell culture was maintained in minimum essential medium (MEM) (Invitrogen, Carlsbad, CA, USA), supplemented with 5% heat-inactivated fetal bovine serum (Hyclone, South Logan, Utah, USA) and 5% horse serum (Invitrogen, Carlsbad, CA, USA). The media were changed once a week. After two weeks in culture, microglial cells were separated by gentle shaking for 20 min at room temperature and then plated in 6-well plates and cultured at 37°C in a 95% air/5% CO_2 incubator for additional 48 hours in MEM containing 10% fetal bovine serum (Hyclone, South Logan, Utah, USA) and 1% penicillin and streptomycin (Invitrogen, Carlsbad, CA, USA). The purity of the cells was determined by immunostaining for the microglia specific marker, OX42 (sc-53086, Santa Cruz Biotechnology, Santa Cruz, CA, USA); cell nuclei were counter-stained with 4',6-

diamidino-2-phenylindole (DAPI) (VECTASHIELD Mounting Medium with DAPI, H-1200, Burlingame, CA, USA).

MTT Assay and LDH Assay

The cytotoxic effect of MeHg in microglial cells was evaluated by 3-[4,5- dimethylthiazol-2-yl]-2,5 diphenyltetrazolium bromide (MTT) assay (Sigma *in vitro* Toxicology Assay Kit, MTT based, M-5655, St. Louis, MO, USA). 10X MTT stocking solution was prepared by reconstituting 15mg stock MTT reagent in 3ml of OPTI- MEM culture media (Invitrogen, Carlsbad, CA, USA) in the absence of phenol red immediately before the experiment. Primary cultured microglial cells were maintained in 96-well plates at a density of 20,000 cell/well for 2 days prior to experiment. Cells were treated for 6 hours. Treatment with 100 μM H_2O_2 was used as a positive control of cell death. After treatment, 10X MTT stocking solution was directly added to each well at a final concentration of 0.5 mg/ml. The formazan crystal precipitates were dissolved by adding an equal volume of MTT solubilization solution (Sigma, M-8910, St. Louis, MO, USA) and gently shaking for 20 min. The absorbance was measured by spectrophotometer (Molecular Device, VMax® Kinetic Microplate Reader, Sunnyvale, CA, USA) at a wavelength of 570 nm. The background absorbance was measured at 690 nm and subtracted from the 570 nm measurement.

Cellular membrane integrity was measured by the lactate dehydrogenase (LDH) assay. After treatment, the culture media were collected for LDH analysis. The LDH assay substrate (L 2402, Sigma, St. Louis, MO, USA) was always freshly prepared. The assay mixture was added in an amount equal to twice of the volume of the culture medium and incubated at room temperature for 30 min in the dark. The reaction was terminated by adding 1/10 volume of 1N HCL. The

absorbance was measured by a spectrophotometer (Molecular Device, VMax® Kinetic Microplate Reader, Sunnyvale, CA, USA) at a wavelength of 490 nm, and the background absorbance was measured at 690nm.

Detection of intracellular ROS formation

Microglial cells were pre-incubated with H_2DCF-DA (C6827, Invitrogen, Carlsbad, CA, USA) at a final concentration of 25 μM for 30 min at 37°C. The MeHg solution was directly added in the MEM culture media containing H_2DCF-DA. After treatment, the microglial cells were washed with 4°C PBS twice and precipitated by centrifugation at 400x g. The cell pellets were then dissolved in 1% Triton X- 100 (Promega, Madison, Wisconsin, USA). Fluorescence was measured at a wavelength of 480/530nm (excitation/emission) by SpectraMax M5 (Molecular Devices, Sunnyvale, CA, USA). The DCF fluorescent signal in microglial cells was obtained with a Nikon microscope (Nikon Eclipse 80i, Shinagawa-ku, Tokyo, Japan) at 480/530nm.

Measurement of GSH

The intracellular GSH concentration was measured by high-performance liquid chromatography (HPLC) as previously described [153]. After MeHg treatment, microglial cells were derivatized with iodoacetic acid and dansyl chloride. HPLC analysis was carried out with a propylamine column (YMC Pack, NH2, Waters, Milford, MA, USA) and an automated HPLC system (Alliance 2695, Waters Corporation, Milford, MA, USA). The GSH and GSSG concentrations were normalized to the protein concentration of the samples as measured by colorimetric detection and quantitation using BCA Protein Assay Reagent (23225, Rockford, IL, USA).

Immunohistochemistry

Microglial cells were cultured on coverslips coated with poly-L-lysine. After MeHg treatment, cells were fixed with ice-cold 4% paraformaldehyde (PFA) for 15 min, followed by two washes with 30 mM glycine to quench the PFA. Cells were permeated for 3 min by 0.25% Triton X- 100 in PBS and blocked in 5% BSA/PBS for 45 min. The samples were incubated for 1h with 1:200 rabbit anti- Nrf2 (Abcam 31136, Cambridge, MA, USA) and washed in PBS three times before incubation with 1:400 secondary antibody, donkey anti-rabbit IgG conjugated with FITC (Millipore, AP182F, Billerica, MA). Coverslips were mounted with Vectashield Mounting Medium with Propidium Iodide (PI) (VECTOR, H-1300, Burlingame, CA, USA). The fluorescence signal was detected using a Zeiss confocal microscope (LSM 510, Zeiss, Dublin, CA, USA) at the following settings: detector gain 900, amplifier offset -0.085 and pinhole 98. The propidium iodide (PI) signal was detected with the following settings: detector gain 844, amplifier offset -0.068 and pinhole 110.

Measurement of Nrf2 by Western Blot Analysis

Western blot analysis was conducted with the primary antibodies, rabbit-anti Nrf2 (1:400) (sc-722, Santa Cruz Biotechnology, Santa Cruz, CA, USA) and mouse anti β-Actin (1:2,000) (A1978, Sigma, St. Louis, MO, USA). Secondary antibodies were donkey anti-rabbit IgG conjugated with horseradish peroxidase (HPR) (1:1000) (W4011, Promega, Madison, Wisconsin, USA) and donkey anti-mouse IgG conjugated with horseradish peroxidase (HPR) (1:4,000) (W4021, Promega, Madison, Wisconsin, USA). The cytosolic and nuclear fractions were prepared with NE-PER Nuclear and Cytosolic Extraction Reagents (78833, Thermo Scientific, Rockford, IL, USA). Briefly, after treatment, microglial cells were lysed in ice-cold hypotonic

buffer containing 10mM HEPES, 1.5mM $MgCl_2$, 10mM KCl and 1mM dithiothreitol (DTT) and cocktail of protease inhibitors (Thermo Scientific, Rockford, IL, USA). After 30 min incubation on ice, the samples were centrifuged at 4°C at 12,000g and the supernatant was collected as the cytosolic fraction. The pellet was further extracted for 30 min in a high salt lysis buffer containing 50mM HEPES, 500 mM NaCl, 1 mM dithiothreitol (DTT) and protease inhibitors (Thermo Scientific, Rockford, IL, USA). After 10 min centrifugation at 4°C at 12,000g, the supernatant was collected as the nuclear fraction. The density of the Nrf2- specific bands was normalized to β-Actin.

Measurement of *Ho-1, Nqo1* and *xCT* Genes Expression by Quantitative Real-Time PCR

mRNA of *Ho-1, Nqo1* and *xCT* were measured by real-time PCR using the Universal Probe Library (Roche, Indianapolis, IN, USA). Table 1 lists the primer sequences and UPL probes. Average threshold cycle (*ΔCt*) values were used to determine the relative difference between control and treated samples. All data were normalized to β-Actin levels.

Table 1

primer sequences used for real- time PCR analysis			
gene	forward (5'-3')	backward (5'-3')	UPL probe
xCT	5'-TCC ATG AAC GGT GGT GTG T-3'	5'- CCC TTC TCG AGA TGC AAC AT-3'	#80
HO-1	5'-GTC AGG TGT CCA GGG AAG G-3'	5'-CTC TTC CAG GGC CGT ATA GA-3'	#9
NQO1	5'-AGC GCT TGA CAC TAC GAT CC-3'	5'-CAA TCA GGG CTC TTC TCA CC-3'	#50
beta actin	5'- CCC GCG AGT ACA ACC TTC T- 3'	5'- CGT CAT CCA TGG CGA ACT- 3'	#17

Table 1: Primer sequences and UPL probe numbers used to measure expression levels of *Ho-1, Nqo1* and *xCT* in real-time PCR.

Nrf2 Knockdown by Small Hairpin RNA (shRNA)

Primary microglial cells at ~50-60% confluence were infected with 15µl lentiviral particles with $1X10^6$ infectious units of virus (IFU) for 24 hours. The lentiviral particles contained an expression construct encoding specific shRNA against Nrf2 (sc-37049-V, Santa Cruz Biotechnology, Santa Cruz, CA, USA). The infection rate was tested by copGFP Control Lentiviral particles (sc-108084, Santa Cruz Biotechnology, Santa Cruz, CA, USA). Primary microglial cells were also infected with control lentiviral particles containing scrambled shRNA sequence (sc-108080, Santa Cruz Biotechnology, Santa Cruz, CA, USA) as a negative control.

Statistical analysis

All results were expressed as means ± standard errors. Unless otherwise specified, differences among treatment groups were analyzed by one-way analysis of variance (ANOVA), followed by Bonferroni's *post hoc* test. Statistical significance was set at $p<0.05$. All experiments were repeated with at least three independently isolated microglial cultures, and data analysis was carried out with GraphPad Prism (GraphPad Software, San Diego, CA, USA).

Results

Overall Cytotoxic Effects of MeHg on Microglia

As the first step, the purity of primary microglial cultures was assessed by immunostaining with the microglial specific marker, OX42 [154] (Fig 2A). As shown in the merged image (Fig 2C), when co-stained with DAPI (Fig 2B), a nuclear dye, nearly all cells appeared to be of the microglial cells lineage. In addition, cells exhibited characteristic microglial morphology in the differential interference contrast (DIC) image (Fig 2D).

Fig 2

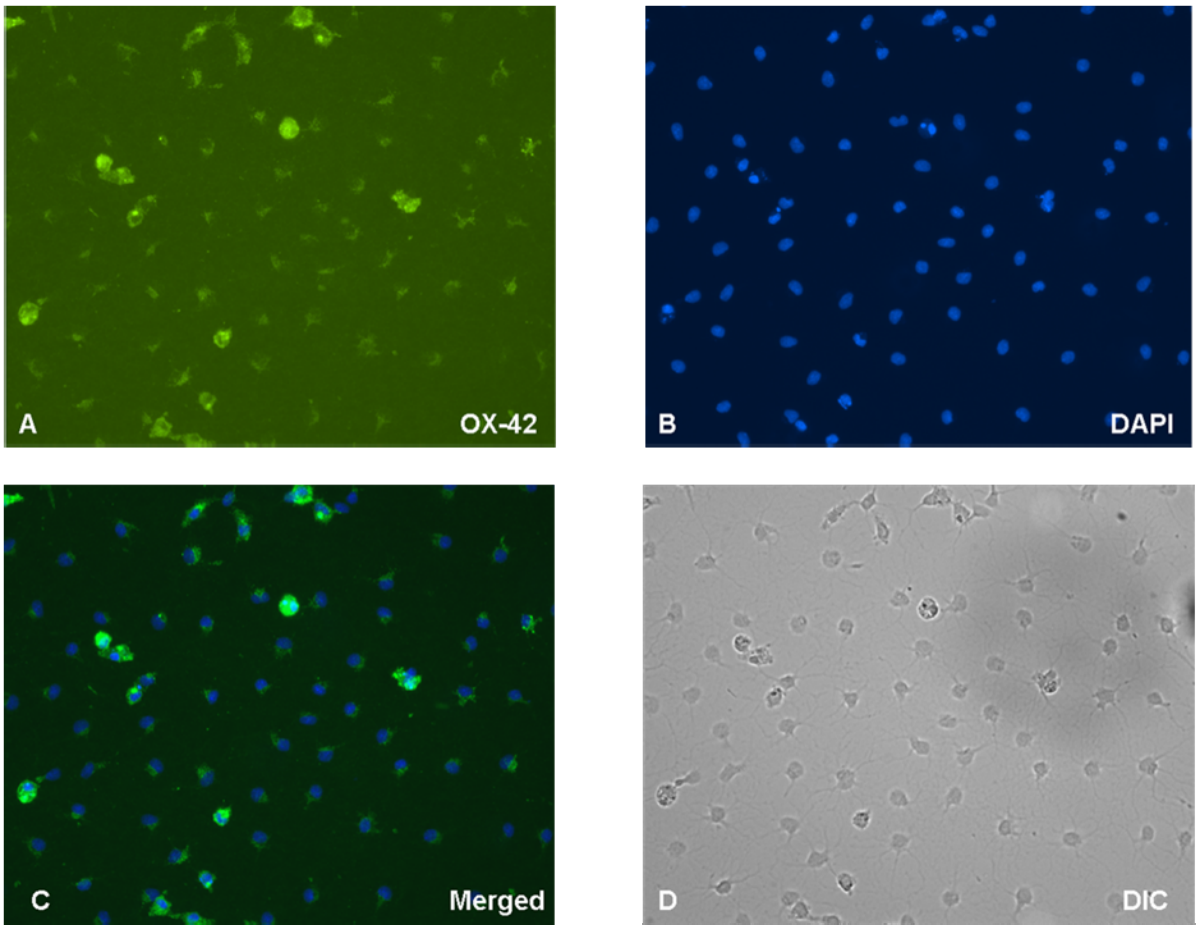

Fig 2. The purity of primary microglial culture was tested on day 3 after separation from mixed glial culture by immunostaining for OX42. **[A]**: Microglial cells were fixed and immunostained for OX42. **[B]**: Microglial nuclei were counter-stained with DAPI. **[C]**: Merged image of OX-42 and DAPI demonstrated the purity of microglial culture close to 100%. **[D]**. DIC image of microglial cells. Photographs show representative fields observed in twelve coverslips from three independent experiments.

Next, we tested the overall cytotoxic effects of MeHg on microglial cells with the MTT assay. The absorbance of MTT (wavelength of 570nm) is positively correlated with cell viability. As shown in Fig 3A, after MeHg treatment for 6 hours, the absorbance was indistinguishable between control and 0.1μM MeHg-treated cells. However, higher concentrations of MeHg (1 and 5 μM) reduced the absorbance to 0.86± 0.09 ($p<0.05$) and 0.59± 0.08 ($p<0.001$), respectively, reflecting reduced cell viability. As the positive control, H_2O_2 at 100 μM reduced MTT absorbance to 0.27± 0.07 ($p<0.001$). Cell viability was also measured by the LDH assay. The absorbance of LDH (wavelength of 490nm) is reversely correlated with cell viability. As shown in Fig 3B, the absorbance of LDH increased after 6-hour treatment with 1 ($p<0.01$) and 5 μM MeHg ($p<0.001$), respectively, reflecting decreased cell viability.

Fig 3A

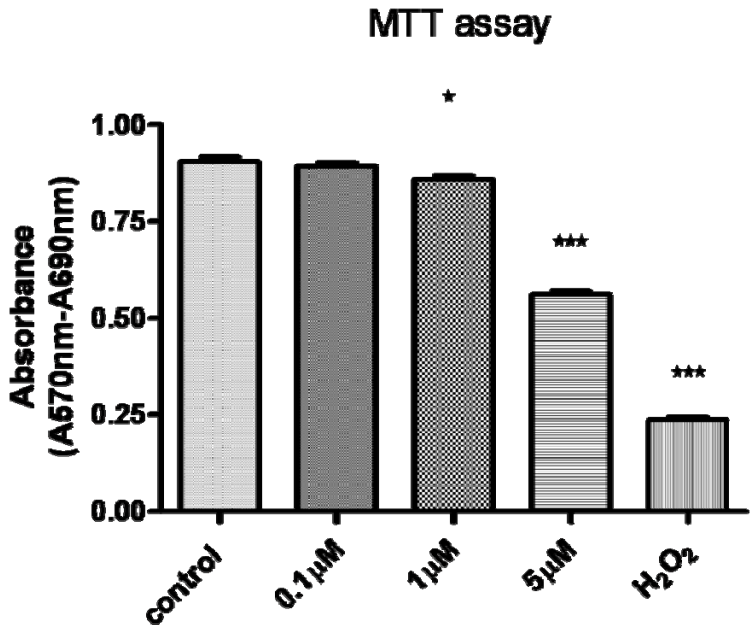

Fig 3B

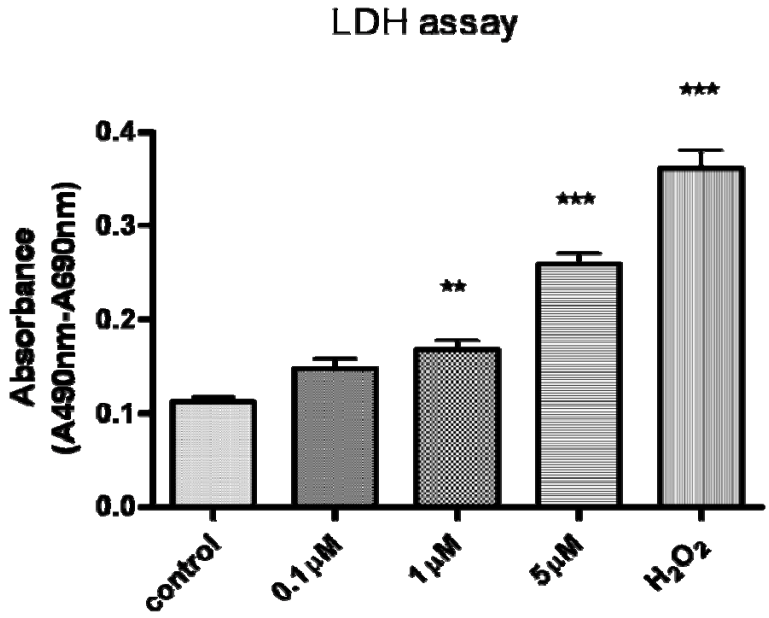

Fig 3. Effect of MeHg cytotoxicity on microglial cells was measured by MTT assay [A] and LDH assay [B]. **[A]**: Result of MTT assay of microglial cells after MeHg treatment for 6h showed the concentration-dependent decrease in absorbance. Microglial cells were treated with MeHg with the concentrations indicated in the graph. 100μM H_2O_2 was used as a positive control. **[B]**: Result of LDH assay using microglial culture media after the same treatment demonstrated a concentration-dependent increase in absorbance. Values are expressed as the mean ± SEM derived from five independent experiments. ★ P<0.05, ★★ P<0.01, ★★★ P<0.001

MeHg Caused Acute Oxidative Stress in Microglia

Next, we tested whether MeHg induces ROS generation in microglial cells with the H_2DCF-DA assay. The lipophilic H_2DCF-DA diffuses freely through the cell membrane and it is intracellularily converted to hydrophilic DCF. Once in the cells, DCF reacts with ROS and fluoresces, providing a tool for intracellular ROS level analyses. As shown in Figure 4, a significant increase in fluorescence intensity was readily detectable after 1min treatment with 5 μM MeHg (222.6±39.01, $p<0.01$) and 100 μM H_2O_2 (229.03±40.08, $p<0.001$). Treatments with 1μM and 5 μM MeHg for 10 min further increased DCF fluorescence in a concentration-dependent manner (Fig 4). Furthermore, increased DCF fluorescence in living microglial cells was also visualized under a Nikon microscope at 480/530nm corroborating the findings in Fig 4 (see Fig 5).

Fig 4

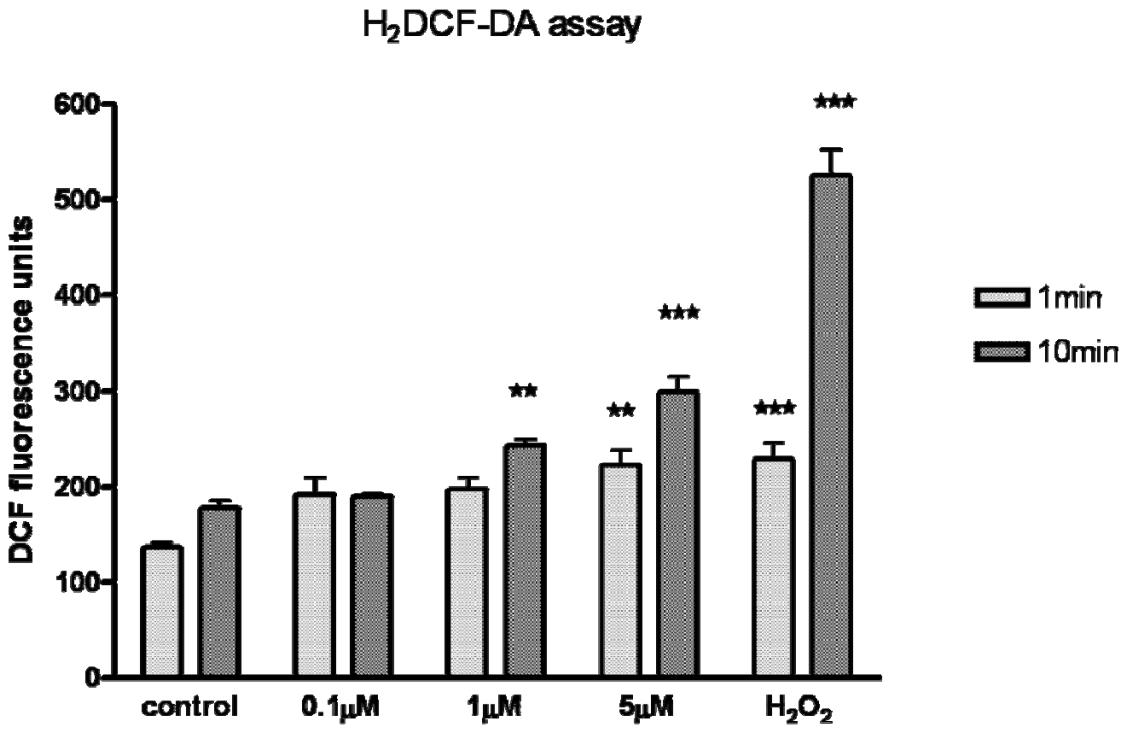

Fig 4. ROS production was measured by DCF fluorescence in microglial cells. Microglial cells were treated with MeHg at the concentrations indicated in the graph. 100μM H_2O_2 was used as a positive control. DCF fluorescence levels were measured after 1 min and 10 min treatment, respectively. The results demonstrated that higher MeHg concentration and longer exposure time led to higher ROS level. Values are expressed as the mean ± SEM derived from six independent experiments. ★ P<0.05, ★★ P<0.01, ★★★ P<0.001

Fig 5A

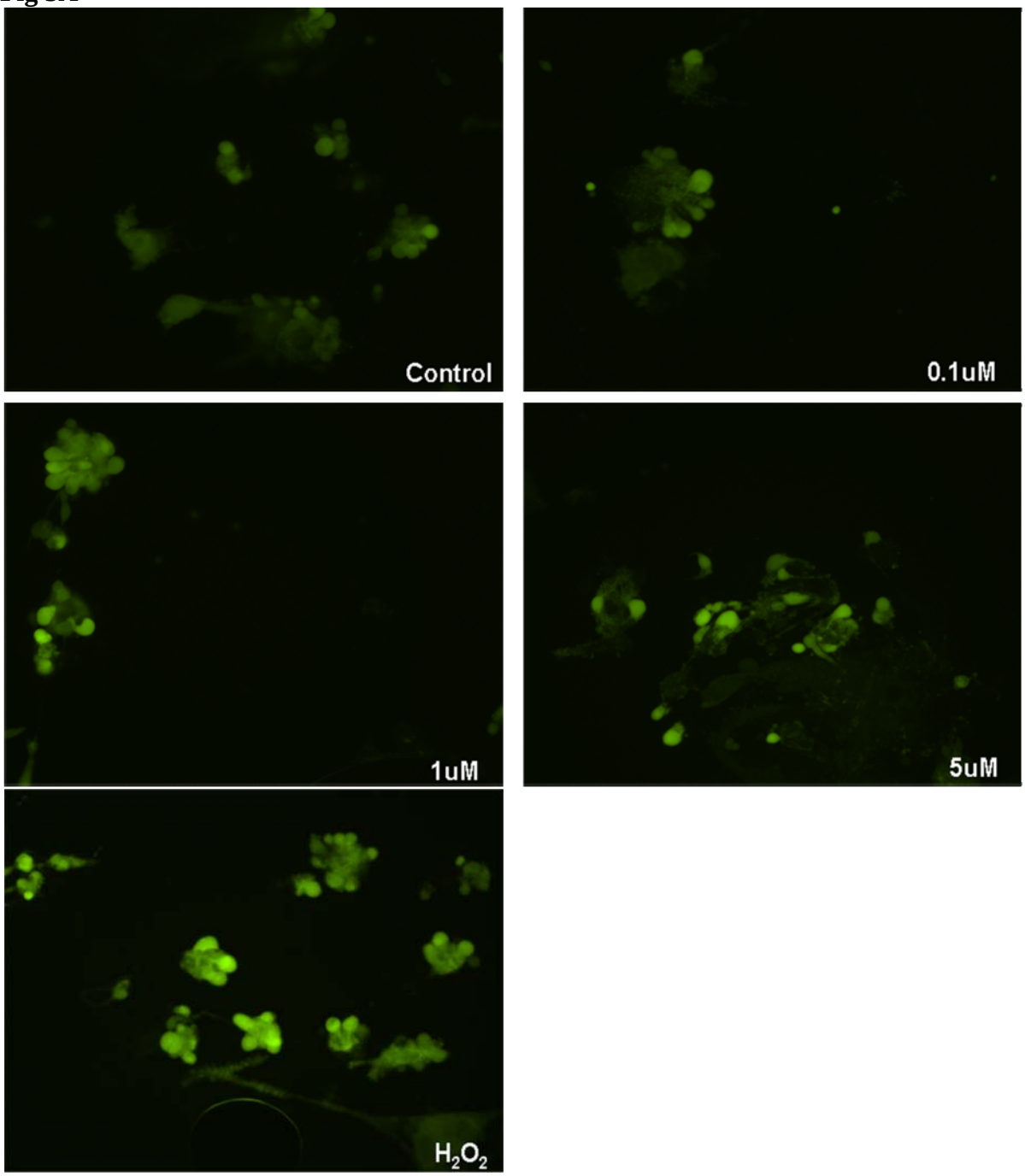

Fig 5B

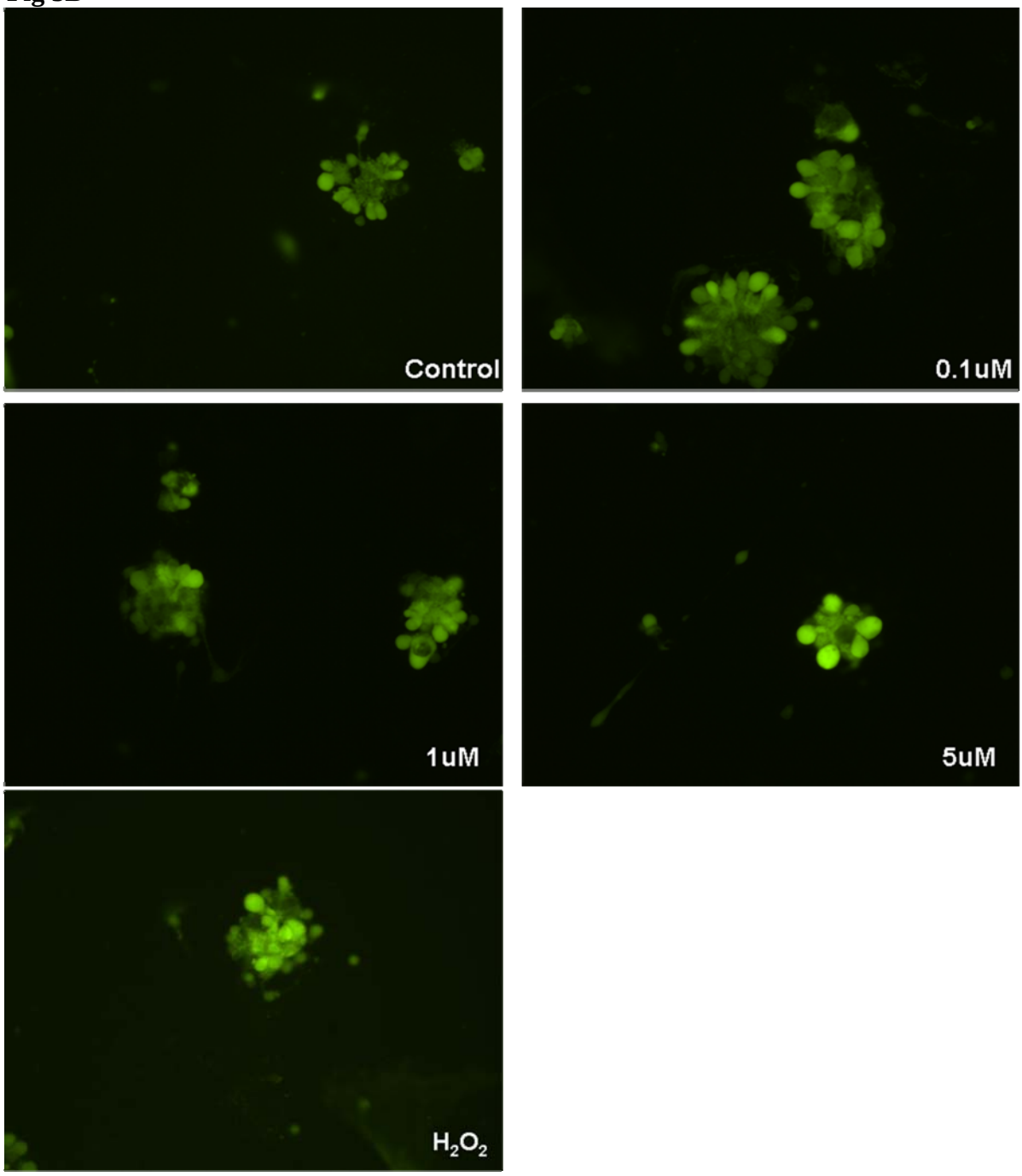

Fig 5. DCF fluorescence levels in living microglial cells were visualized by microscopy. **[5A]**: Microglial cells were treated with MeHg at the concentrations indicated in the figures. 100μM H_2O_2 was used as a positive control for 1 min. **[5B]**: Microglial cells were treated under the same concentrations for 10 min. The intensity of the fluorescence signal was indicative of the intracellular ROS production. Photographs show representative fields observed from three independent experiments.

MeHg Caused Microglial GSH Reduction

GSH can detoxify ROS, resulting in the formation of GSSG, the oxidized form of GSH. Therefore, we sought to determine if microglial ROS generation could cause a decline in the GSH level. As shown in Fig 6, after 0.1 μM MeHg treatment for 1 min, the GSH/GSSG ratio remained statistically unchanged as compared to the control. However, higher concentrations of MeHg (1 and 5 μM) produced a concentration-dependent reduction in the GSH/GSSG ratio (69.01±16.9% and 51.32±20.9% of the control level, respectively). Further reduction in the GSH/GSSG ratio was observed after prolonged MeHg treatment for 10min and 1h in a concentration- and time-dependent manner.

Fig 6

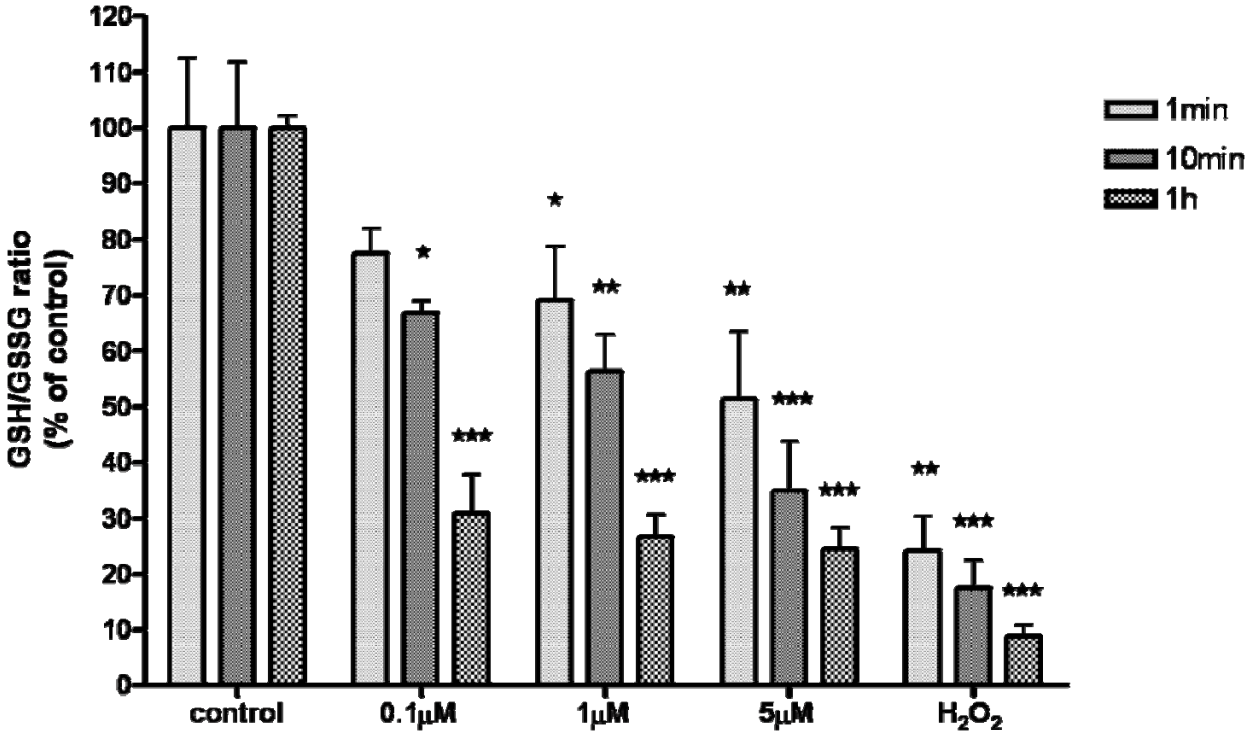

Fig 6. GSH and GSSG levels were measured by HPLC after MeHg treatment. Microglial cells were treated with MeHg at the concentrations indicated in the graph for 1min, 10min and 1h. 100μM H_2O_2 was used as a positive control. The ratios of GSH/GSSG were calculated and the percentages of control were used to plot the graph. Each treatment group was compared to its corresponding control level. The results demonstrated that MeHg caused acute and robust reduction in microglial GSH level in a concentration- and time-dependent manner. Values are expressed as the mean ± SEM derived from three independent experiments. ★ P<0.05, ★★ P<0.01, ★★★ P<0.001

MeHg–induced Oxidative Stress Upregulated Nrf2 and Promoted its Nuclear Translocation

As mentioned before, Nrf2 plays a pivotal role in maintaining redox balance. Therefore, we sought to determine if Nrf2 was altered in microglial cells post MeHg exposure in order to counteract ROS generation. Indeed, the upregulation of the Nrf2 protein level and its nuclear translocation were detected in microglial cells by confocal microscopy after MeHg exposure. As shown in Fig 7, the basal level of Nrf2 (green fluorescence) was low. After 10 min treatment with 0.1 μM MeHg, Nrf2 staining was sparsely detected in the cytosol. In contrast, treatment with 1 or 5 μM MeHg increased Nrf2 staining in both the cytosol and nuclei. Compared to 1 μM MeHg treatment, the staining intensity was greater in 5μM MeHg-treated cells. The co-localization of Nrf2 and propidium iodide (PI) staining in the nuclei indicated the nuclear translocation of Nrf2.

Fig 7

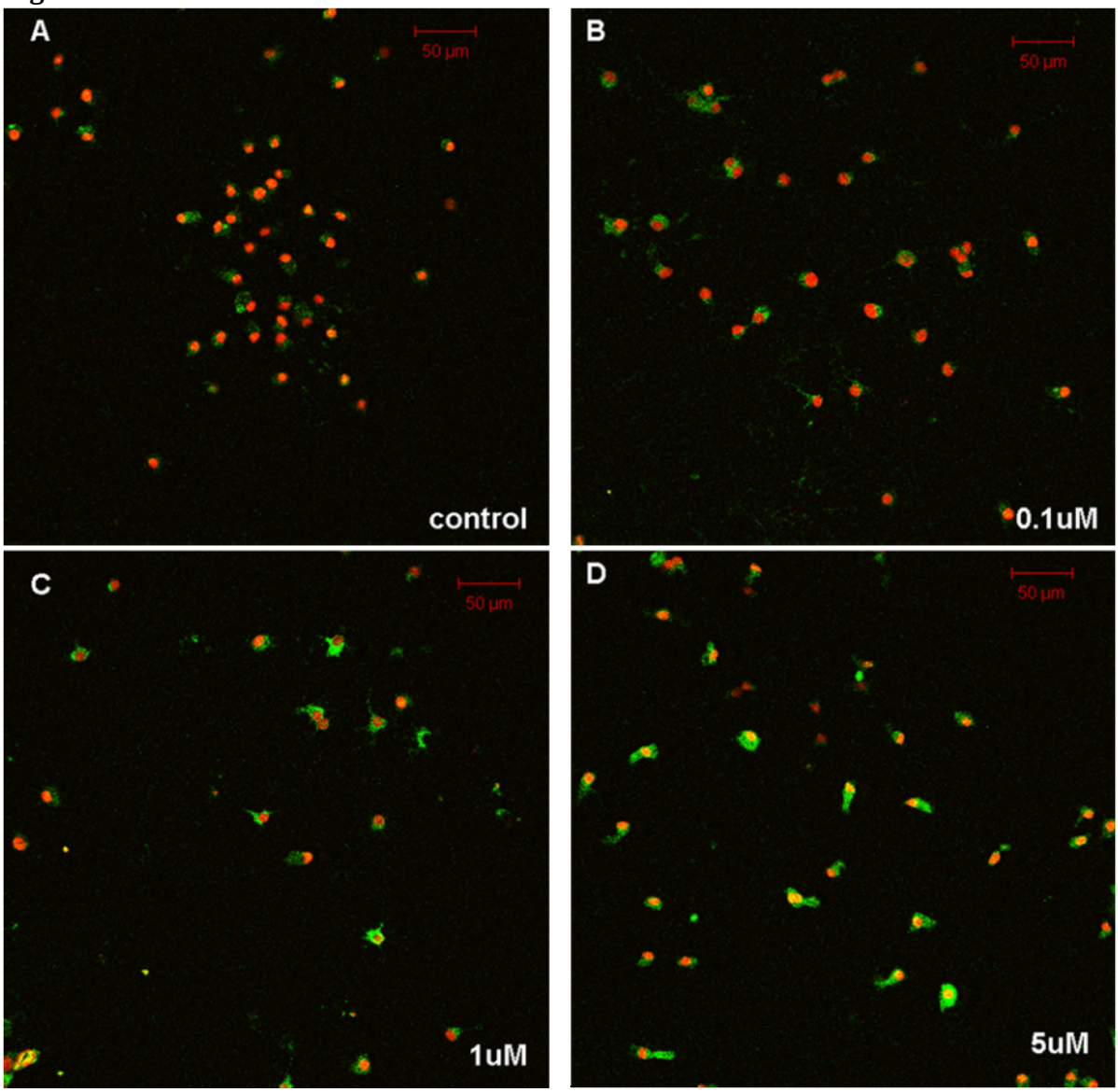

Fig 7. Nrf2 protein level and intracellular localization were assessed by immunostaining. **[A]**: Control group showed minimal Nrf2 (Green) in the cytosol. Cell nuclei were stained by PI (Red). **[B]**: 0.1µM MeHg treatment increased Nrf2 in the cytosol, but not in the nuclei. **[C]**: 1µM MeHg treatment for 10 min increased Nrf2 in both the cytosol and the nuclei. **[D]**: 5µM MeHg treatment for 10 min resulted in a higher level of Nrf2 in both cytosol and nuclei, as compared to 1µM MeHg-treated cells. The yellow color indicates the colocalization of Nrf2 and DNA in microglial nuclei. Photographs show representative fields observed from four independent experiments.

Next, we delineated the dynamic changes in Nrf2 level in both the cytosol and nuclei. As shown in Fig 8, cytosolic Nrf2 protein increased in a concentration-dependent manner after 1 min MeHg treatment. However, under the same conditions, the nuclear Nrf2 protein level remained unchanged. After 10 min, Nrf2 protein level was increased in both the cytosolic and nuclear fractions after 1 and 5 μM MeHg treatments as well as 100 μM H_2O_2 treatment. After 1 h of MeHg treatment, increased Nrf2 accumulated in the nuclei, but not in the cytosol. The quantitative results in Fig 8 show that 1 and 5μM MeHg treatment for 1 hour increased nuclear Nrf2 by 2.60±0.56- ($p<0.05$) and 3.99±1.32- ($p<0.01$) fold over the control value, respectively. The representative western blot bands are shown below the quantified data in Fig 8.

Fig 8

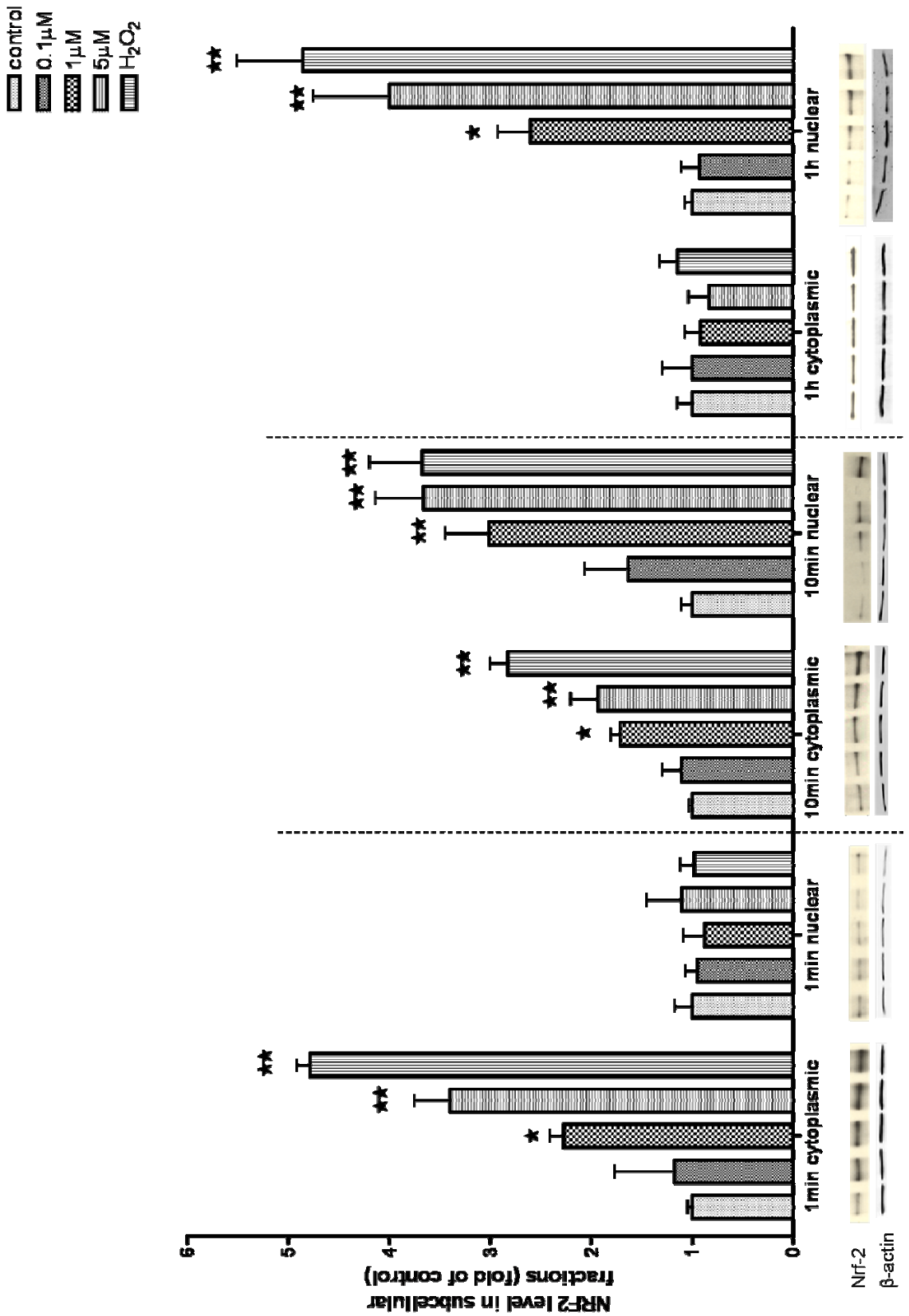
control
0.1μM
1μM
5μM
H2O2
NRF-2 level in subcellular fractions (fold of control)
0
1
2
3
4
5
6
1min cytoplasmic
1min nuclear
10min cytoplasmic
10min nuclear
1h cytoplasmic
1h nuclear
Nrf-2
β-actin

Fig 8. Cytosolic and nuclear fractions of Nrf2 were analyzed by western blot. Microglial cells were treated with MeHg at the concentrations indicated in the graph for 1min, 10min and 1h. 100μM H_2O_2 was used as a positive control.Nrf2 protein levels in cytosolic and nuclear fractions were measured by western. Density of each band was measured by Image J, and the values were normalized with β-Actin. After 1 min MeHg treatment, Nrf2 increased in the cytosolic fraction but not in the nuclear fraction. **A**fter 10 min MeHg treatment, however, Nrf2 increased in both subcellular fractions. **A**fter 1 h MeHg treatment, Nrf2 remained increased in the nuclear fraction, but returned to control level in the cytosol. Values are expressed as the mean ± SEM derived from three independent experiments. ★ P<0.05, ★★ P<0.01, ★★★ P<0.001

MeHg-induced Nrf2 Nuclear Accumulation Upregulated the Transcription of *Ho-1, Nqo1* and *xCT* Genes

After treatment with MeHg for 30 min, the mRNA levels of *Ho-1, Nqo1* and *xCT* were quantified by real-time PCR. The treatment time was based on the observation that Nrf2 was translocated to the nuclei commencing at 10 min post MeHg treatment and remained detectable at 1 hour post treatment. The transcription level of *Ho-1* (Fig 9A) and *Nqo1* (Fig 9B) was upregulated in response to MeHg treatment with 1 and 5 μM. However, *xCT* gene expression was increased by 2.3±1.46-fold over the control value ($p<0.01$) after treatment with the highest concentration of MeHg (5 μM), as shown in Fig 9C.

Fig 9A

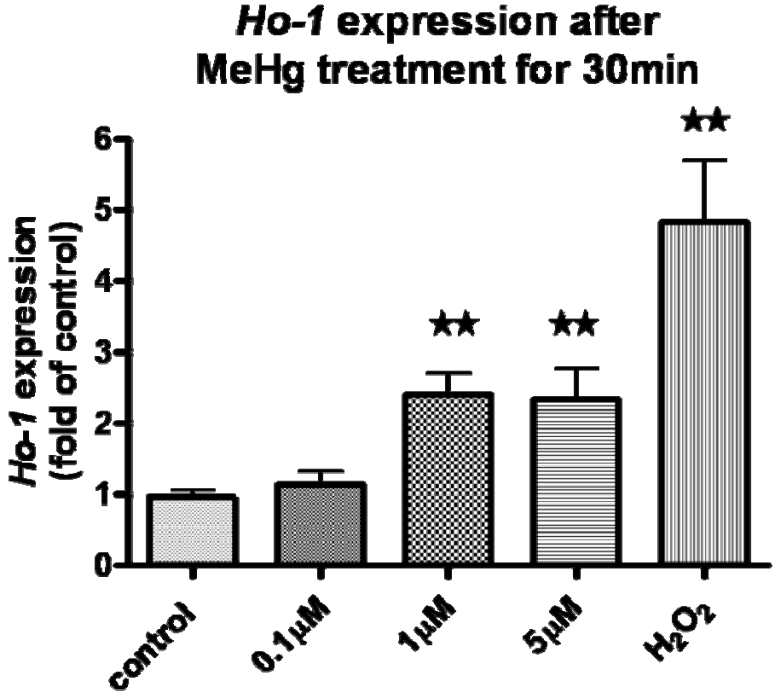
Ho-1 expression after
MeHg treatment for 30min
Ho-1 expression
(fold of control)
0
1
2
3
4
5
6
control
0.1μM
1μM
5μM
H_2O_2

Fig 9B

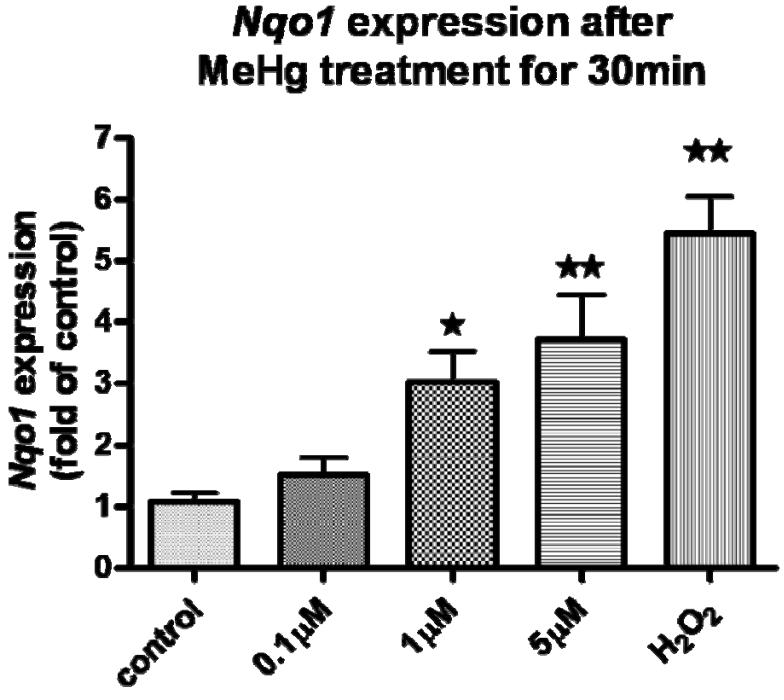
Nqo1 expression after
MeHg treatment for 30min
Nqo1 expression
(fold of control)
0
1
2
3
4
5
6
7
control
0.1μM
1μM
5μM
H_2O_2

Fig 9C

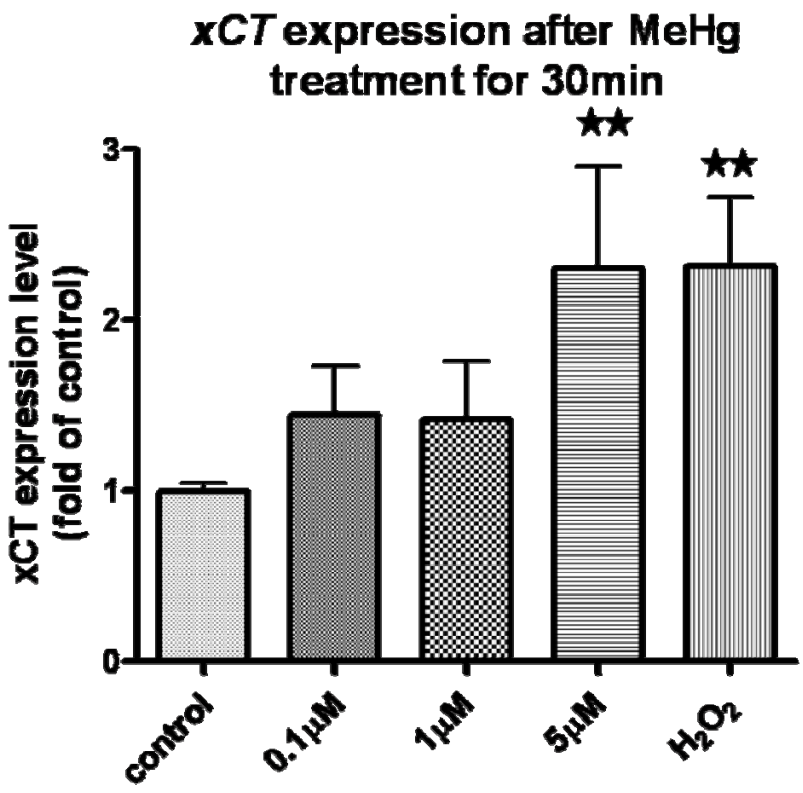

Fig 9. The expression of *Ho-1, Nqo1* and *xCT* were measured by real-time PCR after MeHg treatment. Microglial cells were treated with MeHg at the concentrations indicated in the graph for 30min. 100μM H_2O_2 was used as a positive control. The mRNA levels of *Ho-1* [8A], *Nqo1* [8B] and *xCT* [8C] were measured by real-time PCR. The differences in the average threshold cycle (*ΔCt*) values were determined and normalized to the expression of β-actin. Values are expressed as the mean ± SEM derived from five independent experiments. ★ P<0.05, ★★ P<0.01, ★★★ P<0.001

Next, we carried out an *Nrf2* knockdown experiment to confirm that the transcriptional upregulation of these tested genes is dependent on Nrf2 activity. Compared to the control group, 5 μM MeHg treatment caused a significant increase in the *Ho-1* mRNA levels in both uninfected and scramble shRNA-infected microglial cells ($p<0.05$). In contrast, the Nrf2 knockdown group did not demonstrate an increased *Ho-1* mRNA level after the same treatment as compared to the control level ($p>0.05$) (Fig 10A). Fig 10B shows that no significant increase in *Nqo1* mRNA level was present in the *Nrf2* knockdown group after 5μM MeHg, in contrast to uninfected or scramble shRNA-treated groups. Similar changes in *xCT* mRNA level were also observed after *Nrf2* knockdown (Fig 10C). Therefore, the upregulation of *Ho-1*, *Nqo1* and *xCT* transcription upon MeHg treatment is dependent upon nuclear Nrf2 activity.

Fig 10A

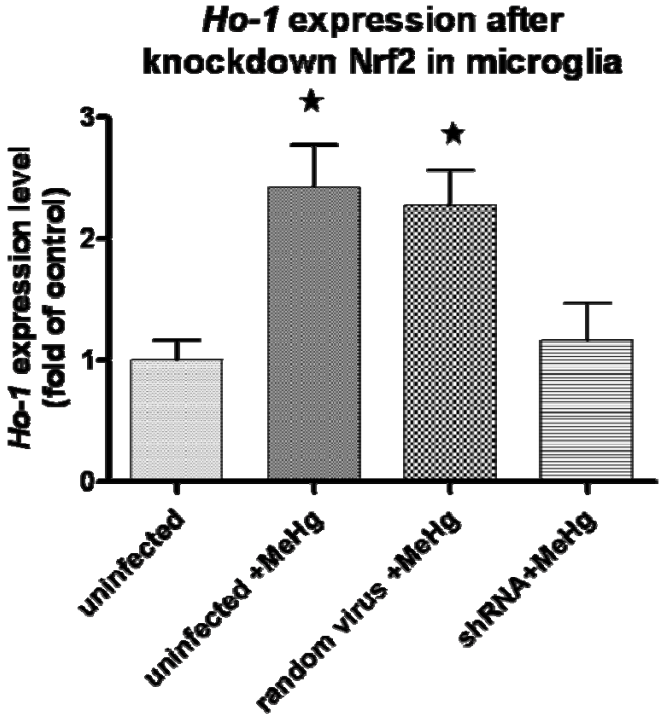

Fig 10B

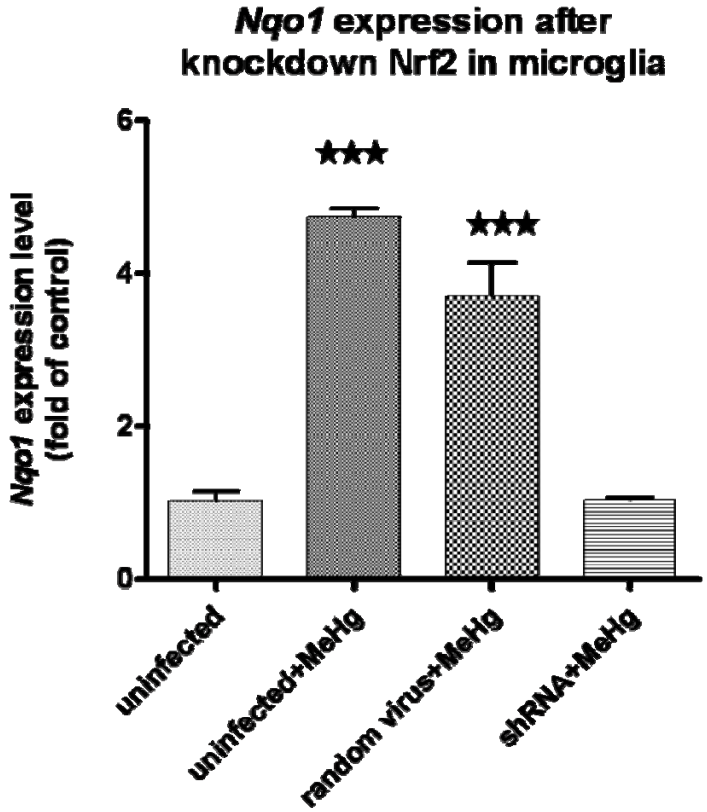

Fig 10C

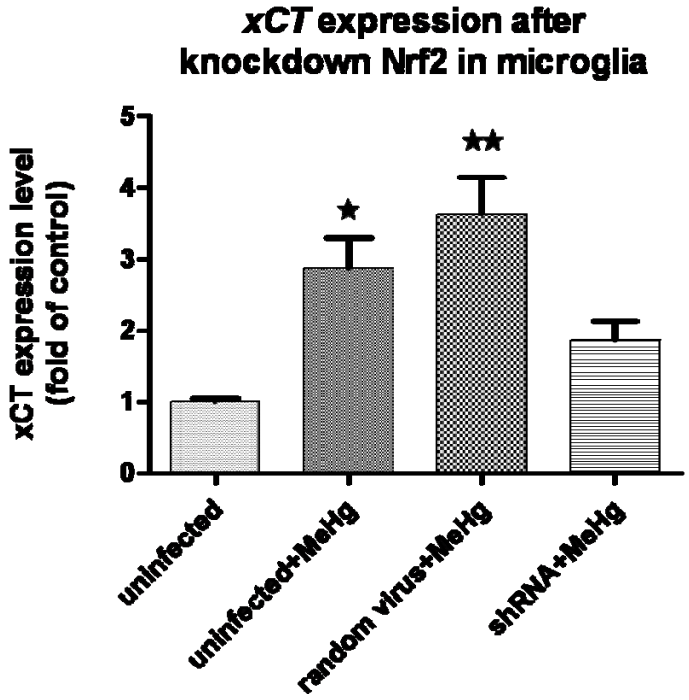

Fig 10. The effects of *Nrf2* knockdown on MeHg-induced *Ho-1, Nqo1* and *xCT* expression were analyzed by real-time PCR. Primary microglial cells were first infected with lentivirus as indicated for 24 hours and then treated with 5μM MeHg for 30 min. Then, the mRNA levels of *Ho-1* [9A], *Nqo1* [9B] and *xCT* [9C] were measured by real-time PCR. The difference in the average threshold cycle (*ΔCt*) values was determined and normalized to the expression of β-actin. The uninfected and untreated microglial cells were used to determine the basal gene expression levels. The uninfected cells treated with 5μM MeHg for 30min served as a positive control. The random virus with no known gene target was also used to infect microglial cells in order to reveal any possible effects of lentiviral backbone on gene expression. Microglial cells treated *Nrf2* specific shRNA showed no significant increase in downstream gene expression compared to basal levels after 5uM MeHg treatment for 30min. Values are expressed as the mean ± SEM derived from three independent experiments. ★ P<0.05, ★★ P<0.01, ★★★ P<0.001

Nrf2 Protected Microglial Cells against MeHg Toxicity

To further evaluate the cytoprotective function of Nrf2 against MeHg-induced cell death, we assessed cell viability upon MeHg treatment under *Nrf2* knockdown condition. As shown in Fig 11A, compared to uninfected microglial cells in the absence of MeHg exposure, both uninfected cells and random virus infected cells treated with 5μM MeHg for 6h demonstrated a significant decrease in MTT absorbance; , knockdown of *Nrf2* further decreased MTT absorbance after the same treatment ($p<0.001$). Notably, compared to uninfected cells post MeHg treatment, knockdown of *Nrf2* caused a significant decrease in MTT absorbance ($p<0.001$, compare 2nd column with 4th column in Fig 11A). Consistent with the MTT assay results, the *Nrf2* knockdown group demonstrated the highest absorbance after 5μM MeHg treatment for 6h in the LDH assay (Fig 11B). Furthermore, compared to uninfected microglial cells treated with MeHg, *Nrf2* knockdown of microglia displayed increased LDH absorbance, indicating decreased viability in *Nrf2* deficienct cells ($p< 0.001$, compare 2nd column with 4th column of Fig 11B).

Fig 11 A

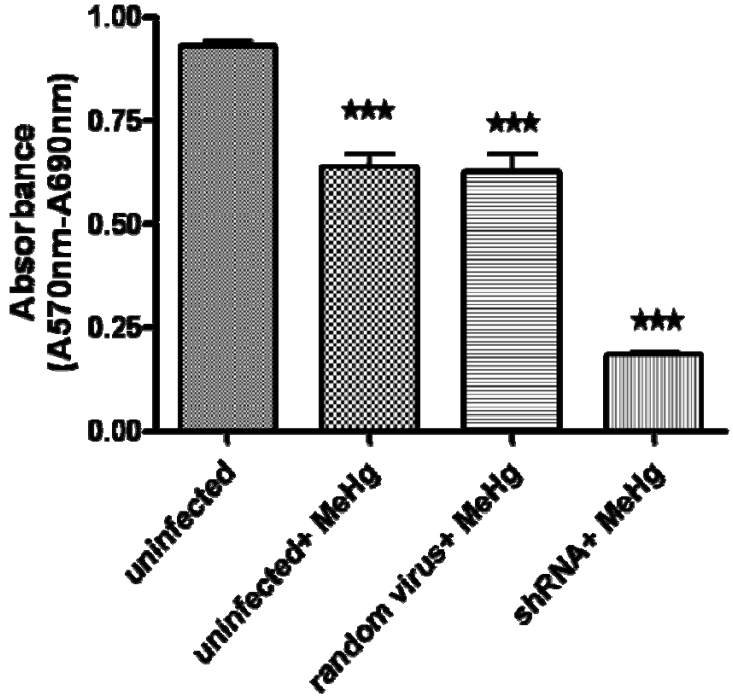

Fig 11 B

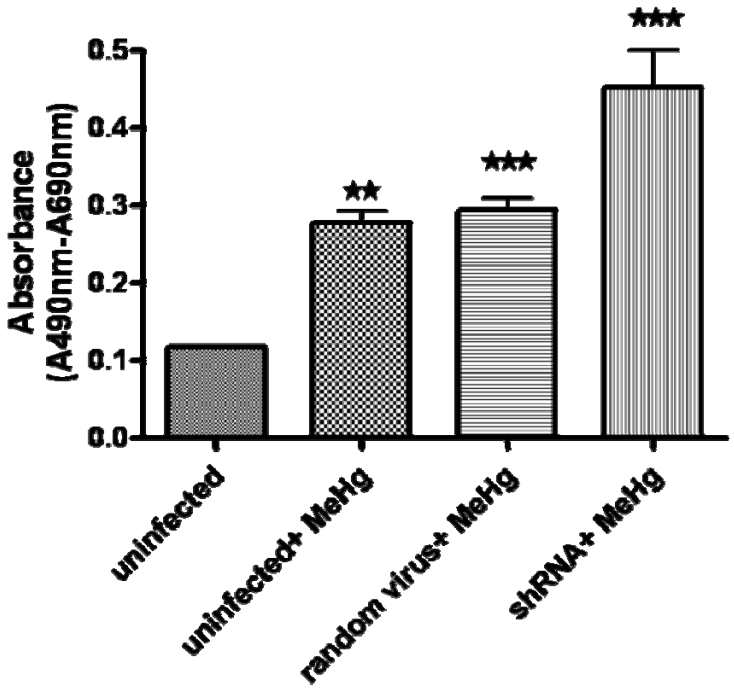

Fig 11. The effects of *Nrf2* knockdown on microglial cell viability were assessed by MTT and LDH assay. Primary microglial cells were first infected with lentivirus for 24 hours and then treated with 5μM MeHg for 6h. The uninfected microglial cells without MeHg exposure were used to measure the maximal cell viability. The uninfected cells treated with 5μM MeHg for 6h served as a positive control for cell death. The random virus with no known gene target was also used to infect microglial cells in order to reveal any possible cytotoxicity effects of the lentiviral backbone **[A]:** Result of MTT assay showed lowest absorbance in *Nrf2* knockdown cells, indicative of lowest cell viability **[B]:** Result of LDH assay using culture media from the same treatment groups demonstrated the highest absorbance in *Nrf2* knockdown cells, which indicated the highest level of LDH released from damaged microglial cells to culture media. Values are expressed as the mean ± SEM derived from four independent experiments. ★ P<0.05, ★★ P<0.01, ★★★ P<0.001

Discussion

To our knowledge, this is the first study to investigate the response of primary microglial cells to acute MeHg exposure. We have demonstrated that MeHg leads to rapid ROS generation and GSH depletion commencing at one minute post MeHg exposure, well before changes in astrocytes or neurons are observed (data not shown). In response, microglial Nrf2 is upregulated and undergoes nuclear translocation to activate the expression of downstream genes such as *Ho-1, Nqo1* and *xCT*. Our data suggest that microglial cells are the first line of cellular defense against MeHg toxicity in the CNS.

Previous studies have reported an increase in ROS in microglial cells after prolonged MeHg treatment at high concentrations [143, 144, 155]. However, these studies do not capture the acute microglial response to lower concentrations of MeHg as detected in early stage of Minamata disease patients. Here, we have revealed that 5μM MeHg exposures cause a significant increase in ROS generation in primary microglial cells commencing at one minute post MeHg exposure (Fig 4, 5). Similar acute ROS generation in microglial cells was also observed after TiO2 exposure [156]. Although increased generation of ROS also occurs in neurons [157, 158] and astrocytes [107, 153], it is only detected after much longer exposure to MeHg.

GSH is used to detoxify ROS and itself is converted to the oxidized form, GSSG. In response to MeHg, microglial ROS is increased (Fig 4,5) and, correspondingly, the GSH/GSSG ratio is decreased (Fig 6). Previous studies have established the cytoprotective effects of GSH in MeHg-induced toxicity [159, 160]. GSH binds to Hg compounds via its sulfhydryl groups, and the conjugated products are actively pumped out of the cells by multidrug resistance proteins

(MRPs), leading to the decrease in intracellular Hg and its toxicity [161]. Our data have also revealed that a lower intracellular GSH level is correlated with greater microglial death. For example, treatment with 5μM MeHg causes maximal reduction in GSH levels (Fig 6) as well as maximal cell death (Fig 3). In agreement with our observations, Miura and Clarkson reported a significant inverse correlation between the GSH level and MeHg toxicity using a MeHg-resistant rat pheochromocytoma PC12 cell line. The levels of GSH in these resistant cells were four-fold higher than in the nonresistant cells, which led to greater efflux and less intracellular retention of MeHg [162, 163]. Furthermore, microglial GSH levels are only 25% of those in astrocytes (data not shown), which likely reflects their diminished capability to buffer MeHg-induced ROS generation. In addition, lower GSH levels in microglial cells may lead to reduced MeHg efflux and increased intracellular Hg levels. This may explain previous findings of the earliest and highest accumulation of Hg deposits in microglial cells in the rat brain [164] and non-human primates [102].

Intracellular ROS generation is the pivotal event in regulating Nrf2 levels [153]. As the major regulator of the antioxidant system in cells, Nrf2 protein levels in microglia increased rapidly within 1 min of MeHg treatment (Fig 8). The increase in Nrf2 (Fig 8) protein levels was paralleled by the MeHg-induced increase of ROS (Fig 4, 5), as well as the decrease in GSH (Fig 6). We also observed Nrf2 nuclear translocation commencing at 10 min post MeHg exposure. Our data corroborate Li's model supporting a role for oxidative stress in disrupting the interaction between Nrf2 and Keap1, which leads to decreased rate of proteasomal degradation of Nrf2 in the cytosolic fraction. This model explains why the increase of cytosolic Nrf2 was detected as early as 1 min post MeHg exposure [133]. Based on the fact that Nrf2 activation was

not observed in primary astrocytes until 90 min after MeHg treatment at the same concentration [153], our results support the notion that microglia are the first glial cell type to respond to MeHg [165].

We observed increased microglial death upon *Nrf2* knockdown with the shRNA approach (Fig 11). Consistent with our result, Toyama et al. reported that primary mouse hepatocytes isolated from *Nrf2*- deficient mice were highly susceptible to MeHg-induced cytotoxicity, and *Nrf2* overexpression attenuated MeHg-induced cytotoxicity in SH-SY5Y neuroblastoma cells [166]. Nuclear translocation of Nrf2 is critical for attenuation of oxidative stress. Once in the nuclei, Nrf2 orchestrates the expression of *Ho-1, Nqo1* and *xCT*, all of which detoxify xenobiotics and endogenous reactive electrophiles. Previous studies have also confirmed the critical function of Nrf2 in regulating the expression of these genes in other cell types. For example, in human lumphoma cells, gallium nitrate upregulated the *Ho-1* mRNA level as a result of Nrf2 activation [153, 167]. Similarly, Nrf2 in renal epithelial cells upregulated the *Nqo1* reporter construct after exposure to hypoxia/reoxygenation [168].

Upon activation, microglial cells secrete numerous bioactive factors such as interleukins, prostaglandin, TNF-α and nitric oxide (NO). The nature of the released factors appears to be dependent on the nature of the causative agents. For example, lipopolysaccharides **(**LPS) and trimethyltin (TMT) were reported to increase the microglial release of IL-6, TNF-α and NO [143]. In contrast, MeHg leads only to IL-6 release, leaving TNF-α and NO unchanged [155]. As the first cell type to respond to MeHg, the microglial response to this metal may influence other cell types via the secretion of IL-6. Current literature suggests that IL-6 has differential effects on

different cell types. For example, microglial IL-6 induces astrogliosis, associated with MeHg-induced microglial clusters in 3D brain cell cultures. In contrast, neurons were decreased in the vicinity of such clusters [143]. Interestingly, as a proinflammatory factor, IL-6 may have a neuroprotective function. IL-6 co-administered with MeHg prevented MeHg-induced degeneration of the neuronal cytoskeleton [143]. Similar protective effects of IL-6 against the toxic effects of glutamate have also been previously described [169] and MPP+ [170]. Furthermore, Nrf2 has been shown to regulate the production of microglial biofactors [171]. Thus, in future studies, it is essential to address the functions of microglial IL-6 and the regulatory effect of Nrf2 in response to MeHg treatment.

On the other hand, microglial activity can be modulated by other cell types in the brain. Neurons can increase microglial reactivity [172]. Co-culturing with neurons leads microglial cells to differentiate to a macrophagic state, which suggests certain diffusible factors released from neurons could result in the activation of microglial cells [173]. In contrast to neurons, astrocytes appear to dampen microglial reaction. The current study was performed in purified microglial cells after acute MeHg treatment, given the cross-talk between the various cell types. It is imperative to extend the findings regarding MeHg's function on microglial cells to more complex cellular networks, such as co-cultures and, ultimately, to in vivo preparations.

In summary, our work demonstrates that microglial cells are the first CNS cell type to respond to MeHg. Future studies on either the attenuation of intracellular ROS generation or the upregulation of GSH and Nrf2 in microglial cells could afford potential therapeutic value and

more efficacious treatment techniques and protocols to address and ameliorate MeHg poisoning at early stages of exposure.

CHAPTER III

COMPARATIVE STUDY ON THE RESPONSE OF RAT PRIMARY ASTROCYTES AND MICROGLIAL CELLS TO METHYLMERCURY TOXICITY

This chapter has been published as an article under the title as

"Comparative study on the response of rat primary astrocytes and microglia to methylmercury toxicity"

In Glia. 2011 May;59(5):810-20

Summary

As two major glial cell types found in the brain, astrocytes and microglial cells play pivotal and yet differential roles in maintaining normal brain functions. Even though both cell types been implicated as major targets of methylmercury (MeHg), their sensitivity and adaptive response to MeHg can vary given their distinctive properties under physiological conditions. This study was carried out to compare the response of astrocytes with microglial cells upon MeHg treatment, in order to delineate their different roles in mediating MeHg neurotoxicity. The study addressed the effects of MeHg on their cell viability, reactive oxygen species (ROS) generation and glutathione (GSH) levels. Results showed that microglial cells are more sensitive than astrocytes to MeHg treatment, consistent with higher mercury concentration, but lower basal GSH level in microglial cells, compared to astrocytes. Furthermore, NF-E2-related factor 2 (Nrf2), a major regulator of intracellular antioxidant response and its downstream genes were upregulated in both cells, but with notably different kinetics. In summary, microglial cells and astrocytes exhibit distinct

sensitivity to MeHg treatment, which contributes to their differential temporal adaptive responses to MeHg toxicity.

Key words: methylmercury, microglial cells, astrocytes, reactive oxygen species, glutathione, Nrf2.

Introduction

Mercury, a global pollutant, is methylated to MeHg in the aquatic environment by sulfate-reducing bacteria [174]. It is then rapidly taken up by living organisms and biomagnified through the food chain, reaching concentrations 10,000-100,000 times greater in fish than in the water [175]. MeHg accumulates at higher concentration in fish-eating populations [176, 177]. Congenital Minamata disease is the most well-documented neurological disorder caused by MeHg poisoning [178].

MeHg readily crosses the blood-brain barrier via the L-type large neutral amino acid transporter and distributes in all brain cell types [32]. The majority of studies on MeHg-induced central nervous system (CNS) damage focused on its effects on neurons [121, 179]. Recently, the mechanisms of MeHg neurotoxicity have been extended to other CNS cell types, predominately glial cells [180, 181]. Glial cells, including astrocytes and microglial cells, are not electrically excitable [182], however, they have diverse and important functions, such as providing support and nutrition [1], maintaining CNS homeostasis [103], removing pathogens [183], inducing neuronal differentiation [184] and mediating CNS immune responsiveness [185, 186]. Dysfunction of glial cells has been reported to contribute to MeHg-induced brain damage [107,

187]. MeHg causes ROS generation in astrocytes due to the disruption of cellular redox homeostasis [107]. Furthermore, MeHg inhibits astrocytic glutamate uptake, while stimulating glutamate efflux [90], which result in excessive glutamate in the extracelluar milieu and subsequent neuronal excitotoxicity. Microglial cells are the first known activated cells under various pathological conditions, such as inflammation, infection, trauma and degenerative diseases [165]. This activation and the consequent free radical generation were also observed after MeHg treatment [144, 187-189]. In the active state, microglial cells release proinflammatory cytokines, including interleukin 6 (IL-6), tumor necrosis factor-α (TNF-α) and prostaglandin E2 (PGE2), all of which influence neighboring cells [190]. Given the fact that glial cells are critical in maintaining CNS homeostasis and different glial cells have distinct functions, it was deemed important to test the hypothesis that glial subtypes will respond in distinct temporal manner in response to MeHg treatment.

As a key protective factor against oxidative stress, Nrf-2 was found to be upregulated in both astrocytes and microglial cells upon MeHg treatment [153, 187]. Nrf2 is bound to Kelch-like ECH-associating protein 1 (Keap1) in the cytoplasm under physiological conditions [129]. The interaction between Nrf2 and Keap1 is disrupted upon oxidative stress and the unbound Nrf2 is more resistant to proteasomal degradation [191]. Accordingly, *de novo* Nrf2 is built up within the cells, leading to increased translocation of Nrf2 into nuclei [133]. Once in the nucleus, Nrf2 interacts with antioxidant response element (ARE) to initiate the transcription of target genes, of which the protein products are used to detoxify xenobiotics and endogenous reactive electrophiles [136-138]. Accordingly, the study was designed to study differences in the kinetics

of Nrf2 activation in glial cell subtypes in order to gain better understanding on their respective roles in mediating adaptive responses to MeHg treatment.

Although some previous studies have assessed the effects of MeHg on microglial cells and astrocytes [107, 187], they did not systemically compare the responses between astrocytes and microglial cells after MeHg treatment. We hypothesized that even though common factors and pathways are shared by astrocytes and microglial cells in response to MeHg toxicity, their sensitivity and regulation kinetics might differ, therefore allowing astrocytes and microglial cells to play different roles in mediating MeHg toxicity. Our data supported this hypothesis by showing that microglial cells are more sensitive than astrocytes to MeHg as measured by cell viability, reactive oxygen species (ROS) generation, glutathione depletion and Nrf2 activation.

Experiment Procedures

Cell Culture

Primary astrocytes and microglial cells were isolated from postnatal day-1 neonatal Sprague-Dawley rats, according to a published protocol [187, 192]. The mixed glial cell culture was maintained in minimum essential medium (MEM) (Invitrogen, Carlsbad, CA, USA), supplemented with 5% heat-inactivated fetal bovine serum (Hyclone, South Logan, Utah, USA) and 5% horse serum (Invitrogen, Carlsbad, CA, USA). After two weeks in culture, microglial cells and astrocytes were separated by gentle shaking for 20 min at room temperature. Cells were then plated in 6-well plates and cultured at 37°C in a 95% air/5% CO_2 incubator.

MTT Assay and LDH Assay

The cytotoxic effects of MeHg were evaluated by 3-[4,5- dimethylthiazol-2-yl]-2,5 diphenyltetrazolium bromide (MTT) assay (Sigma *in vitro* Toxicology Assay Kit, MTT based, M-5655, St. Louis, MO, USA) and lactate dehydrogenase (LDH) assay. 10X MTT stocking solution was freshly prepared by reconstituting 15mg stock MTT reagent in 3ml of OPTI- MEM culture media (Invitrogen, Carlsbad, CA, USA) in the absence of phenol red. After MeHg treatment, 10X MTT stocking solution was directly added to each well at a final concentration of 0.5 mg/ml. The formazan crystal precipitates were dissolved by adding an equal volume of MTT solubilization solution (Sigma, M-8910, St. Louis, MO, USA) and gently shaking for 20 min. Its absorbance at 570nm was measured and the background absorbance at 690nm was also measured and subtracted out. Cell viability was expressed as the 570nm-690nm ratio over control. Culture media (50µl) after treatment were collected for LDH analysis. Fresh assay mixture 100µl (L2402, Sigma, St. Louis, MO, USA) was added to the culture media and incubated at room temperature for 30 min in dark. The reaction was terminated by adding 1/10 volume of 1N HCL. The absorbance at 490nm was measured and the background absorbance at 690nm was subtracted out. Cytotoxicity was expressed as 490nm-690nm ratio over control.

Detection of intracellular ROS formation

Astrocytes and microglial cells were pre-incubated with dichlorodihydrofluorescein diacetate acetyl ester (H2DCFDA) (C6827, Invitrogen, Carlsbad, CA, USA) at a concentration of 25 µM for 30 min at 37°C. MeHg was added without aspirating H2DCFDA solution. After treatment as indicated, cells were washed with 4°C PBS twice and then precipitated at 400x g. The cell pellets were dissolved in 1% Triton X- 100 (Promega, Madison, Wisconsin, USA). Fluorescence was

measured at 530nm (excitation of 480nm) by SpectraMax M5 (Molecular Devices, Sunnyvale, CA, USA). The fluorescence units were plotted in the graph.

Measurement of GSH

The intracellular GSH concentration was measured by high-performance liquid chromatography (HPLC) as previously described [153, 187]. Cells were derivatized with iodoacetic acid and dansyl chloride. HPLC analysis was carried out with a propylamine column (YMC Pack, NH2, Waters, Milford, MA, USA) and an automated HPLC system (Alliance 2695, Waters Corporation, Milford, MA, USA). GSH and GSSG concentrations were normalized to the protein concentration of the samples analyzed with the BCA Protein Assay Reagent (23225, Thermo, Rockford, IL, USA).

Immunocytochemistry

Astrocytes and microglial cells were cultured on coverslips coated with poly-L-lysine. Immunocytochemistry was performed using the published protocol [187]. Cells were incubated for 1h with 1:200 rabbit anti-Nrf2 (Abcam 31136, Cambridge, MA, USA) before incubation with 1:400 secondary antibody, donkey anti-rabbit IgG conjugated with fluorescein isothiocyanate FITC (Millipore, AP182F, Billerica, MA). Coverslips were mounted with Vectashield Mounting Medium with Propidium Iodide (PI) (VECTOR, H-1300, Burlingame, CA, USA). The fluorescence signal was detected using a Zeiss confocal microscope (LSM 510, Zeiss, Dublin, CA, USA) at the following settings: detector gain 900, amplifier offset -0.085 and pinhole 98. The propidium iodide (PI) signal was detected with the following settings: detector gain 844, amplifier offset -0.068 and pinhole 110.

Western Blot Analysis

Total cellular proteins were prepared in radioimmunoprecipitation assay (RIPA, R0278-50ML, Sigma, St. Louis, MO, USA) buffer with protease inhibitor (Complete Protease Inhibitor Cocktail, 04693116001, Roche, Indianapolis, IN, USA) and Halt Phosphatase Inhibitor Cocktails (78427, Thermo Scientific, Rockford, IL 61105). Western blot analysis was conducted with primary antibodies, rabbit-anti Nrf2 (1:400) (sc- 722, Santa Cruz Biotechnology, Santa Cruz, CA, USA) and mouse anti β-actin (1:2,000) (A1978, Sigma, St. Louis, MO, USA). Secondary antibodies were donkey anti-rabbit IgG conjugated with horseradish peroxidase (HPR) (1:1000) (W4011, Promega, Madison, Wisconsin, USA) and donkey anti-mouse IgG conjugated with horseradish HPR (1:4,000) (W4021, Promega, Madison, Wisconsin, USA). The density of the Nrf2- specific bands was normalized to β-actin.

Quantitative Real-Time PCR

The transcription levels of heme oxygenase 1 (*Ho1*), NAD(P)H dehydrogenase, quinone 1 (*Nqo1*) and x- C-type transporter (*xCT*) were measured by real-time PCR using the Universal Probe Library (Roche, Indianapolis, IN, USA). Table 1 lists the primer sequences and UPL probes. Average threshold cycle (*ΔCt*) values were used to determine the relative difference between control and treated samples. All data were normalized to β-actin levels.

Table 1

Primer Sequences and UPL Probes Used for Real-time PCR Analysis			
Gene	**Forward (5'-3')**	**Backward (5'-3')**	**UPL probe**
Ho-1	5'-GTC AGG TGT CCA GGG AAG G-3'	5'-CTC TTC CAG GGC CGT ATA GA-3'	#9
Nqo1	5'-AGC GCT TGA CAC TAC GAT CC-3'	5'-CAA TCA GGG CTC TTC TCA CC-3'	#50
xCT	5'-TCC ATG AAC GGT GGT GTG T-3'	5'- CCC TTC TCG AGA TGC AAC AT-3'	#80
β-actin	5'- CCC GCG AGT ACA ACC TTC T- 3'	5'- CGT CAT CCA TGG CGA ACT- 3'	#17

Nrf2 Knockdown by Small Hairpin RNA (shRNA)

At ~50-60% confluence, primary astrocytes and microglial cells were infected with 15µl lentiviral particles containing $1X10^6$ infectious units of virus (IFU) for 24 hours before MeHg treatment. The lentiviral particles containing expression constructs of specific shRNA against Nrf2 (sc-37049-V, Santa Cruz Biotechnology, Santa Cruz, CA, USA) were used to knock down Nrf2. Lentiviral particles containing scrambled shRNA sequence with no known gene target (sc-108080, Santa Cruz Biotechnology, Santa Cruz, CA, USA) were used as the negative control.

Measurement of Intracellular Mercury Level

^{14}C-MeHg (82 nCi/µg Hg, American Radiolabeled Chemical, Inc., St. Louis, MO) was added into regular MeHg at the volume ratio of 1:1,000. Cells were maintained in 6-well plates and treated with radiolabeled ^{14}C-MeHg/"cold" MeHg mixture at concentrations indicated. At the end of the treatments, cells were washed three times with a cold mannitol buffer [290 mM mannitol, 10 mM Tris nitrate and 0.5 mM calcium nitrate ($Ca(NO_3)_2$] and lysed with 1M sodium hydroxide. Cell lysates (750 µl) were combined with 75 µl 10 M HCl, and radioactivity was measured in a liquid scintillation counter (Tri-Carb 2900TR, Perkin Elmer Life Science). For each well, radioactivity was corrected for cellular protein content determined by the BCA assay.

Statistical analysis

All results were expressed as means ± standard errors. Unless otherwise specified, differences among treatment groups were analyzed by one-way analysis of variance (ANOVA), followed by Bonferroni's *post hoc* test. Statistical significance was set at $p<0.05$. All experiments were

repeated with at least three independently isolated cell cultures, and data analysis was carried out with GraphPad Prism (GraphPad Software, San Diego, CA, USA).

Results

Microglial Cells Are More Vulnerable to MeHg Compared with Astrocytes

As a first step, we compared the vulnerability of primary microglial cells and astrocytes in response to MeHg. Either cell type was treated for 6 h with MeHg and viability was determined by the MTT and LDH assays. The absorbance of MTT (570nm) is positively correlated with cell viability [193, 194].

As shown in Fig.12, MeHg (≥ 1μM) caused a significant decrease ($p<0.05$) in microglial cell viability. In contrast, the same treatment in astrocytes did not lead to significant cell death. A positive control, 100μM H_2O_2 treatment reduced cell viability to 24±0.08% ($p<0.001$) and 66.8±5.3% ($p<0.001$) of controls in microglia and astrocytes, respectively. The absorbance of LDH (490nm) is reversely correlated with cell viability [195]. Microglial LDH absorbance was significantly increased after 1μM ($p<0.01$) and 5μM ($p<0.001$) MeHg treatment for 6h, while MeHg (up to 5μM) did not cause a significant increase in LDH absorbance in astrocytes (Fig.13). These results are consistent with the MTT assay results (Fig.12) reflecting increased rate of cell death in microglia *vs*. astcocytes.

Fig 12

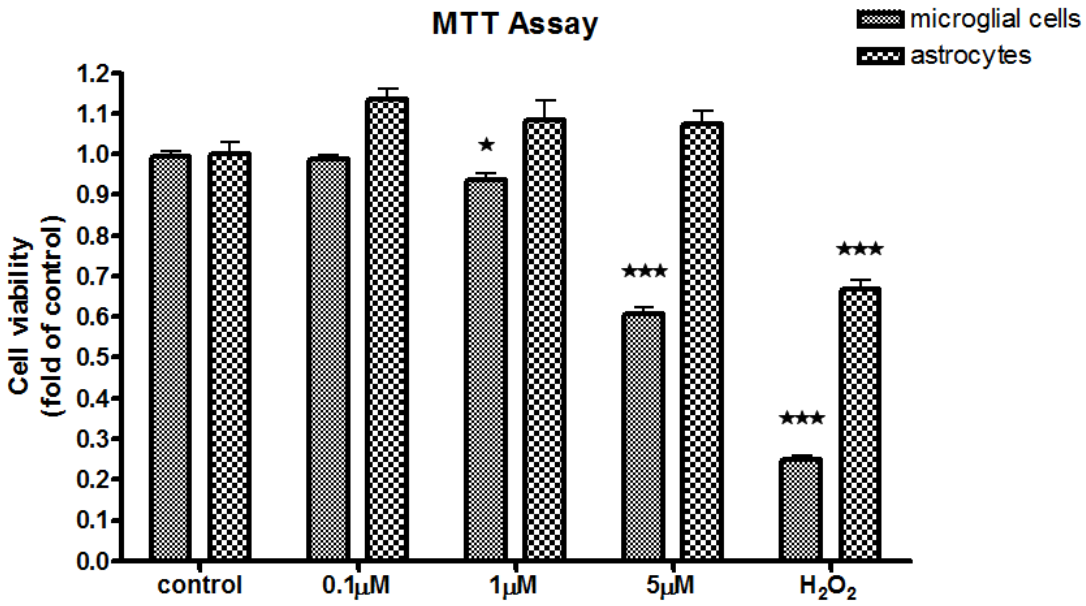

Fig12. MTT assay result of astrocytes and microglial cells. Effects of MeHg cytotoxicity on astrocytes and microglial cells were measured by MTT assay after MeHg treatment for 6 hours. MeHg at 1 and 5μM caused a decrease in cell viability in microglial cells. In contrast, MeHg up to 5μM did not decrease astrocyte viability. 100μM H_2O_2 was used as a positive control. Values are expressed as the mean±SEM derived from three independent experiments.

Fig 13

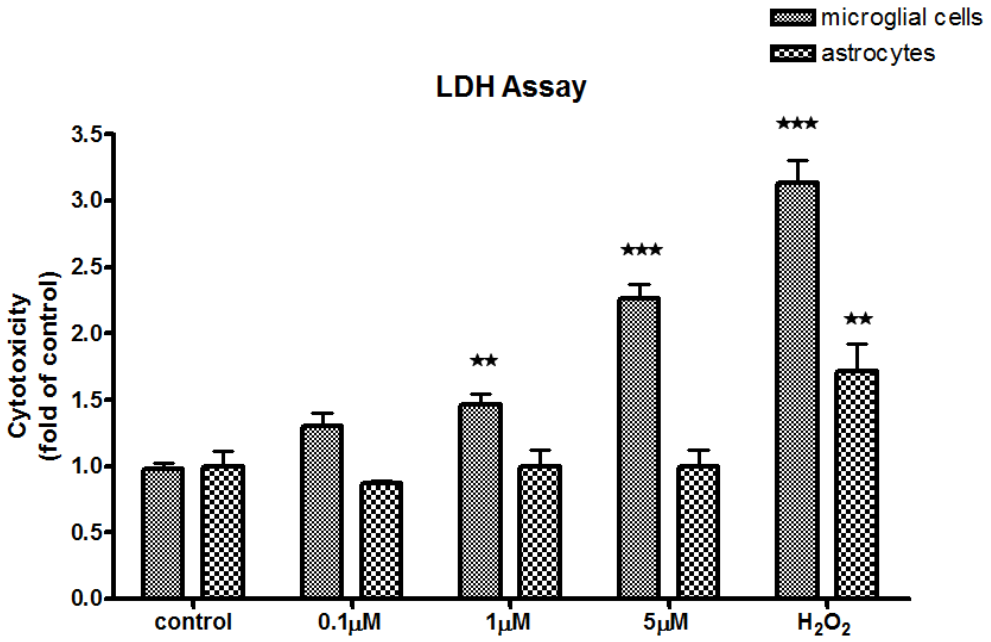

Fig 13. LDH assay result of astrocytes and microglial cells. Effects of MeHg cytotoxicity on astrocytes and microglial cells were measured by LDH assay after MeHg treatment for 6 hours. The results showed 1 and 5μM MeHg treatment significantly increased the number of damaged microglial cells, but not astrocytes. Only 100μM H_2O_2, the positive control, resulted in increased number of damages astrocytes. Values are expressed as the mean±SEM derived from three independent experiments.

Microglial Cells and Astrocytes Exhibit Distinct Kinetics and Levels of ROS Generation

To explain the difference in cell vulnerability (Figs. 12 and 13), we tested whether the kinetics and levels of ROS generation, a common cause of cell death, differed between astrocytes and microglial cells. The H_2DCFDA based assay was used to measure intracellular ROS. Lipophilic H_2DCFDA diffuses freely through the cell membrane and converted to hydrophilic 2',7'-dichlorofluorescin (DCF) intracellularly [196]. Once in the cell, DCF reacts with ROS and fluoresces, providing a tool for measuring intracellular ROS. As shown in Fig. 14, increased ROS levels in microglial cells were detected as early as 1min after 5μM MeHg treatment (222.6±39.01, $p<0.01$) or 100μM H_2O_2 treatment (229.03±40.08, $p<0.01$). . ROS continued to rise to 243.11±15.25 ($p<0.01$) of control at 1μM MeHg and 298.45±40.30 ($p<0.001$) at 5 μM MeHg treatment for 10min. MeHg treatment at 5μM for 1h increased ROS to 338.99±28.92 ($p<0.001$) of control. In astrocytes, however, the increase in ROS generation was only observed after 5μM MeHg treatment for 6h.

Fig 14

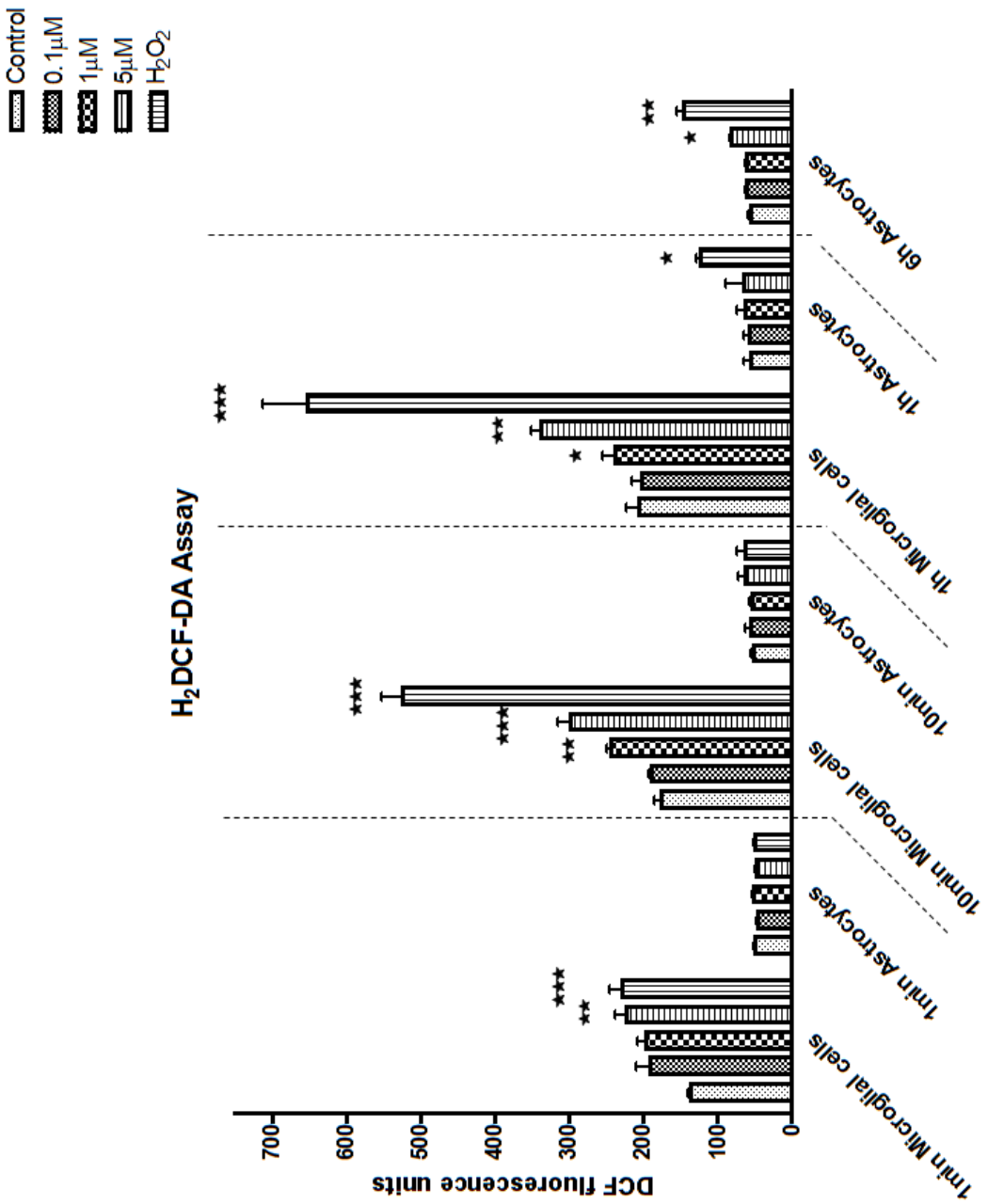

Fig 14. ROS production in astrocytes and microglial cells. DCF fluorescence was measured 1min, 10min and 1h after MeHg was added in both cell types, and 6 hour treatment data were only collected in astrocytes. The increased ROS level in microglial cells was first detected at 1min in 5μM MeHg treatment group. Higher MeHg concentration and longer treatment time led to more ROS generation in microglial cells. In astrocytes, however, only 5μM MeHg treatment for 6h increased intracellular ROS level. Astrocytes had constantly lower ROS level than microglial cells after the same treatment. H_2O_2 at 100μM was used as positive control. Values are expressed as the mean±SEM derived from six independent experiments.

MeHg Causes Rapid GSH Reduction in Microglial Cells, but not in Astrocytes

GSH detoxifies ROS and in the process generates GSSG, the oxidized form of GSH [197]. Given the different kinetics in ROS production in astrocytes and microglial cells (Fig. 14), additional studies were carried out to compare the GSH levels in the two cell types in response to MeHg treatment. The GSH/GSSG ratio of the control group was standardized to 100% (Fig. 15). MeHg (1μM and 5μM) treatment for 1min decreased the microglial GSH/GSSG ratio to 69.01±16.9% ($p<0.05$) and 51.32±20.9% ($p<0.01$) of control levels. A further reduction in the microglial GSH/GSSG ratio was observed after longer MeHg treatment (for 10min and 1h) in a concentration- and time-dependent manner. In contrast, a reduction in the astrocytic GSH/GSSG ratio was not detected until 6 h after treatment with 5μM MeHg treatment ($p<0.01$).

Fig 15

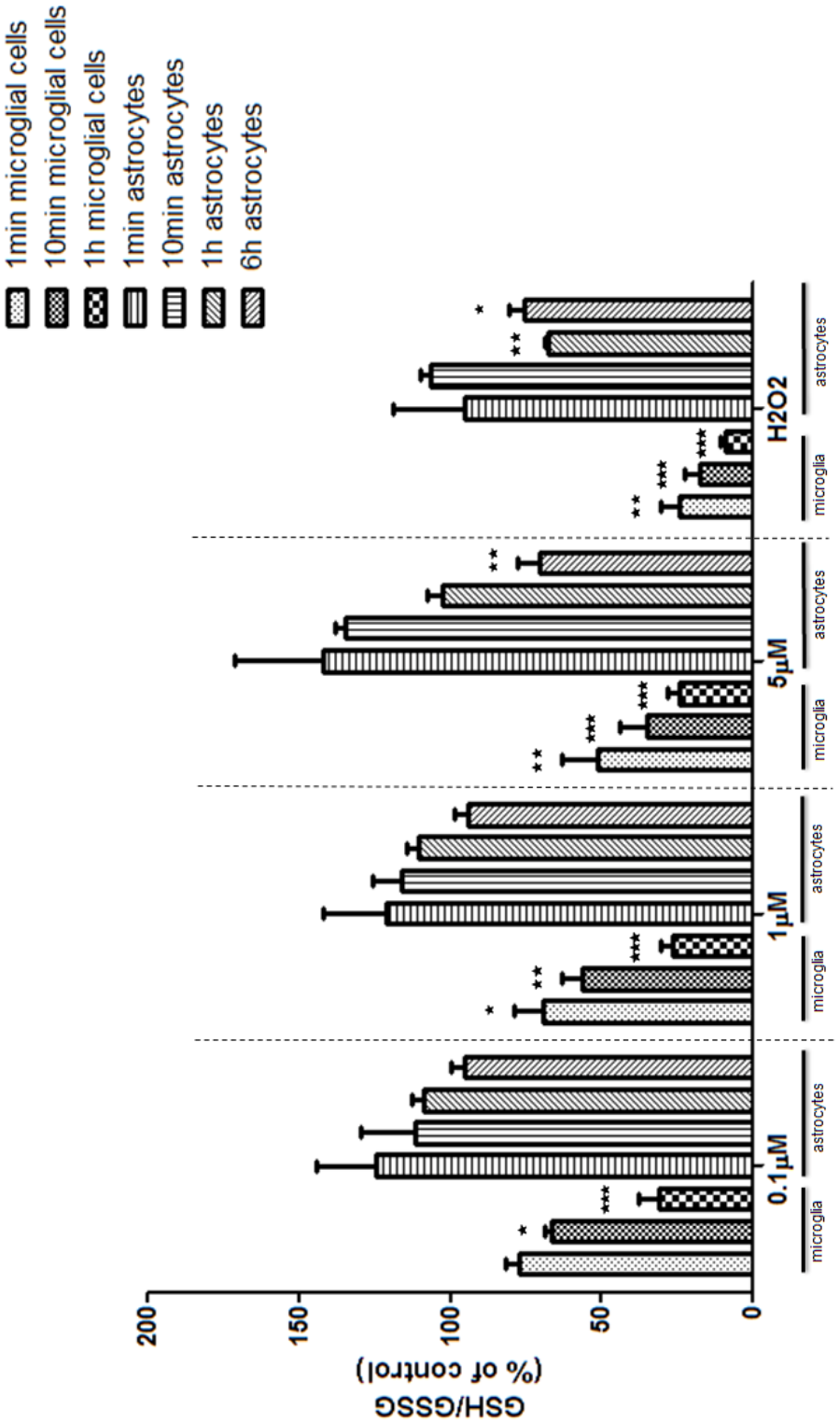
1min microglial cells
10min microglial cells
1h microglial cells
1min astrocytes
10min astrocytes
1h astrocytes
6h astrocytes
GSH/GSSG
(% of control)
200
150
100
50
0
0.1µM
1µM
5µM
H2O2
microglia
astrocytes

Fig 15. GSH/GSSG ratios in microglial cells and astrocyters. GSH and GSSG concentrations were measured by HPLC and the ratios of GSH/GSSG were calculated. The ratio of control group was set to 100% and each treatment group was compared with its corresponding control level and the percentage of control was used to plot the graph Both cell types were treated with MeHg at concentrations indicated in the graph for 1min, 10min and 1h. Only astrocytes were treated for 6h. . The results demonstrated that MeHg caused acute and robust reduction in microglial GSH/GSSG ratio in a concentration-dependent manner. In contrast, only 5μM MeHg treatment for 6h caused reduction in GSH/GSSG ratio in astrocytes. Values are expressed as the mean±SEM derived from three independent experiments.

Kinetic profiles of Nrf2 Upregulation differ between Microglial Cells and Astrocytes

Nrf2 plays a pivotal role in maintaining the redox balance upon MeHg treatment [153, 187]. Given the differences in ROS generation (Fig. 14) and GSH reduction (Fig. 15) after MeHg treatment in astrocytes *vs*. microglial cells, additional studies were performed to determine if Nrf2 kinetics showed a cell-specific signature. The upregulation of Nrf2 protein level and its nuclear translocation were detected by confocal microscopy.

As shown in Fig. 16A, the basal level of Nrf2 (green fluorescence) was low in both cell types. After 10min treatment with 0.1μM MeHg, Nrf2 fluorescence was sparsely detected in microglial cells, but a higher MeHg concentration (≥1μM), appreciably increased the Nrf2 fluorescence intensity and promoted its nuclear translocation, as indicated by the colocalization of Nrf2 (green) and PI staining (counterstaining nuclei in red). In contrast, changes in Nrf2 fluorescence intensity and nuclear translocation were observed in astrocytes only at a much later time point (after 6-hour treatment) and only at the highest MeHg concentration (5μM) of MeHg (Fig 16B). Consistent with the profile of ROS generation (Fig. 14) and GSH reduction (Fig. 15), these data suggest that changes in Nrf2 protein level in astrocytes occur on a more protracted time-scale compared to microglial cells.

Fig 16
16A

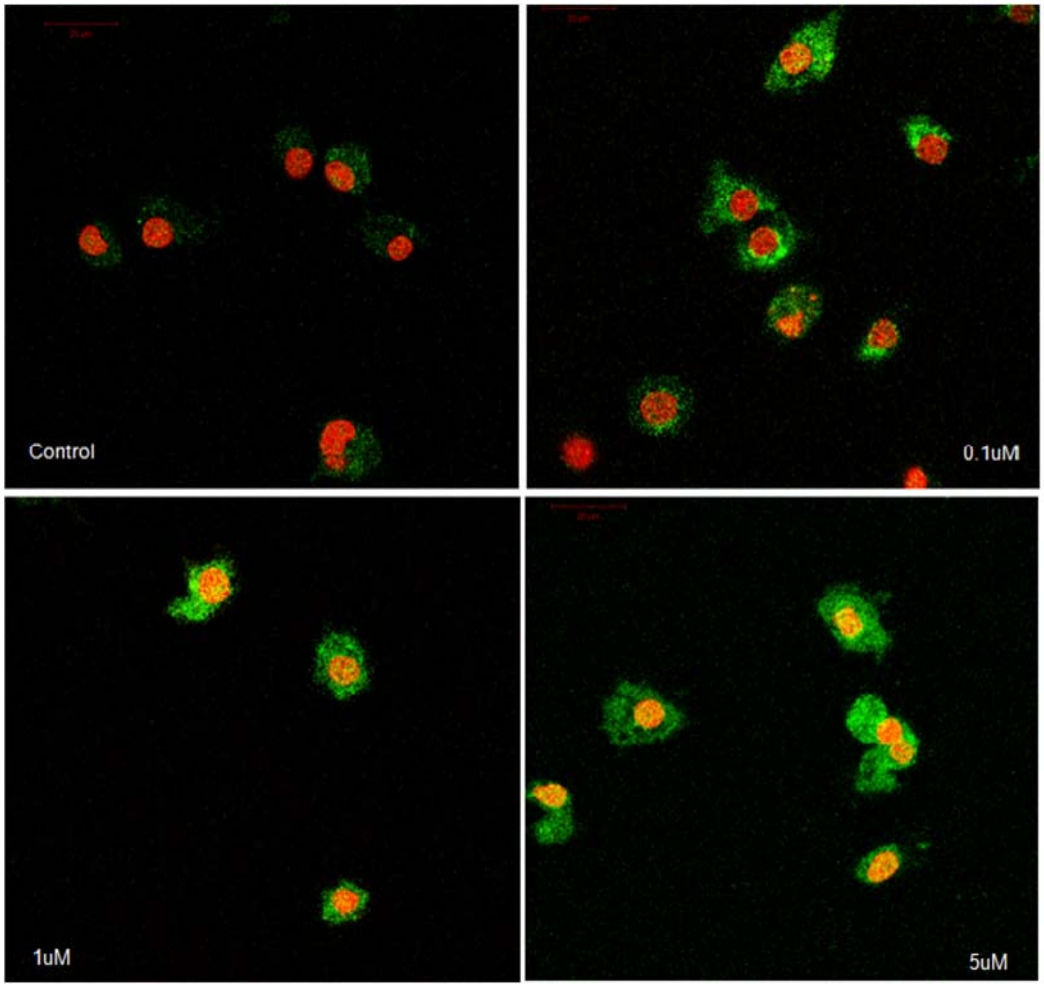

16B

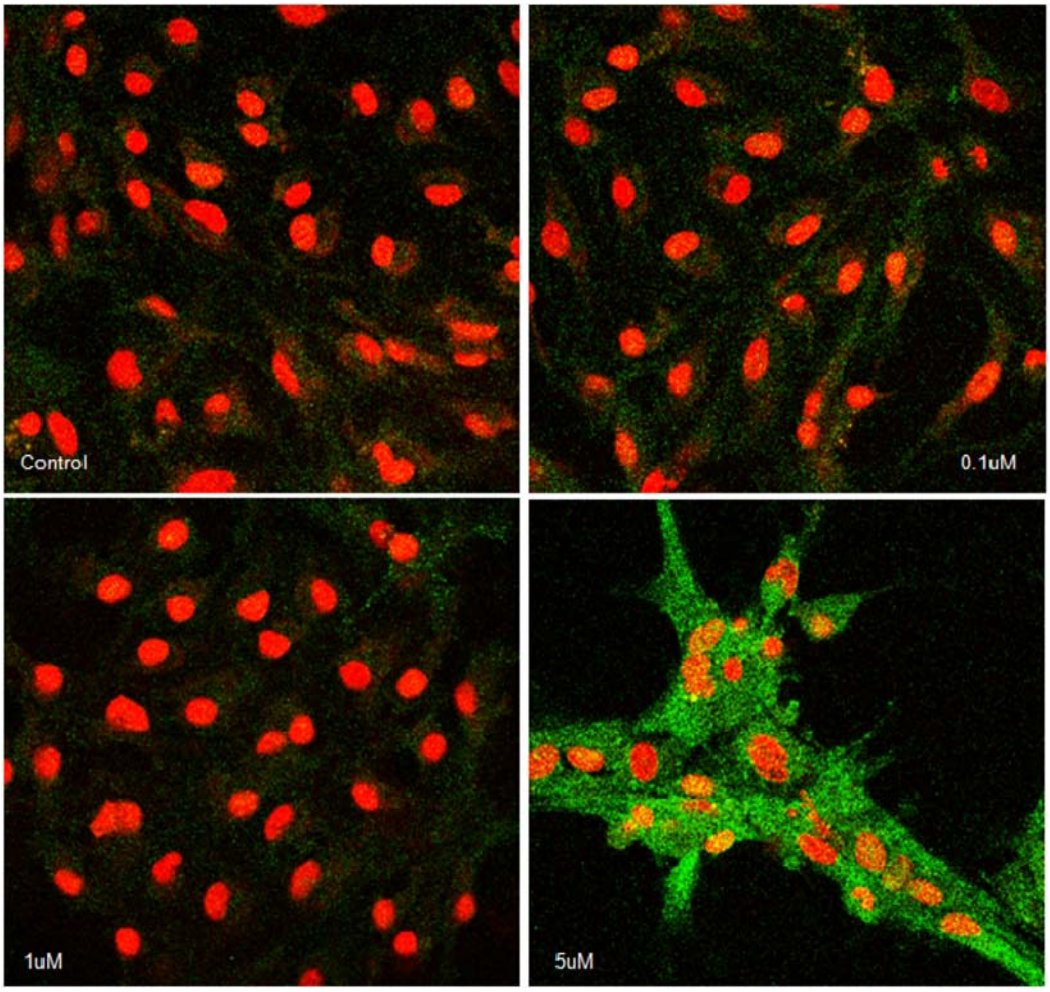

Fig 16 Immunostaining of Nrf2 in microglial cells and astrocytes. Nrf2 was labeled in green and cell nuclei were stained by PI dye in red. (A) In microglial cells, control group showed minimal Nrf2 in the cytosol. MeHg treatment at 0.1μM for 10min increased Nrf2 in the cytosol but not in the nuclei. Higher concentration of MeHg increased Nrf2 in both cytosol and nuclei. Yellow color indicated the colocalization of Nrf2 and DNA in microglial nuclei. (B) In astrocytes, only 5μM MeHg treatment for 6h increased Nrf2 in both cytosol and nuclei. Photographs show representative fields observed from four independent experiments.

Changes in microglail and astrocytic Nrf2 fluorescent intensities (Fig. 16) were also corroborated by means of western blot analysis. As shown in Fig. 17, MeHg treatment in microglial cells caused a concentration- and time-dependent increase in Nrf2. However, in astrocytes, Nrf2 remained unchanged after 1h MeHg treatment at all three concentrations tested (0.1~5 μM). After prolonged MeHg treatment (6h), MeHg only at 5μM appreciably increased astrocytic Nrf2 protein level ($P<0.05$).

Fig 17

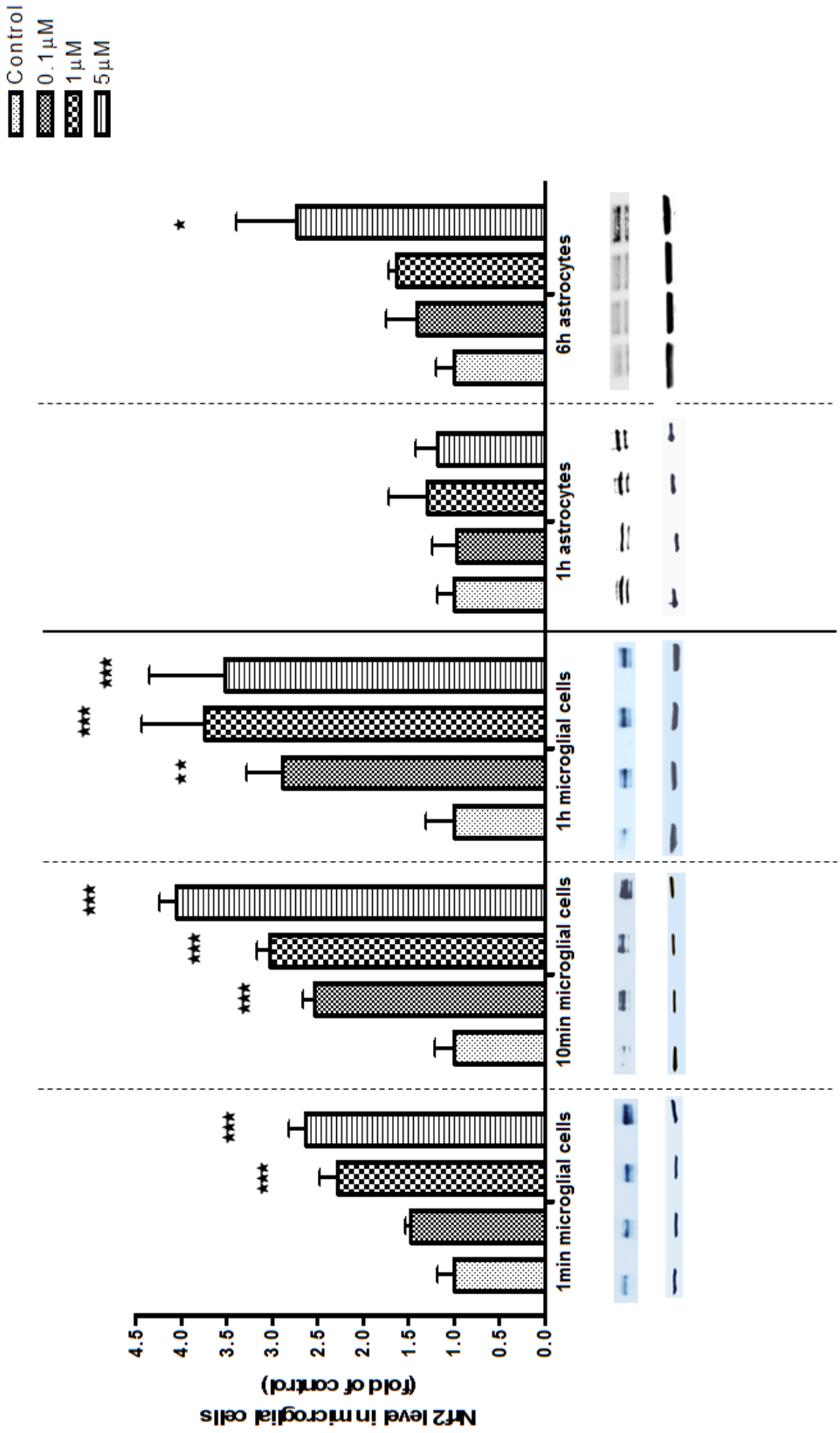
Control
0.1μM
1μM
5μM
Nrf2 level in microglial cells
(fold of control)
4.5
4.0
3.5
3.0
2.5
2.0
1.5
1.0
0.5
0.0
1min microglial cells
10min microglial cells
1h microglial cells
1h astrocytes
6h astrocytes

Fig 17. Nrf2 protein level in the whole cell lysate of microglial cells and astrocytes. The Nrf2 protein level in whole cell lysate was measured by western blot. Both cell types were treated with MeHg at concentrations indicated in the graph for 1min, 10min and 1h. Only astrocytes were treated for 6h. Nrf2 protein level increased in microglial cells commencing at 1min into 1 and 5μM MeHg treatment. After 10min MeHg treatment, MeHg ≥ 0.1μM increased Nrf2 protein level in microglial cells and the increase remained after 1h MeHg treatment. However, in astrocytes, only 5μM MeHg treatment for 6h increased Nrf2 protein level.. Values are expressed as the mean±SEM derived from three independent experiments.

The Temporal Upregulation of Nrf2 Downstream Genes Differs in Microglial Cells *vs*. Astrocytes

Based on the changes noted above (Figs. 16, 17), microglial cells were treated for 30 min, while astrocytes were treated for 6h with MeHg before the mRNA was harvested for real-time PCR analysis. As shown in Fig. 18A, in microglial cells, the transcription levels of *Ho1* and *Nqo1* were upregulated in response to 1 and 5μM MeHg treatment. xCT gene expression was increased by 2.3±1.46 fold over the control value ($p<0.01$) after 5μM MeHg treatment for 30min. In contrast, the increased transcription levels of these genes in astrocytes were detected only after MeHg treatment at highest concentration (5μM) for 6h (Fig 18B).

Fig 18

18A

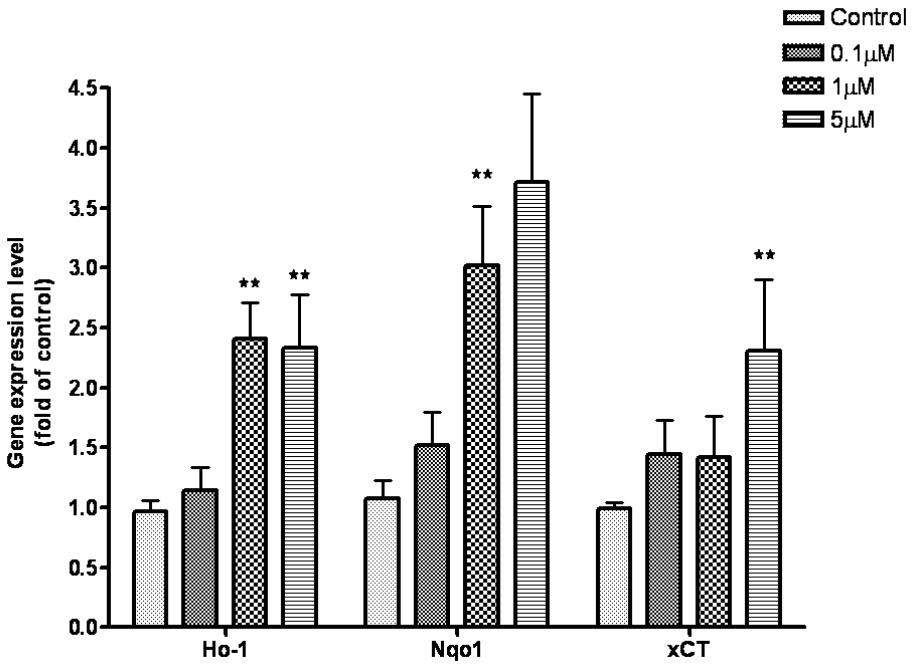

18B

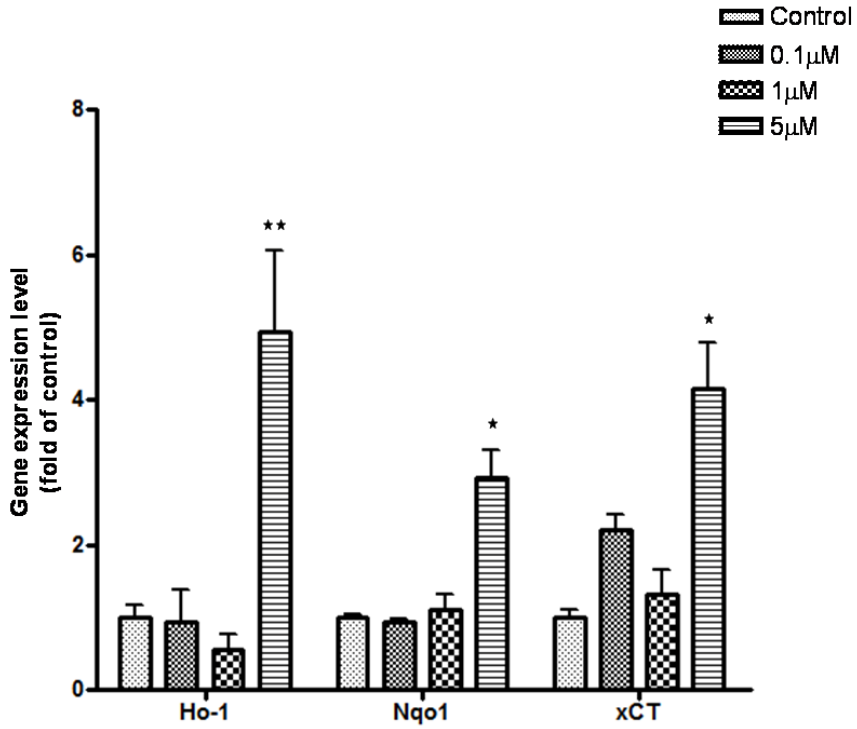

Fig 18. The expression of *Ho1, Nqo1* and *xCT* in microglial cells and astrocyts. Gene expression level was measured by real-time PCR. The differences in the average threshold cycle (*ΔCt*) values were determined and normalized to the expression of β-actin. (A) Microglial cells were treated for 30min. The transcription levels of *Ho1* and *Nqo1* were upregulated in response to MeHg treatment at 1 and 5μM. xCT gene expression was increased after 5μM MeHg treatment. (B) Astrocytes were treated with MeHg for 6 hours. The increased transcription levels of these genes in were detected only after MeHg treatment at highest concentration (5μM) for 6 hours. Values are expressed as the mean±SEM derived from three independent experiments.

Next, we tested the hypothesis that the transcriptional upregulation of these genes was dependent upon Nrf2 activity. Nrf2 activity was inhibited by knocking down *Nrf2* gene expression with shRNA. As shown in Fig. 19A, 5μM MeHg treatment for 30min resulted in a significant increase in *Ho1* mRNA levels in both uninfected and scramble shRNA-infected microglial cells ($p<0.05$) compared with controls. In contrast, microglial cells' *Ho1* transcription level of Nrf2 knockdown was indistinguishable from control levels. Similar changes in microglial *Nqo1* and *xCT* were also observed after Nrf2 knockdown (Fig. 19A). In astrocytes (Fig. 19B), 5μM MeHg treatment for 6 h caused a significant increase in *Ho1* and *Nqo1* mRNA levels in both uninfected and scramble shRNA infected astrocytes. Nrf2 knockdown in astrocytes brought down their transcription to control level. Interestingly, Nrf2 knockdown in astrocytes decreased xCT transcription level compared to the uninfected or scramble shRNA infected cells, but it remained significantly higher than in the controls ($p<0.05$).

Fig 19

19A

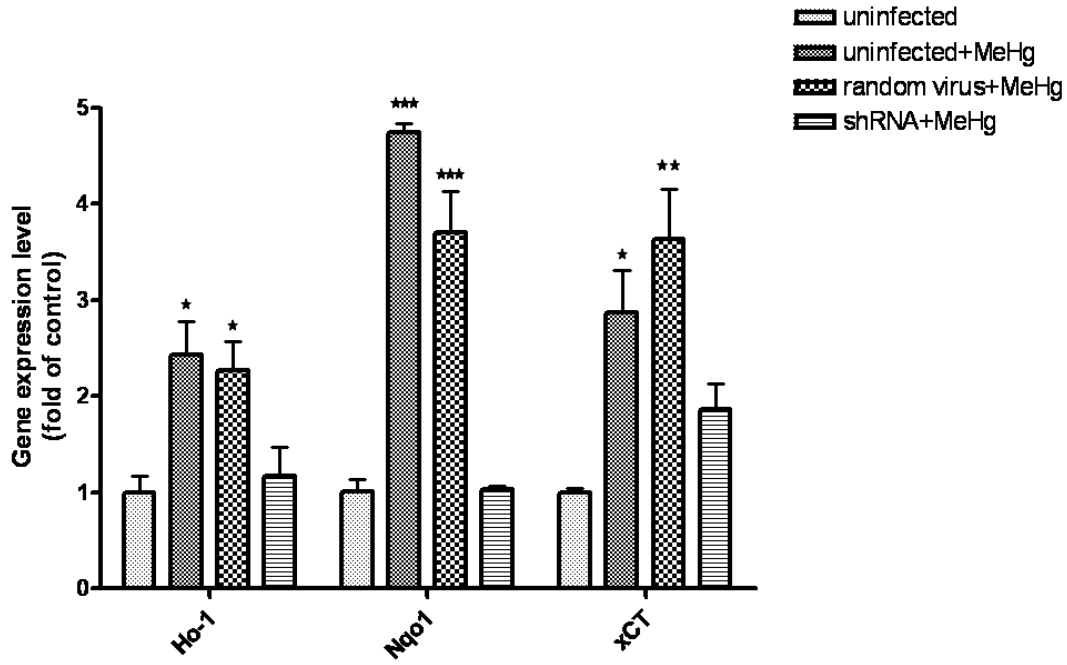

19B

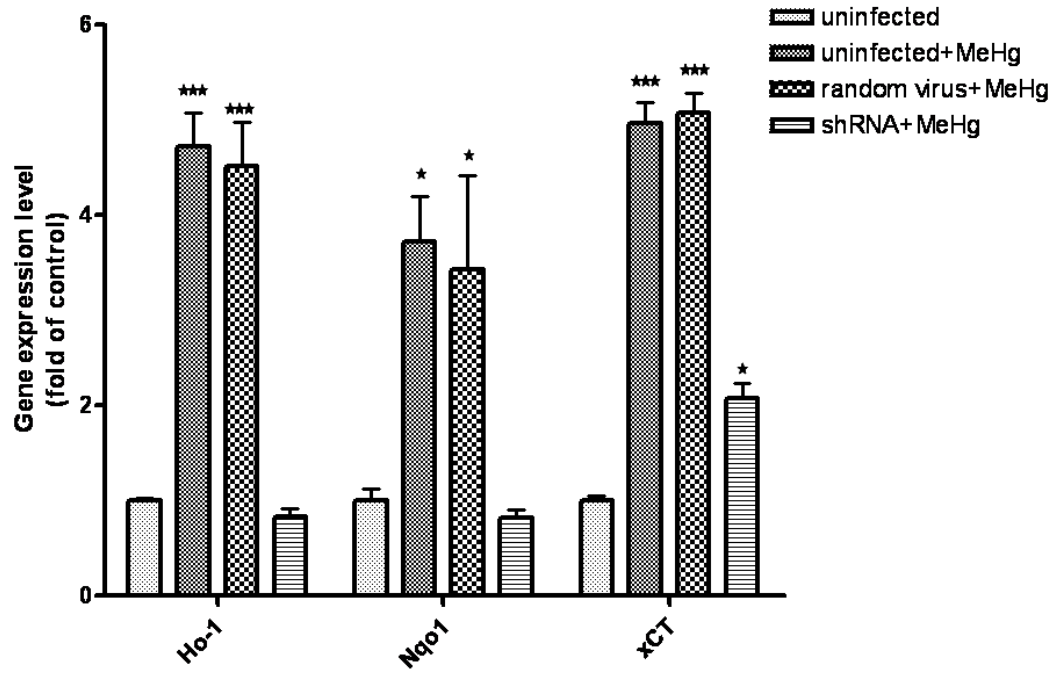

Fig 19. The effect of Nrf2 knockdown on *Ho1, Nqo1* and *xCT* expression in microglial cells and astrocytes. Both cell types were first infected with lentivirus as indicated for 24h and then treated with 5μM MeHg for 30min in microglial cells and 6h in astrocytes. The uninfected cells without MeHg treatment were used to measure basal gene expression level. mRNA levels of *Ho1, Nqo1* and *xCT* were measured by real-time PCR. The difference in the average threshold cycle (*ΔCt*) values was determined and normalized to the expression of β-actin. (A) Microglial cells treated with Nrf2-specific shRNA showed no significant increase in downstream gene expression as compared basal expression level. (B) In astrocytes, the expression of *Ho1*and *Nqo1* from Nrf2 knockdown group showed no signicant increase as compared to basal expression level. Even though *xCT* was upregulated in Nrf2 knockdown group, its increase was less than that of uninfected and random shRNA infected groups after MeHg treatment. Values are expressed as the mean±SEM derived from three independent experiments.

Nrf2 Protects Microglial Cells and Astrocytes against MeHg Toxicity

To further evaluate the cytoprotective function of Nrf2 against MeHg-induced cell death, we assessed cell viability upon MeHg treatment in Nrf2 knockdown cells. As shown in Fig. 20, compared to uninfected microglial cells in the absence of MeHg treatment, both in uninfected cells and random virus infected cells, 5μM MeHg treatment for 6h caused a significant decrease in cell viability ($P<0.001$) (assessed by the MTT assay). Notably, Nrf2 knockdown further decreased cell viability after the same treatment ($p<0.001$). In astrocytes, MeHg (5μM) treatment for 6h did not significantly reduce cell viability in either uninfected cells or random virus infected cells. However, Nrf2 knockdown caused a significant decrease ($P<0.001$) in astrocyte viability after the same treatment.

Fig 20

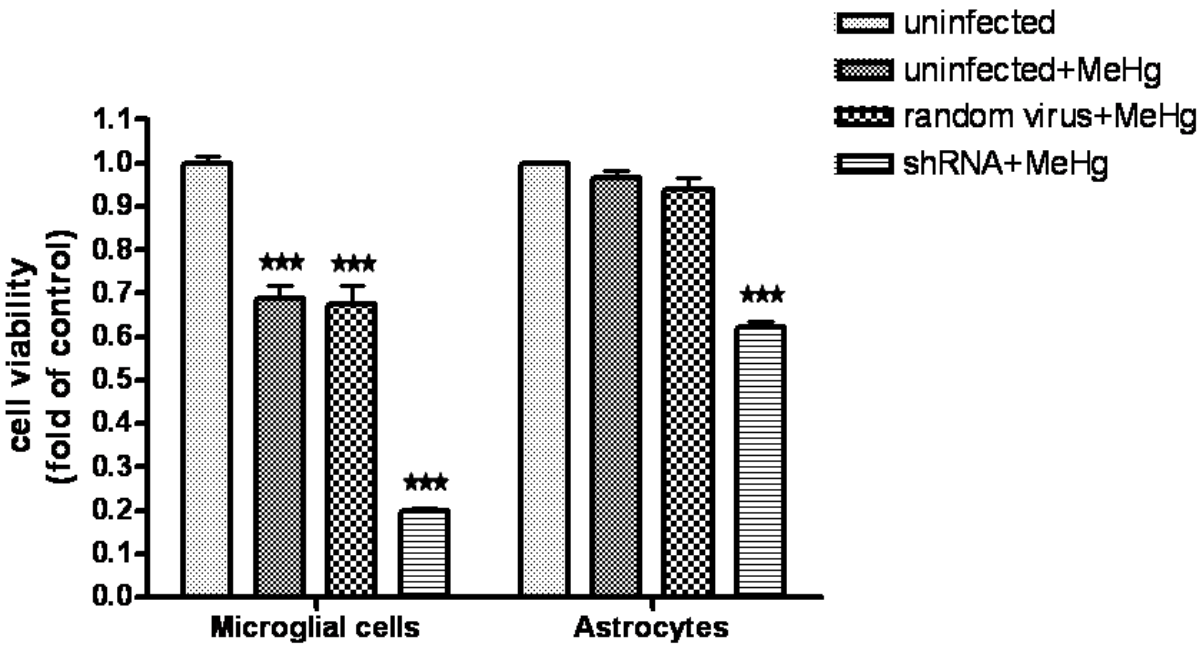

Fig 20. The effect of Nrf2 knockdown on cell viability in microglial cells and astrocytes. Cell viability was assessed by MTT assay. Both cell types were first infected with lenvivirus for 24h and then treated with 5μM MeHg for 6h. The uninfected cells without MeHg treatment were used to measure the maximal cell viability. The results demonstrated Nrf2 knockdown caused significant further reduction of cell viability in both microglial cells and astrocytes as compared to uninfected and random shRNA infected groups after MeHg treatment. Values are expressed as the mean±SEM derived from three independent experiments.

Astrocytes and Microglial Cells Show Differences in Intracellular Mercury Concentration and GSH Level

To further address the distinctive vulnerabilities of microglial cells *vs*. astrocytes in response to MeHg treatment, next, we measured intracellular mercury (Hg) concentration and basal level of GSH in each cell type. The intracellular Hg concentration was measured using ^{14}C-MeHg (refer to Methods for details). As shown in Fig 21, MeHg (≥1μM) treatment in microglia led to a significant increase in Hg accumulation within 1min of its addition to the medium (1μM, $p<0.05$; 5μM, $p<0.01$). Notably, the intracellular microglial Hg concentration reached its peak after 5μM MeHg treatment for 1h. In contrast, astrocytic Hg concentration remained unchanged after 0.1μM and 1μM MeHg treatment for up to 6 hours. Only the highest concentration of MeHg (5μM) increased the intracellular Hg concentration, commencing at 10min. Notably, the intracellular Hg concentration in astrocytes at each time point was significantly lower *vs*. microglial cells ($p<0.01$).

As noted above, MeHg caused rapid GSH reduction (Fig. 15) and ROS production (Fig. 14) in microglial cells, but not in astrocytes. Given that GSH is the major detoxifying molecule of free radicals, we tested if microglial cells have a reduced GSH pool (*vs*. astrocytes) to cope with the increased intracellular levels of MeHg (Fig. 21) and ROS generated by MeHg treatment. The intracellular basal level of GSH was measured by HPLC (see Methods for details). As shown in Fig. 22, the basal GSH level in microglial cells was 26.71±3.85 nmol/mg protein, which was significantly lower than that in astrocytes (93.43±16.62 nmol/mg protein) ($p<0.001$).

Fig 21

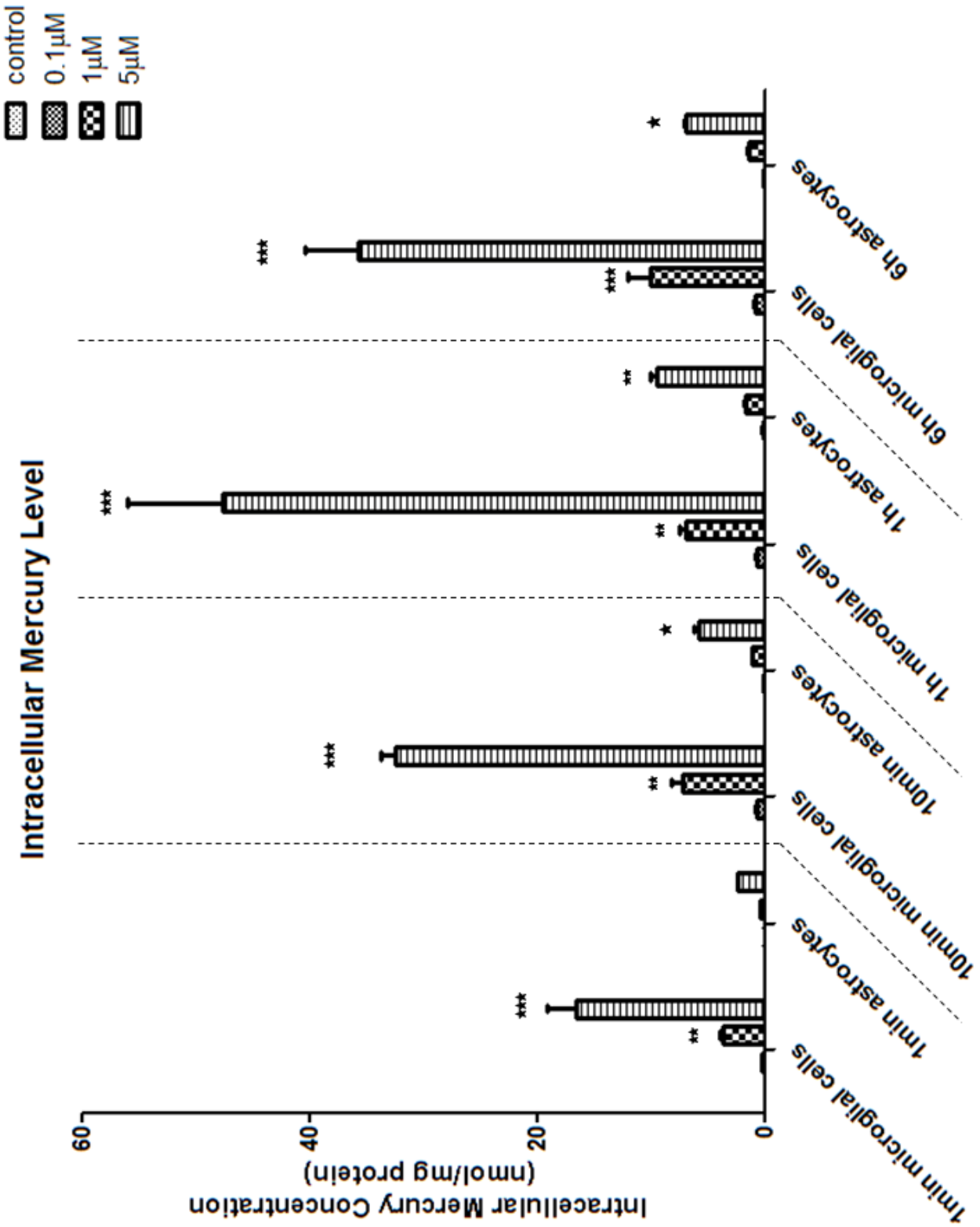
control
0.1μM
1μM
5μM
Intracellular Mercury Level
Intracellular Mercury Concentration
(nmol/mg protein)
0
20
40
60
1min microglial cells
1min astrocytes
10min microglial cells
10min astrocytes
1h microglial cells
1h astrocytes
6h microglial cells
6h astrocytes

Fig 21. Intracellular mercury concentration in microglial cells and astrocytes. Both cell types were treated with the mixture of ^{14}C-MeHg and non-radioactive MeHg (volume ratio of 1:1000) at concentrations indicated in the graph for 1min, 10min, 1h and 6h. The radioactivity was measured and intracellular mercury level was calculated and normalized to protein concentration. The results showed that 1μM and 5μM MeHg treatment increased intracellular mercury concentration in microglial cells at all time points in a concentration-dependent manner. MeHg up to 1μM failed to change intracellular mercury concentration in astrocytes within 6h. Only 5μM MeHg treatment increased intracellular mercury concentration in astrocytes commencing at 10min into treatment. Notably, astrocytes had constantly lower intracellular mercury level than microglial cells. Values are expressed as the mean±SEM derived from three independent experiments.

Fig 22

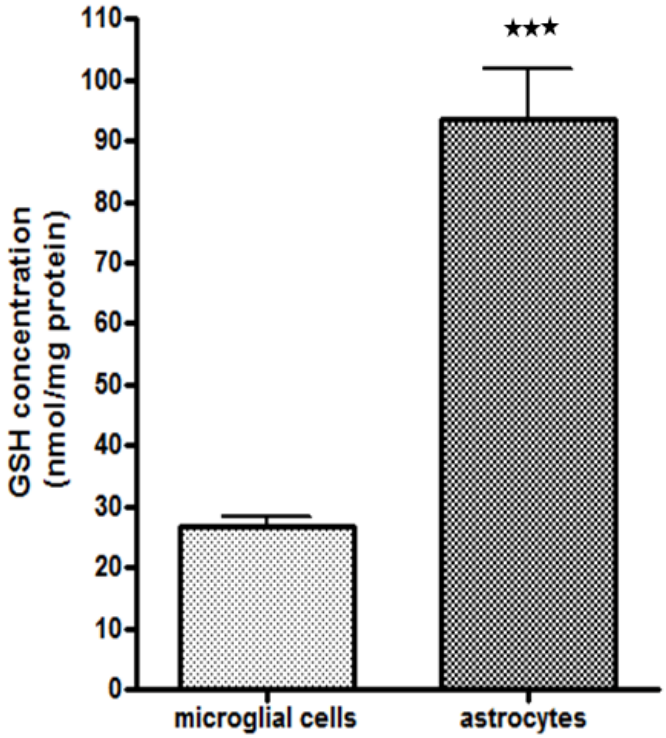

Fig 22. The basal level of intracellular GSH in microglial cells and astrocytes. GSH level was measured by HPLC. The result showed almost four-fold higher GSH level in astrocytes(93.43±16.62nmol/mg protein) than that in microglial cells (26.71±3.85 nmol/mg protein). Values are expressed as the mean±SEM derived from three independent experiments.

Discussion

To our knowledge, this is the first study to systematically compare the differences between primary microglial cells and astrocytes in response to physiologically relevant MeHg treatments. The concentrations of MeHg (0.1-5μM) used in this study well represent the common brain MeHg level as reported by Akagi et al. [151]. Several measurements of responsiveness to MeHg established that microglial cells responded to this organometal more rapidly than astrocytes, and these responses occurred to inherently lower MeHg concentrations. For example, MeHg (≤1μM) treatment led to rapid ROS generation and GSH depletion in microglial cells commencing at 1min after treatment, and well before the 6 h time point where similar changes were observed in astrocytes treated with 5μM MeHg (Figs. 14,15). Consistent with the time scale we observed, Long et al reported that microglial cells responded to TiO_2 at ≥60ppm with a rapid (1-5min) release of H_2O_2 [156]. However, various toxins, such as 1mM dibutyryl cAMP and 1μg/ml Lipopolysaccharide (LPS), are reported to activate astrocytes after 6h treatment [198].

MeHg, like other toxins, first stimulates microglial cells and the microglial response is not causative agents dependent [156]. Consistently, comparative studies carried out in cultured cells and animals treated with neurotoxins have shown that astrocytes are less sensitive than microglial cells [117, 118] and astrocytic reactions occur much later than in microglial cells [119, 120]. For example, in vitro experiment demonstrated that low concentration of neurotoxicant trimethyltin (TMT), 10^{-9}M, activates microglial cells. However, at least 10 folds higher concentration of TMT is required to stimulate astrocytes [118]. Furthermore, in vivo experiment showed that reactive microglia in rat brain were evident 2 days after TMT treatment, but the astrocytosis was not observed until 14 days after TMT treatment at the same

concentration [120]. Similarly, the activation of either glial cell types could play a different role in mediating MeHg neurotoxicity due to the different kinetics of their responses to MeHg. Based on our observation, the response of microglial cells occurred much faster than astrocytes, suggesting that microglial cells may participate in mediating the earlier phases of MeHg toxicity. Astrocytes, on the other hand, may mediate MeHg neurotoxicity on a protracted time scale.

The difference in sensitivity to MeHg could allow microglial cells and astrocytes to act at different time windows of MeHg toxicity. Indeed, we found Nrf2 exhibited distinctive upregulation kinetics between these two cell types after MeHg treatment. Consistent with previous observations [187], the upregulation of microglial Nrf2 occurred 1min after MeHg treatment (Fig. 17) with Nrf2 undergoing nuclear translocation 10min post MeHg treatment. In contrast, these changes in astrocytes were not inherent only to the highest MeHg treatment (5μM MeHg), and were evident only at 6h post treatment (Figs. 16,17). Consistent with the difference in Nrf2 kinetics in the two cell types, the temporal expression of Nrf2 downstream genes was distinctively regulated in these two cell types (Figs. 18,19). The expression of *Ho1, Nqo1* and *xCT* rapidly increased in microglial cells but delayed in astrocytes (6h post MeHg treatment). As we confirmed the cytoprotective function of Nrf2 in both cell types by shRNA apporoach (Fig. 20), the protective effects of Nrf2 in these two cell types are different given the truth that the regulatory kinetics of Nrf2 is different in microglial cells *v.s.* astrocytes.

The earlier responsiveness of microglia *vs*. astrocytes to MeHg treatment was corroborated by distinct differences in the intracellular Hg concentrations as well as the basal GSH levels in the two cell types (Fig 21,22). Consistent with earlier reports that microglial cells accumulated the

largest concentration of Hg following MeHg treatment in non-human primates [102], we observed that intracellular Hg concentration in microglial cells were significantly higher than that in astrocytes after the same MeHg treatment. This may reflect the faster and more robust response of microglial cells *vs*. astrocytes to MeHg. Previous studies have established the cytoprotective effects of GSH in MeHg-induced toxicity [159, 160]. GSH readily binds to MeHg via its sulfhydryl groups, and the conjugated products are actively pumped out of the cells by multidrug resistance proteins, leading to a decrease in intracellular MeHg and its toxicity [161]. In addition, GSH detoxifies ROS generated by MeHg to maintain the redox balance in the cell [199]. As shown in Fig. 22, a greater than four folds higher basal GSH level were noted in astrocytes compared to microglial cells, which may explain the more rapid changes in ROS levels and GSH/GSSG ratio in microglial cells, where GSH would be expected to be depleted more rapidly given its lower basal levels. It may also reflect the delayed Hg accumulation and lower intracellular Hg level in astrocytes as higher GSH levels may facilitate the extrusion of the metal from these cells vs. microglia (Fig.21).

MeHg not only directly activates glial cells, but also alters normal CNS function via molecules released by glial cells. For example, upon activation, microglia produce free radicals (Figs. 14, 15)[156] and release proinflammatory cytokines such as interleukin 6 (IL-6) [155]. Microglial cells have been shown to influence other cell types via IL-6 secretion. For example, it induces astrogliosis associated with MeHg-induced microglial clusters [143]. Interestingly, as a proinflammatory factor, IL-6 may have a neuroprotective function. IL-6 co-administered with MeHg prevented MeHg-induced degeneration of the neuronal cytoskeleton [143]. Similar protective effects of IL-6 against the toxic effects of glutamate have also been previously

described [169]. In contrast, astrocytic dysfunction might mediate MeHg toxicity at later stages. For example, Yin et al. reported that the disrupted amino acid homeostasis plays the critical role in astrocytes- mediated MeHg toxicity [200]. Among these amino acids, glutamate is profoundly affected [200]. MeHg inhibits astrocytic glutamate uptake, while stimulating glutamate efflux [90], consequently resulting in an excessive concentration of synaptic glutamate, which ultimately leads to neuronal excitotoxicity and cell death [147]. Astrocytes also appear to dampen microglial activation under physiological conditions [173]. Therefore, MeHg-induced astrocytic dysfunction may hasten microglial dysfunction by removing astrocytic inhibitory function.

In summary, results presented herein demonstrated the different response kinetics of astrocytes and microglial cells to MeHg treatment. Microglial cells exhibited a faster and more robust response to MeHg compared to astrocytes. The microglial response to MeHg reflects a significantly greater accumulation of Hg in these cells vs. astrocytes, as well as lower basal GSH pool to detoxify ROS generated by MeHg and possibly direct binding to MeHg itself. Collectively, these studies suggest that microglial cells and astrocytes assume different role on a protracted time-scale, with microglia representing the early responders and astrocytes assuming a similar role later on upon treatment. A better understanding of the distinctive roles of these cells in mediating MeHg toxicity under in vivo conditions is clearly warranted, as it may facilitate potential therapeutic modalities to ameliorate MeHg-induced CNS damage.

CHAPTER IV

CONCLUSION AND DISCUSSION

To our knowledge, this is the first study to investigate the response of primary astrocytes and microglia to acute MeHg exposure, as well as to compare responses in glial cell types upon treatments with physiologically relevant concentrations of MeHg. Furthermore, the protective functions of Nrf2 and its downstream genes in both astrocytes and microglia have been systematically studied. As stated above, some previous studies [144] were carried out to study glial response to MeHg treatment, but the concentrations used in those studies were higher than the concentrations of MeHg (0.1-5μM) used in my studies which are within the range of brain MeHg levels in human pathological conditions as reported by Akagi et al. [151]. The majority cell lines used in previous studies are cancer- derived immortalized glia [143, 144], whose response may not represent the "normal" glia. More importantly, I compared the kinetics of microglial response with astrocytic response after MeHg treatment by using the cells harvested from the same animals, which minimized the individual variations.

In the first part of my thesis project, we have demonstrated that MeHg leads to rapid ROS generation and GSH depletion in primary microglia commencing at one minute post MeHg exposure. Previous studies have reported an increase in ROS in microglial cells after prolonged MeHg treatment at higher concentrations [143, 144, 155]. However, these studies do not capture the acute microglial response to lower concentrations of MeHg as detected in early stages of Minamata disease patients. Notably, the primary cell culture used in my project best represents

the vulnerability of developing brains since all cells were harvested from 1-day-old neonatal rats. As stated above, the developing glial cells are more sensitive to MeHg poisoning, and therefore, the cell culture I used in my project is the best model system since it fills in the gap missed by previous studies using glial cell cultures after multiple passages. Here, we have revealed that 5μM MeHg treatment causes a significant increase in ROS generation in primary microglial cells commencing at one minute post MeHg exposure. The acute response of microglia appears to be independent to the stimuli, since the similar acute ROS generation in microglial cells was also observed after TiO2 exposure [156].

In the second part of my thesis project, I compared the difference in the kinetics of microglial response to that of astrocytes after MeHg treatment. The two major glial cell types in the brain, astrocytes and microglia play pivotal yet different roles in maintaining optimal brain function. Comparing to microglia, astrocytes also produce excessive ROS in response to MeHg treatment, but it is only detected after much longer exposure to MeHg (6 hours) (Fig 14), which is consistent with previous reports [107, 153]. Our data clearly suggest that microglia are the first line of cellular response to MeHg poisoning in the CNS. Supporting this notion, comparative studies in cultured cells treated with trimethyltin (TMT) found significantly greater sensitivity in microglia compared to astrocytes [117, 118]. A low in vitro concentration of TMT (10-9M) led to microglial activation, while at least a 10-fold higher concentration was required for the activation of astrocytes [118]. As mentioned above, even though both cell types have been implicated as major targets of MeHg, their unique sensitivities and adaptive responses to this metal can vary given their distinctive properties and physiological functions. Thus, the distinct sensitivities of microglia and astrocytes likely indicate different roles for the two cell types along

a temporal axis in response to MeHg. Accordingly, the second part of thesis project was carried out to compare the respective responses of astrocytes and microglia following treatment with MeHg, examining and addressing the effects of MeHg on cell viability, reactive oxygen species (ROS) generation and glutathione (GSH) levels, as well as mercury (Hg) uptake and the expression of NF-E2-related factor 2 (Nrf2).

In mammalian cells, GSH:GSSG balance is dynamically maintained stable. GSH is used to detoxify ROS and itself is converted to the oxidized form, GSSG. As my data showed, ROS in microglia and astrocytes are increased in response to MeHg treatment (Fig 4, 5, 14) and, correspondingly, the GSH/GSSG ratio is decreased in microglia (Fig 6) and astrocytes (Fig 15). The mechanism of GSH protective function has been studied extensively [159, 160]. Konig [161] reported that GSH binds to Hg compounds via its sulfhydryl groups, and the conjugated products are actively pumped out of the cells by multidrug resistance proteins (MRPs), leading to the decrease in intracellular Hg and its toxicity. In addition, Farina [201] and Das [199] reported that GSH prevents the interaction of Hg with protein thiols and detoxifies ROS generated by MeHg to maintain the redox status in the cell.

Previous studies revealed that lower intracellular GSH level is correlated with greater glial cell death. For example, Miura and Clarkson [162, 163] studied the correlation between GSH level and MeHg toxicity using MeHg-resistant rat pheochromocytoma PC12 cell line. Compared to nonresistant cells, the levels of GSH in resistant cells were four-fold higher, which led to greater efflux and less intracellular retention of MeHg. Consistent with previous study [202], in my experiments, the basal level of astrocytic GSH was measured to be 80±10nmol/mg protein [203].

Compared to astrocytes, microglial GSH levels are only 25% of those in astrocytes (Fig 22), which likely reflects their diminished capability to buffer MeHg-induced ROS generation. Thus, lower GSH levels in microglial cells may lead to reduced MeHg efflux and increased intracellular Hg levels. This may explain previous findings of the earliest and highest accumulation of Hg deposits in microglial cells in the rat brain [164] and non-human primates [102]. Our data also show that the lower intracellular GSH level is correlated with greater glial cell death. In microglia, treatment with 5μM MeHg causes maximal reduction in GSH levels (Fig 6) as well as maximal microglial death (Fig 3), which supports the notion that GSH plays a critical role as a protective molecule against MeHg toxicity.

As shown before, microglia are more sensitive to MeHg exposure and respond much faster than astrocytes. It is reasonable hypothesize that the distinct sensitivities of microglia and astrocytes likely indicate different roles for the two cell types along a temporal axis in response to MeHg. Previous studies revealed that intracellular ROS generation parallel to the increase in Nrf2 protein and it is also the pivotal molecule in regulating Nrf2 levels [153]. Consistent with the previous literatures, the increase in Nrf2 (Fig 8) protein levels was paralleled by the MeHg-induced increase of ROS (Fig 4,5), as well as the decrease in GSH (Fig 6). Indeed, Nrf2 expression exhibited distinct upregulation kinetics after MeHg treatment in microglia *vs.* astrocytes. For example, the upregulation of microglial Nrf2 occurred as early as 1 min after MeHg treatment at 1μM (Fig. 7), however, the phenomenon was not observed in astrocytes until 5μM MeHg treatment for 6 hours. Nrf2 is the transcription factor and undergoes nuclear translocation [153]. In my project, I also observed Nrf2 nuclear translocation commencing at 10 min post MeHg exposure. Our data support the new model proposed by Li et al [133], that

oxidative stress disrupts the interaction between Nrf2 and Keap1 leading to the decreased rate of proteasomal degradation of Nrf2 in cytosolic fraction. This model explains why the increase of cytosolic Nrf2 was detected as early as 1 min post MeHg exposure [133]. In contrast, these changes in astrocytes were inherent only with the highest MeHg treatment (5μM MeHg) and were evident only at 6 h post-treatment (Figs. 16,17). Based on the fact that Nrf2 activation in primary astrocytes after MeHg treatment occurred much later than microglia, our results further support the notion that microglia are the first glial cell type to respond to MeHg treatment[165].

Nrf2 is the key protective molecule regulating its downstream antioxidant genes and the nuclear translocation of Nrf2 is critical for attenuation of oxidative stress [166]. It is reported that primary mouse hepatocytes isolated from *Nrf2*- deficient mice were highly susceptible to MeHg-induced cytotoxicity, and *Nrf2* overexpression can attenuate MeHg- induced cytotoxicity in SH-SY5Y neuroblastoma cells [166]. Consistent with these studies, we also observed increased astrocytic and microglial death upon *Nrf2* knockdown by using shRNA approach (Fig 20). Previous studies also confirmed the critical function of Nrf2 in orchestrating the expression of *Ho-1, Nqo1* and *xCT*, all of which detoxify xenobiotics and endogenous reactive electrophiles in numerous cell types. For example, Nrf2 in renal epithelial cells upregulated the *Nqo1* reporter construct after exposure to hypoxia/reoxygenation [168]. Similarly, in human lymphoma cells, gallium nitrate upregulated the *Ho-1* mRNA level as a result of Nrf2 activation [153, 167]. Once I observed the difference in Nrf2 expression kinetics in microglia and astrocytes, I further carried out experiments to investigate the difference in temporal regulation of Nrf2 downstream genes (Figs. 18,19). My results clearly showed that the expression of *Ho1, Nqo1* and *xCT* rapidly

increased in microglia, but the increase was delayed in astrocytes (6 h post MeHg treatment; Figs.18,19).

Based on the combined data generated in my project, it is reasonable to conclude that the difference in the kinetics of ROS generation, Nrf2 activation and the upregulation of its downstream genes could reflect the temporal difference in the activation of these two cell types. Notably, the timescale of the changes is not dependent on stimuli, since it is also reported in earlier studies. For example, Long and colleagues reported that microglia responded to titanium dioxide (TiO_2; ≥60ppm) with a rapid (1-5min) release of H_2O_2 [156]. In contrast, 1mM dibutyryl cAMP and 1μg/ml Lipopolysaccharide (LPS) led to astrocytic activation after 6h treatment [198]. The faster activation of microglia in comparison to astrocytes was also observed *in vivo* upon TMT treatment. Reactive microglia in the rat brain were noted within 2 days after TMT treatment, while astrocytosis was not evident until 14 days after TMT treatment [120]. From a molecular point of view, the differences between microglial and astrocytic responsiveness to MeHg appear to be related, at least in part, to differences in their respective cellular thiol statuses. This idea is based on three important events: (i) microglia accumulate higher levels of Hg (Fig. 21), which interact with and oxidize thiols; (ii) microglia contain lower GSH levels (Fig. 22), which maintains the normal cellular thiol status; and (iii) Nrf2 activation is regulated by oxidative modifications of its cysteine thiol groups, as well as by thiol oxidation in Kelch-like ECH-associated protein-1 (Keap1) [204]. The differential thiol status in microglia and astrocytes also explains the observed changes in ROS levels and the GSH/GSSG ratio during MeHg exposure, where microglial GSH was depleted faster given its lower basal levels. Intracellular MeHg has been reported to be exported out of cells as the GSH complex [205]; thus, the higher

basal GSH levels in astrocytes lead to delayed Hg accumulation and lower intracellular Hg levels in these cells (compared to microglia).

As stated above, the major function of glia is to maintain the hemostasis of CNS and the dysfunction of glia adversely affect the normal function of brain via molecules released by these cells. There are numerous studies showing microglia, upon activation, release proinflammatory cytokines, such as interleukin 6 (IL-6) [155]. IL-6 has very complicated effects on CNS. For example, Eskes [143] reported that IL-6 induces astrogliosis associated with MeHg-induced microglial clusters. Interestingly, as a proinflammatory factor, IL-6 may have also a neuroprotective function. IL-6 co-administered with MeHg has been shown to prevent the MeHg-induced degeneration of the neuronal cytoskeleton [143]. Similar protective effects of IL-6 against the toxic effects of glutamate have also been previously described [169].

As shown in my results, astrocytic dysfunction might mediate MeHg toxicity at later stages. For example, disrupted amino acid homeostasis after MeHg treatment may ensue upon MeHg-induced inhibition of astrocytic glutamate uptake [200] while stimulating glutamate efflux [90], resulting in an excessive concentration of synaptic glutamate, which ultimately leads to neuronal excitotoxicity and cell death [147]. As mentioned above, neurons, microglia and astrocytes form the complex cell-cell network, and therefore the dysfunction of one cell type affects the function of the other cell type. For example, Eskes [172] reported that neurons can increase microglial reactivity Co-culturing with neurons leads microglial cells to differentiate to a macrophagic state, which suggests certain diffusible factors released from neurons could result in the activation of microglial cells [172]. In contrast to neurons, Thomas [173] reported that astrocytes dampen microglial activation under physiological conditions. Notably, my thesis project was performed

in purified glial cells after acute MeHg treatment. Given the cross-talk between the various cell types, it is imperative to extend the findings regarding MeHg's function on microglial cells to more complex cellular networks, such as co-cultures and, ultimately, to *in vivo* preparations.

In summary, the results of my thesis project demonstrate different response kinetics in astrocytes and microglia upon MeHg treatment. Microglia exhibited a faster and more robust response to MeHg compared to astrocytes. The microglial response to MeHg reflects a significantly greater accumulation of Hg in these cells than astrocytes, as well as a lower basal GSH pool for detoxifying ROS generated by MeHg. The faster microglia activation of Nrf2 and its downstream genes (*Ho1, Nqo1* and *xCT*) is likely related to its lower thiol status. Collectively, these studies suggest that microglia and astrocytes assume different roles on a protracted time-scale, with microglia representing the early responders and astrocytes taking on a similar role at a later stage following MeHg treatment (see Fig 23). A better understanding of the distinctive roles of these cells in mediating MeHg toxicity under *in vivo* conditions is clearly warranted. As suggested by the results of my project, increasing intracellular GSH or upregulating Nrf2 are very promising therapeutic strategies to treat MeHg poisoning. Indeed, additional insight gained from future studies offers tremendous promise for the identification and development of potential therapeutic modalities to ameliorate MeHg-induced CNS damage.

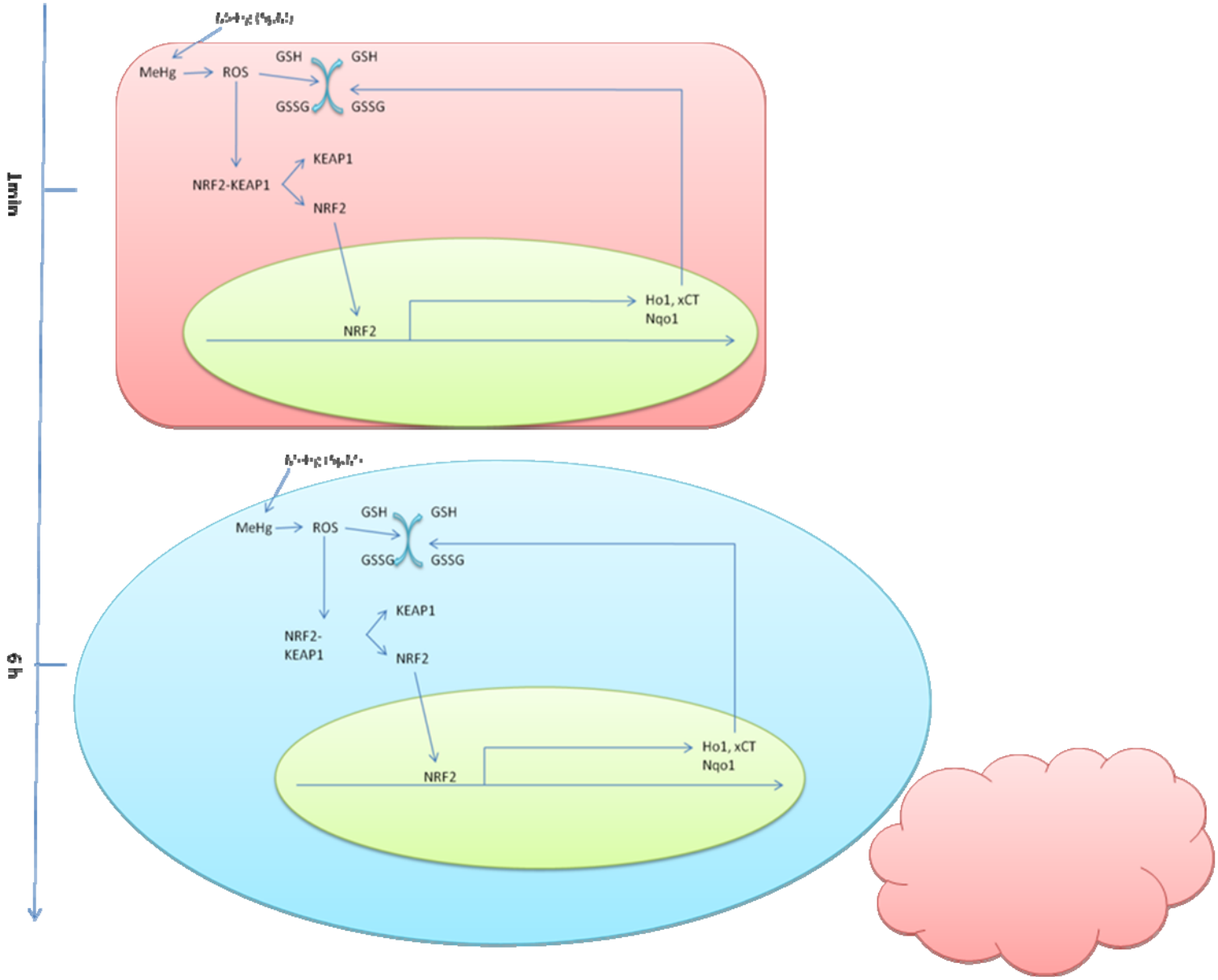

Fig 23. The responses of microglia and astrocytes are summarized. The time axis is listed on the left. [Top panel] 1min post MeHg treatment, the MeHg concentration in microglia (pink) is elevated and intracellular ROS is produced, which leads to the conversion of GSH to GSSG in order to detoxify the excessive ROS. The elevated ROS also disrupts the NRF2-KEAP1 complex that results in the dissociation of NRF2. The free NRF2 is translocated into the nucleus where it stimulates downstream detoxifying gene expression, including Ho1, xCT and Nqo1. Notably, there is no astrocytic (blue) response at this time point. [Bottom panel] 6 hours after MeHg

treatment, there is similar cellular response observed in astrocytes. There is significant microglial (pink) death due to overwhelming oxidative stress and MeHg toxicity.

Appendix

A. Book chapter: Neonatal Rat Primary Microglia: Isolation, Culturing and Selected Applications

This chapter has been published in

Chapter 12:Unit 12.17.

Curr Protoc Toxicol. 2010 Feb;

INTRODUCTION

Neurons are the major cell type in the central nervous system (CNS), their unique electrical excitability distinguishing them from other cell types. Glial cells, including astrocytes, microglia and oligodendrocytes are non-electrically excitable. The term glia is derived from the Greek language and means “glue”. Yet glial cells have diverse functions, well beyond the original scope ascribed to them as being the mere glue that holds the neurons in place. They provide support and nutrition [1], maintain CNS homeostasis [103], form myelin [103] and participate in signal transmission [104, 105], just to name a few of their functions. The majority of glial cells are astrocytes, which are intimately involved in maintaining the extracellular milieu. Some selected functions of astrocytes include secretion of growth factors, release of cytokines and modulation of synaptic transmission by removal of neurotransmitters such as glutamate from the synaptic cleft. Oligodendrocytes are the myelin-forming cells in the CNS and are analogues to Schwann cells of the peripheral nervous system.

Microglia comprise approximately 12% of total cell population in the brain and are the second largest glial cell type. Microglia are derived from myeloid lineage [113]. In postnatal rodents, immunocytochemical studies using antibodies to F4/80 (ERM1), CR3 and FcγRII/III establish that the microglia enter the brain from the circulation and are derived from circulating monocytes [113]. In the brain, they possess phagocytic activity and survey the parenchyma. Microglia express low level of Major Histocompatibility Complex (MHC-II) and function as antigen presenting cells (APC) of the CNS [113]. They are in close contact with other cells in the brain, mainly astrocytes, thus establishing cross-talk that mediates and synergizes responses both in physiological and pathological conditions. Under optimal conditions microglial surface receptors, such as TREM2 and Siglecs maintain the microglia in an inactivated state [113]. In the presence of inflammation, infection, trauma and degenerative diseases, microglia are the first cell type to become activated. Their activation is inherent to Alzheimer's disease [114], Parkinson's disease [115], HIV dementia [116] as well as numerous other pathological conditions. Once activated, microglia produce soluble proinflammatory cytokines, prostaglandins and interleukins, such as tumor necrosis factor-α (TNF-α), PGE2, interleukin-1 (IL-1) and interleukin-6 (IL-6), which not only contribute to the neighboring neuronal damage, but also recruit immune cells into the CNS.

The culture technique introduced here is based on the method first published by Barger and Basile [206] and has undergone minor modification in our laboratory. From one litter of 1-day old neonatal rats (10-14 pups) we routinely get sufficient amount of mixed cells (100 millions) for approximately 15 225 cm^2 culture flasks. These mixed cell cultures reach confluence in approximately 2 weeks post seeding; the culture media are changed twice weekly. Microglia are

isolated from the mixed cell culture before the end of the 2nd week by gentle physical shaking and tapping on the flasks. After isolation, the microglia are re-seeded into three 6-well plates (other seeding options are possible and should be dictated by the end-points of the experiments you wish to conduct taking into account the numbers of replicates) with fresh culture media. The cell purity is routinely examined by immunohistochemistry staining for OX-42, a microglia specific integrin marker. In our hands, the cultures reach >95% purity. Other cells types in the cultures, mainly astrocytes in the mixed culture system lend the process ideal for the concomitant isolation of primary astrocyte cultures. These can be characterized with specific antibodies for intermediate skeletal proteins, such as glial fibrillary acidic protein (GFAP). The method for culturing and maintaining astrocytes has been previously published ([207]).

The mechanical isolation protocol discussed in this chapter offers an economical method to isolate large amount of microglia in a short and not too labor intensive manner. Most importantly, it assures a high yield of cells with great reproducibility. Given the ever increasing importance of microglia to the field of neurotoxicology research, the ability to isolate high yield of primary microglia makes it possible to investigate the role and mechanisms associated with microglial modulation of neurotoxicity. Next, we provide a detailed description on the methods that is routinely used in our laboratory for the isolation and culturing of microglia, with emphasis on the steps which are deemed most critical for obtaining pure and healthy cultures.

ISOLATION AND MAINTENANCE OF PRIMARY MICROGLIAL CELL CULTURES

MATERIALS

Solutions and Reagents

Coating Cell Culture Plates

1. 70% ethanol
2. Borate buffer
3. Borax (71997), Sigma, 3050 Spruce St. St. Louis, MO 63103;
4. Poly-L-lysine (P-1274), Sigma, 3050 Spruce St. St. Louis, MO 63103;
5. Autoclaved distilled water
6. Minimum Essential Medium (MEM) culture media, Gibco, Invitrogen, Grand Island, NY (11095)
7. Minimum Essential Media, with Earle's salts, modified for suspension cultures (S-MEM), Gibco, Invitrogen, Grand Island, NY (11385).

Mixed Glial Cell Isolation

1. 70% ethanol
2. Minimum Essential Medium (MEM) culture media, Gibco, Invitrogen, Grand Island, NY
3. Dissociation media
4. Heat inactivated horse serum Gibco, Invitrogen, Grand Island, NY (26050070)
5. Heat-inactivated fetal bovine serum, Gibco, Invitrogen, Grand Island, NY (10082-147).
6. Penicillin/Streptomycin, Gibco, Invitrogen, Grand Island, NY (15140-163).
7. Trypan blue staining solution, (T8154, Sigma)
8. Hank's Buffered Salt Solution (HBSS), H2387, Sigma

9. **Sigmacote**® (SL-2), Sigma, 3050 Spruce St. St. Louis, MO 63103.

Microglia isolation

1. 70% ethanol
2. Minimum Essential Medium (MEM) culture media, Gibco, Invitrogen, Grand Island, NY
3. Dissociation media
4. Heat inactivated horse serum Gibco, Invitrogen, Grand Island, NY (26050070)
5. Heat-inactivated fetal bovine serum, Gibco, Invitrogen, Grand Island, NY (10082-147).
6. Penicillin/Streptomycin, Gibco, Invitrogen, Grand Island, NY (15140-163).
7. Trypan blue staining solution, (T8154, Sigma)

Maintenance of Cultures

1. 70% ethanol
2. Heat inactivated horse serum Gibco, Invitrogen, Grand Island, NY (26050070)
3. Heat-inactivated fetal bovine serum, Gibco, Invitrogen, Grand Island, NY (10082-147).
4. Penicillin/Streptomycin, Gibco, Invitrogen, Grand Island, NY (15140-163).
5. Minimum Essential Medium (MEM) culture media, Gibco, Invitrogen, Grand Island, NY
6. Phosphate buffered saline (PBS) (554781, BD biosciences, San Diego, CA 92121, USA)

Equipment

Coating Cell Culture Plates

1. Autoclave
2. 6-well cell culture plate
3. Laminar-flow cell culture hood with ultraviolet (UV) light

4. Portable power pipette filler/dispenser

Mixed Glial Cell Isolation

1. Autoclave
2. Laminar -flow cell culture hood with ultraviolet (UV) light
3. CO_2 incubator (37°C, 95% room air/5% CO_2, 95% humidity)
4. Dissecting microscope
5. Low speed (60 rpm) stir plate
6. Low speed centrifuge (<1000 x g) with swinging bucket rotor and 50ml conical tube adapters
7. Portable power pipette filler/dispenser
8. Inverted phase-contrast microscope
9. Hemocytometer
10. Hand-held counter

Microglial isolation

1. Autoclave
2. Laminar -flow cell culture hood with ultraviolet (UV) light
3. CO_2 incubator (37°C, 95% room air/5% CO_2, 95% humidity)
4. Dissecting microscope
5. Low speed (60 rpm) stir plate
6. Low speed centrifuge (<1000 x g) with swinging bucket rotor and 50ml conical tube adapters
7. Portable power pipette filler/dispenser
8. Inverted phase-contrast microscope

9. Hemocytometer
10. Hand-held counter

Maintenance of Cell Cultures

1. Autoclave
2. Laminar -flow cell culture hood with ultraviolet (UV) light
3. CO_2 incubator (37°C, 95% room air/5% CO_2, 95% humidity)
4. Portable power pipette filler/dispenser

Disposable Tools for Animal Dissection and Cell Dissociation:

Mixed Glial Cell Isolation

1. Sterile pipettes, disposable borosilicate glass: 146 mm (5 ¾ inch) and 229 mm (9 inch)
2. Serological pipettes, cotton-plugged disposable borosilicate glass, 10 ml short length
3. Sterile 5 ml disposable syringes (53500-420 , VWR, Batavia, IL 60510, USA)
4. Syringe filter with 25 cm cellulose acetate membrane, 0.2 μm pore size (4612, Pall corporation, Ann Arbor, MI, 48103, USA)
5. Sterile serological pipettes, cotton-plugged disposable polystyrene, individually wrapped: 1 ml, 5 ml, 10 ml, and 25 ml (Midwest Scientific, 280 Vance Road, St. Louis , MO, 63088, USA)
6. Sterile vented cell culture flasks: 225cm^2 (353138, BD falcon, Franklin Lake, NJ, 07417, USA)
7. 4 x 3 inch sterile dressing sponges (82004-740, VWR, Batavia, IL, 60510, USA)
8. 15 ml polystyrene centrifuge tubes, sterile (21008-216, VWR, Batavia, IL, 60510, USA)

9. 50 ml polypropylene tubes, sterile (82018-052, VWR, Batavia, IL, 60510, USA)

Microglial isolation

1. Sterile serological pipettes, cotton-plugged disposable polystyrene, individually wrapped: 1 ml, 5 ml, 10 ml, and 25 ml (Midwest Scientific, 280 Vance Road, St. Louis , MO, 63088, USA)
2. 50 ml polypropylene tubes, sterile (82018-052, VWR, Batavia, IL, 60510, USA)
3. 6 well cell culture plate (353502**,** BD falcon, Franklin Lake, NJ, 07417, USA)

Maintenance of Microglial Cultures

1. Sterile serological pipettes, cotton-plugged disposable polystyrene, individually wrapped: 1 ml, 5 ml, 10 ml, and 25 ml (Midwest Scientific, 280 Vance Road, St. Louis , MO, 63088, USA)

Non-disposable Tools for Animal Dissection and Cell Dissociation:

Surgical apparatus is non-disposable and must be autoclaved before use. Clean it thoroughly immediately after use.

1. Dumont forceps (Pattern #5), 110 mm length, tip 0.1 x 0.06 mm, 2 each (25719-066, VWR, Batavia, IL, 60510, USA)
2. Curves forceps, 4 inch length, full curve, 0.8 mm tip width, 2 each (82027-392, VWR, Batavia, IL, 60510, USA)
3. Curves forceps, 4 inch length, full curve, 0.4 mm tip width, 2 each (82027-406, VWR, Batavia, IL, 60510, USA)

4. Micro-dissecting scissors, 4 inch length, 25 mm angled blade, 3 each (89049-674, VWR, Batavia, IL, 60510, USA)
5. Mayo scissors, 7 inch length, 50 mm curved blade (95039-258, VWR, Batavia, IL, 60510, USA)
6. 50 ml beaker and stir bar (length, 25 mm) *Cover top with foil prior to autoclaving*
7. Pipette sterilizing metal boxes: for 5 ¾ inch Pasteur pipettes, 9 inch Pasteur pipettes, and 10 ml glass serological pipettes (20171-042, VWR, Batavia, IL, 60510, USA)
8. Surgical instrument tray, autoclavable (62687-069, VWR, Batavia, IL, 60510, USA)

BASIC PROTOCOL

The algorithm is listed below:

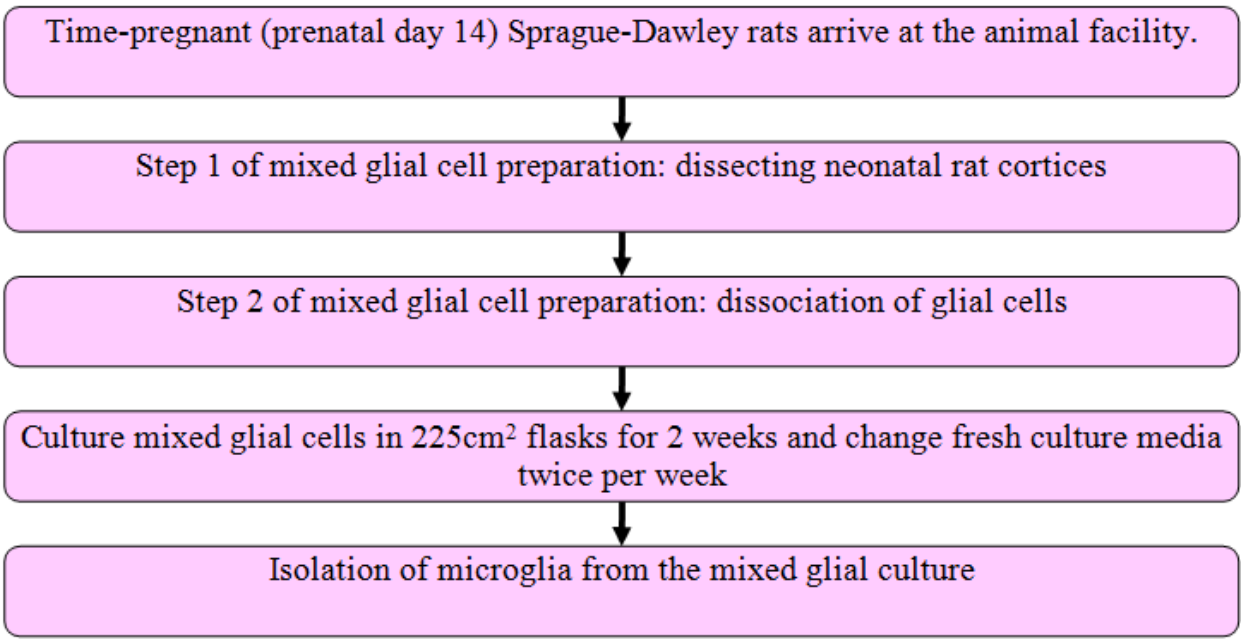

Time-dated Pregnant Rat Delivery Schedule

We schedule pathogen-free time-pregnant (prenatal day 14; PD14) Sprague-Dawley rats to arrive at the animal facility one week prior to their delivery date (PD21). The number of ordered pregnant rats is calculated based on the fact that one female Sprague-Dawley rat normally gives birth to 10-14 pups. The time-dated pregnant rat delivery allows us to isolate cultures on a consistent basis. We prepare cultures every Wednesday afternoon using 1-day-old pups, so we routinely order pregnant rats for Tuesday delivery to allow them to acclimate for a week prior to delivery. This also is cost effective, as we do not need to maintain our own breeding colony and incur extensive per diem charges. In the long run we find it cost effective as it also frees our staff and students from frequenting the animal facility for husbandry checkups, determination of plugs (PD1), etc.

Mixed Glial Cell Preparation

The protocol described here is composed of two continuous steps. The first step focuses on dissecting rat cortices and the second one entails the dissociation of glial cells including astrocytes, microglia and small amount of oligodendrocytes. These two steps should be performed consecutively.

Step 1: Dissection of Neonatal Rat Cortices

1. Gently hold and rinse the head and neck of the pup with 70% ethanol.
2. Decapitate the head on to a sterile gauze pad using sterile curved scissors. The body is placed in the bio-hazard plastic bag for disposal. The surgical apparatus is placed in the 70% ethanol between decapitations to avoid contamination.

3. Use sterile fine angled dissecting scissors to cut the skin as well as skull at a slight upward angle from the foramen magnum to the eyes along the midline. Extra caution is needed to avoid damaging the brain cortices. The skull flaps can be very easily cut off to simplify the removal of the brain tissue
4. With the 0.8 mm tip curved forceps sever the olfactory bulbs at the anterior part and the spinal cord at the posterior part of the brain. Gently move forceps with a slight back angle pulling up the brain. This will separate the whole brain from the skull base. *During the procedure, the optical nerves can be easily identified; it is not necessary to preserve them*.
5. Place the brain in HBSS in 100mm Petri dish on ice and observe the separated brain under the dissecting microscope.
6. Gently slip one side of the 0.4 mm tip curved forceps under the corticies on either side of the brain so the forceps sit astride the brain.
7. Gently move forceps from side-to-side and with a slight back angle pull up of the cortices. This will separate the cortices from the rest of the brain.
8. With the Dumont forceps, gently tease away the meninges coverings on the cortical surface without damaging it.
9. Flip over the cortices to expose the underside of the tissue to make sure remove any extra tissues.
10. You should be able to see the darker hippocampal crescents that need to be gently removed with the curved forceps.
11. Once each cortex is dissected, place in a sterile 50 ml conical tube containing 10 ml S-MEM + antibiotics on ice. *Limit the total procedure within 10 minutes to minimize the damage. We are able to finish the whole procedures within 5 minutes after practice.*

12. Repeat the same procedure in the rest pups.
13. Place the cortices in the 50 ml tube on ice until the desired number of pup brains has been dissected.

Step 2: Dissociation of Glial Cells

1. Carefully remove as much of the S-MEM as possible with a sterile cotton-plugged 9" Pasteur pipette taking care to retain all of the cortices.
2. Add 12 ml of 37°C dissociation media to the 50 ml beaker and gently pulverize the cortices 7 –8 times using a Sigmacote® treated (see Support Protocol 1) 10 ml glass pipette.
3. Stir for 10 minutes at low speed (1 revolution per second) in the laminar-flow hood.
4. While this is stirring, prepare two 15 ml sterile conical tubes for each extraction. Add 5 ml of growth media to each tube. At this time, also thaw the DNase I and place it on ice.
5. After ten minutes of gentle stirring, remove the beaker from the stir plate and place at a 45° angle for 2 - 3 minutes to allow the non-dissociated tissue to collect at the bottom of the beaker. *Resting the edge of the beaker on a lid from a culture dish works well.*
6. Carefully aspirate 10 ml of the dissociated cells with a Sigmacote® treated 10 ml glass pipette. *Take care not to disturb the undissociated tissue pieces.*
7. Place 5 ml into each of the two 15 ml centrifuge tubes containing the 5 ml of growth media. Invert the mixture 2 – 3 times to mix the cell suspension and growth media. *The serum in the growth media acts to inhibit dispase and prevents over digestion of the dissociated cells.*
8. Add another 10 ml of 37°C dissociation media to the 50 ml beaker and add 100 µl of DNase I. Continue to stir for another 10 minutes. *Note the DNase I is added only after the first extraction and is not added again.*

9. Place the 50 ml beaker at an angle for 2 –3 minutes, remove 10 ml of dissociated cells, and place 5 ml into another pair of 15 ml tubes containing 5 ml growth media as before.
10. Add another 10 ml of 37°C dissociation media to the tissue in the 50 ml beaker and stir for 10 minutes. (Do not add DNase I again.) *The removal of dissociated cells and replacement with 10 ml dissociation media is called an extraction.*
11. Extractions are repeated until there is only fibrous tissue remaining in the 50 ml beaker. *The number of extractions is usually equal to the number of dissected brains.*
12. Allow each pair of 15 ml conical tubes to sit undisturbed during the continuing extractions. *During this time, undissociated tissue will settle to the bottom of the 15 ml tube. This undissociated tissue is placed back into the 50 ml beaker for further dissociation during the final two extractions.*
13. To remove undissociated tissue from the 15 ml tubes, insert a sterile cotton-plugged Sigmacote® treated 9" Pasteur pipette to the bottom of the tube and carefully aspirate the undissociated tissue. Place this tissue back into the 50 ml beaker for further dissociation. *This is done only during the final two extractions because serum carried over from the completed extractions can inactivate the dispase.*
14. Once all of the extractions have been processed, pool the dissociated cells and media from the 15 ml centrifuge tubes into 50 ml conical tubes. Centrifuge the 50 ml tubes for 10 minutes at 500 rpm in a swinging bucket rotor to pellet the suspended cells.
15. Carefully aspirate the media from the cell pellets.
16. Resuspend the cells in 20 ml growth media per 50 ml tube by gentle pipetting with a 10 ml Sigmacote® treated glass pipette.

17. Allow cells to sit for an additional 5 minutes and remove any sedimented tissue as before with a 9" Pasteur pipette. Discard this undissociated tissue.
18. Pool the suspended cells into 50 ml tubes on ice.
19. Determine the total and viable cells by gently mixing 100 µl cells with 100 µl diluted trypan blue staining solution. Allow the cells to take up the trypan blue for 5 min and determine cell number and viability with a hemocytometer.
20. Dilute cell suspension to 10,000 viable cells/ml with growth media.
21. Pipette 2,500 viable cells/cm^2 into 225 cm^2 culture plates and then add growth media to the final volume of 75 ml.
22. Unlike culturing astrocytes, the media must not be changed until 7 days after plating to allow mixed glial cells to attach. *Approximately 5~ 10 % of the mixed glial cells plated will attach and grow on the coated plastic surface over the next 1.5~ 2.5 weeks.*
23. When changing media, insert the 5 inch Pasteur pipette and aspirate the media. *Change the Pasteur pipette frequently and when it may have touched anything but inside of the culture flasks. A pipette contaminated during media changes can easily infect the entire culture if it is not changed.*
24. Add 75ml fresh culture media to using a large disposable pipette.
25. Media is changed twice per week. If the culture media turn turbid, the cells should be discarded and the possibility of contamination should be suspected.

Isolation of Microglia from the Mixed Glial Culture:

1. Check the mixed glial cell culture under inverted phase-contrast microscope approximately 2 weeks after the initial plating, when astrocytes reach 100% confluence.

The microglia are growing on the top of single layer of astrocytes as small rounded cells. *Adjusting the fine focus of the microscope assists in distinguishing the different cell layers.*

2. Put the cell culture flask on the flatten surface and gently bang on the side and tap the flasks at the speed of 45 times per minutes. *Try to minimize the amount of foam generated when shaking the cell culture flasks.*
3. While tapping and shaking the cell culture flask, prepare the centrifuge. In our laboratory, we use a PRECISION Durafuge 200R centrifuge (PRECISION, 170 Marcel Drive, Winchester, VA, USA) and set the temperature to 4°C. *Based on our experience, it takes about 20 minutes to cool down from room temperature to 4°C. This may vary based on the type of centrifuge available to you so make sure it is ready for use at the appropriate temperature as you are isolating the cells to prevent any delays.*
4. Check the cell culture flask under the inverted phase- contrast microscope every 3 minutes to make sure the monolayer astrocytes are not disturbed and continue to adhere to the substratum of the flask.
5. The detached microglia float in the media, while the astrocytes remain attached to the bottom.
6. If attached microglia are observed, keep shaking the flasks until almost all microglia are floating. Using this method, after gentle shaking of the flasks for 9-12 minutes we are able to get almost all of the microglia without disturbing the adherent astrocytes.
7. If astrocytes are sheared from the bottom, immediately stop shaking the flasks. If the harvested cells are contaminated with significant amounts of astrocytes, this may be caused by two reasons: 1) shaking is too rigorous; 2) astrocytes are not sufficiently

healthy to remain attached to the substratum of the flask. If astrocytes readily detach from the flask consider changing fresh culture media more frequently (three rather than two times per week). *Please refer to the Troubleshooting section for additional details.*

8. After most microglia are detached, stop shaking and carefully aspirate the culture media and put it into pre-chilled 50 ml conical tube.
9. Spin down the cells at 1000 RPM at 4°C for 5 minutes using PRECISION Durafuge 200R (or a similar device) with a swinging bucket rotor to pellet the suspended cells.
10. Carefully aspirate the media without disturbing the cell pellets.
11. Resuspend the cells in 5 ml growth media per 50 ml tube by gentle pipetting with a 10 ml Sigmacote® treated glass pipette.
12. Pool the suspended cells into 50 ml tubes on ice.
13. Determine the total and viable cells by gently mixing 100 µl of cells with 100 µl of diluted trypan blue staining solution. Allow the cells to take up the trypan blue for 5 minutes and determine cell number and viability with a hemocytometer. *Stained cells are dead; those that exclude the trypan blue are considered alive.*
14. Dilute cell suspension to 20,000 viable cells/ml with growth media.
15. Pipette 5,000 viable cells/cm^2 into each well of six-well cell culture plates and add growth media to a final volume of 2ml/well.
16. The isolated primary microglia are maintained in a CO_2 incubator (NAPCO series 8000DH, Thermo Scientific, San Diego, CA 92121, USA) (37°C, 95% room air/5% CO_2, 95% humidity) for 48 hours before the experiments are initiated. *Our experience dictates the purity of isolated microglia culture is >95% [immunostaining for the microglial specific marker, OX42 (Fig 1)].*

17. The leftover cells in the culture flasks are mainly astrocytes and they are removed by trypsinization. The protocol introduced here is ideal for the concomitant isolation of both microglia and astrocytes. The detailed protocol of isolation and culturing primary astrocytes has been published by our laboratory before [208]. Trypsin is most effective at a pH between 7.0 and 8.0 and between 24°C and 37°C at 0.05 % to 0.5 % concentration. The trypsinization time required for cells removal from the plates depends on their density, serum concentration and temperature. EDTA is often added to the trypsin to intensify enzyme activity by chelating calcium and magnesium.
18. Add 10 ml of warm phosphate buffered saline (PBS) and rock the flask to wash he monolayer briefly. This assures the removal of the last traces of serum. Astrocytes should not be left in PBS for more than 10 minutes to avoid excessive cell damage.
19. Aspirate the PBS with a Pasteur pipette.
20. Add 2ml 1X trypsin (37°C) and rock the flask gently to cover the entire surface with trypsin.
21. Leave the flask in a CO_2 incubator (37°C, 95% room air/5% CO_2, 95% humidity) for 5 minutes.
22. When the cells are loose, add 10 ml of fresh culture media with serum and resuspend the cells.
23. Dilute cells to 10,000 viable cells/ml growth media.
24. Pipet 2,500 viable cells/cm^2 into each well of the six-well cell culture plates and add growth media to a final volume of 2ml/well. The isolated astrocytes are maintained at CO_2 incubator (37°C, 95% room air/5% CO_2, 95% humidity) for 5 minutes. *The purity of*

astrocytes in our hands reaches >95%. We routinely test the purity by immunohistochemistry staining for the astrocyte specific marker, GFAP (Fig 2).

Support Protocols:

Support Protocol 1: Fire Polishing and Sigmacoat® Treatment of Pipettes for Cell Isolation

The fire polished and Sigmacote® treated pipettes are only used for cell isolation, not routine changing of media. These pipettes need to be fire polished and Sigmacoat® treated. In our laboratory, we routinely fire a batch of 50 pipettes for each planned microglial cell isolation.

1. Fire polished tips of 9 inch Pasteur pipettes by placing the small end in an open flame from a Bunsen burner for a few seconds. This will slightly melt the borosilicate glass and will produce a smooth tip to the pipette which helps prevent damage to the cells. *Take care not to make the diameter of the opening too small as this can increase the shear forces during triturating and may lead to increased cell damage*.
2. Plug the large end of the Pasteur pipettes with cotton. *The amount of cotton obtained from a single cotton tipped swab is sufficient for each pipette.*
3. Treat each pipette with Sigmacote® by drawing the viscous solution up into the Pasteur pipette without touching the cotton plug. Allow the Sigmacote® to drain back into the bottle and place the Pasteur pipette in a beaker with paper towels lining the bottom to drain and dry completely.
4. Once the Pasteur pipettes are dried, place them in a metal container and autoclave.10 ml glass serological pipettes should also be Sigmacote® treated and autoclaved. Fire polishing of these pipettes is unnecessary.

Supporting Protocol 2: Coating Cell Culture Plate with Poly-L-Lysine.

We routinely culture isolated microglia in the poly-L-lysine coated six-well cell culture plate. Prepare borate buffer according the following recipe:

1. prepare coating buffer by dissolving 2mg poly-L-lysine into 50ml borate buffer;
2. add 1 ml coating buffer into each well;
3. let it stand for 1 hour in the tissue culture hood with UV light on;
4. aspirate the coating buffer and wash the well with distilled water for three times
5. air dry the cell culture plate in the tissue culture hood for at least one hour with UV light on;
6. Add 1 ml MEM culture media without antibiotics or serum into each well and store the plate in 4°C. The coated plate could be stored safely for one week.

REAGENTS AND SOLUTIONS

Reagents:

1. Culture Media:

Minimal Essential Medium, with Earle's salts and L-Glutamate (MEM), Gibco, Invitrogen, Grand Island, NY (11095)

Minimal Essential Media, with Earle's salts, modified for suspension cultures (S-MEM), Gibco, Invitrogen, Grand Island, NY (11385). S-MEM has been modified to contain no Ca^{+2} which can produce cell clumping due to interactions of extracellular matrix proteins.

2. Antibiotics:

Penicillin G (10,000U/ml)-Streptomycin Sulfate (10,000 μg/ml), Gibco, Invitrogen, Grand Island, NY (15140-163). Avoid repeated freeze- thaw cycles of penicillin/streptomycin by storing 10ml aliquots at -20°C. 10 ml penicillin/streptomycin is enough for 1 L of media.

Fungizone® (Amphotericin B, 250 μg/ml), Gibco, Invitrogen, Grand Island, NY (15290-018). Fungizon *i*s optional, to prevent fungal or yeast contamination.

3. ***Serum:***

Heat-inactivated horse serum, Gibco, Invitrogen, Grand Island, NY (26050070)

Heat-inactivated fetal bovine serum, Gibco, Invitrogen, Grand Island, NY (10082-147). Avoid repeated freeze-thaw cycles of serum. Put the frozen serum in the water bath no warmer than 40°C until serum is thawed. The thawed serum could be safely stored at 4°C for approximately one week.

4. Protease (dispase), Gibco, Invitrogen, Grand Island, NY (17105-041).

5. Deoxyribonuclease I (DNase I) from Bovine Pancreas Type IV, Sigma Chemical Company, St. Louis, MO (D-5025). DNase I is added immediately after the first extraction to prevent the genomic DNA released by damaged cells from making the dissociating media too viscous during the ongoing digestion. Avoid vortex when handling DNase I as it is vulnerable to inactivation by physical damage.

6. Poly-L-lysine Hydrobromide (P-1274), Sigma, 3050 Spruce St. St. Louis, MO 63103.

7. Trypan blue 0.4%, liquid, sterile-filtered, cell culture tested (T8154). Trypan blue is used determine cell viability. Dead or damaged cells cannot exclude trypan blue, so they appear blue under the microscope.

8. Sigmacote® (SL-2), Sigma, 3050 Spruce St. St. Louis, MO 63103. Sigmacote is a special silicone solution in heptane that readily forms a covalent, microscopically thin film on

glass, retards clotting of blood or plasma. It bonds with the uneven surface of the glass pipettes and provides a smooth hydrophobic barrier. The adherence of cells to the glass surface is greatly reduced, and thus minimizing physical damage to the cells.

9. Distilled Water, cell culture tested, Gibco, Invitrogen, Grand Island, NY (15230-147). All solutions used in this protocol should be prepared in cell culture tested double distilled water.

10. Boric Acid, J.T.Baker, 222 Red School Lane, Phillipsburg, NJ (10043-35-3).

11. Borax (71997), Sigma, 3050 Spruce St. St. Louis, MO 63103.

CRITICAL PARAMETERS

Dissecting neonatal rat cortex: The meninges should be completely removed; otherwise the mixed glial culture may become contaminated with large amount of fibroblasts as the proliferation of fibroblast is much faster than glial cells. An efficient surgical technique is critical for obtaining high quality tissue dissection. Avoid spending more than 10 minutes on dissecting brains to minimize the ischemic damage to the brain tissue.

Dissociation of cells: According to our experience, there is significant variability in the quality of dispase used in this protocol. In general, if a rapid and continuing decrease in cell number or viability is observed, dispase should be changed to newly purchased lots. The use of Sigmacote® treated glass pipettes greatly enhances the quality of dissociated cells because it significantly reduces the trauma to cells during the isolation process. We have observed that harsh maneuver results in a large reduction in the cell viability.

Isolation of Primary Microglia: In general, isolation of microglia by shaking flasks should be gentle to avoid forceful trituration that introduces air bubbles into the suspensions. It is important to change culture media twice a week (or more, should astrocytes detach from the substratum during the tapping process) to keep cells healthy; otherwise, astrocytes could be sheared during the isolation procedure very easily. Keep checking the cells under the inverted microscope every 3 minutes in order to minimize the amount of astrocyte contamination.

Cell Culture Purity: The primary microglial culture obtained by our protocol is routinely >95% positive for OX 42 [209] by immunohistochemistry (See Figure 1). Unlike non-glial cells, microglia should be cultured in Poly-L-lysine or collagen I coated plates. It has been suggested that using rat pups 24 to 48 hours old may decrease the number of contaminated neurons [210]. The small spikes in primary microglia could be very easily observed under microscope with DIC settings (Fig 1).

Coating Material: Primary microglia should not be cultured on uncoated plastic surface or glass surface. In our laboratory, we used both poly-L-Lysine and collagen I coated cell culture plates. One of the unique features of primary microglia is that the phenotype could be different based on different coating materials. Cells are wide spread on Poly-L-lysine coated surface, but microglia grow in clusters on the collagen I coated surface. Therefore, choosing which coating material to use should be carefully considered within the context of the experimental design.

Culture Time: Unlike malignant cells, primary microglia stop proliferating and growing once confluence is reached. Consideration should also be directed at the possibility that different

confluence level may cause significant variations in experiment results [144]. Therefore, it is strongly recommended that the effects of confluence be determined by treating cultured microglia at different confluence levels. Furthermore, experiments should be conducted in triplicates (at a minimum) derived from several independently isolated cultures. Experiments must use cultured cells at the same confluence in order to minimize this confounding factor. At our hands cultured microglia reach 50% confluence two weeks after isolation from the mixed glial culture preparations.

Contamination: If the culture media turn turbid, contamination should be suspected and all infected culture flasks must be disposed immediately. Rapid and accurate identification of the offending microbe is very helpful, but rarely could be done in the laboratory settings. The most common pathogenic microbial include *Staphylococcus aureus*, *Staphylococcus epidermidis* or *Streptococci*, though some rare microbe could be possible such as microplasma, fungi or viruses. The contamination caused by microplasma or viruses could be very difficult to identify because the culture media do not turn turbid. The only sign of microplasma or virus infection is that a large number of cells fail to attach to the substratum. The microbial contamination is most likely to occur during the initial cell isolation, thus sterilization of surgical tools and cleaning of all surface with 70% ethanol are critical to minimize microbial contamination.

TROUBLESHOOTING

Clumping of cells during the extraction: Cell clumping causes significant cell damage during the cell isolation. Ca^{2+} in the regular MEM could interact with the extracellular

proteins, which lead to cell clumping. The cell clumping should be differentiated from tissue sedimentation by its size. Cell clumping is much smaller than tissue sedimentation and checking the sedimentation under microscope could be very easily tell them apart. It is recommended to use S-MEM without Ca^{2+} during cell isolation to prevent cell clumping.

Media becomes very viscous during extraction: It is caused by genomic DNA release from damaged cells and adding DNase I immediately after the first extraction could very well solve it. The DNase I solution should not be vortexed as it is vulnerable to inactivation by physical damage.

Large area of monolayer of astrocytes sheared off during isolation of primary microglia: It is most likely caused by too vigorous shaking of the cell culture flask, especially if the researcher has limited experience in the isolation procedure. We recommend starting with less vigorous physical maneuver and checking the cells under the inverted microscope every three minutes, adjusting the level of vigorousness based on the isolation outcome. Changing the old with fresh culture media could also help to mitigate this problem.

COMMENTARY

Background Information

Microglia play a critical role as resident immunocompetent and phagocytic cells, serving as scavenger cells in the event of infection, inflammation, trauma, ischemia and neurodegeneration. Thanks to the advancement of cell culture techniques, research on the biochemical, physiological, pharmacological and molecular aspects of microglial function are possible. The

culture technique provides an ideal model to study the microglial function under controlled and reproducible conditions.

Given the wide array of microglial functions, the possible uses for primary cultures are endless. A brief list includes, studies on the role of microglia in immunity [211], protective effects of microglia on co-cultured neurons [212], modulators of microglial secretion of growth factors [213] and cytokines [155, 214], and the role of free-radicals production in neuropathology [156], just to name a few. The receptors of microglia contribute to the modulation of CNS microenvironment and functions. For example, the main functional ionotropic glutamate receptors (iGluRs) in cultured rat microglia are mostly AMPA (D,L-α-amino-3-hydroxy-5-methyl-4-isoxazole propionic acid) receptor, which inhibits TNF-α release and helps to modulate glutamate level in the CNS. Furthermore, perturbations in the homeostasis of this transmitter have been reported in neurodegenerative diseases [215]. Microglia also express $GABA_B$ (γ-aminobutyric acid) receptor that inhibits IL-6 release from the activated microglia [215]. In addition, these cells express a variety of purinergic receptors ($P2Y_{12,}$ $P2Y_{6,}$ $P2Y_7$ AND $P2Y_4$), which regulate the migration and cytokine release. Furthermore, microglia exhibit anti-inflammatory effects by expressing adrenergic, dopaminergic and cholinergic receptors [215]. Studies on the function of the above parameters are all amenable to in vitro cultured microglia, and indeed, over the last several decades a plethora of experimental approaches have enriched our understanding on the role of these cells in health and disease.

Though microglial cells can be readily isolated and have clearly received experimental attention, many studies have utilized microglial cell lines instead of primary cells to test their functions in

various physiological and pathological conditions[144]. Although immortalized cell lines, such as murine N9 are less expensive and less time consuming to prepare and maintain, and there is less culture- to- culture variation in these cell lines, it needs to be considered that cell lines are derived from either tumors or are genetically modified to proliferate unlimitedly. Thus results generated from cell lines may lead to erroneous interpretations. Primary microglia have advantages over the immortalized cells more closely representing their in situ counterparts. However, analogous to any type of cultured cells, one must be cautious when relating processes seen in cultured microglia and extrapolating to *in vivo* conditions as primary cells are grown in isolation and lack the normal CNS microenvironment. The interaction between multiple cell types in the brain such as neurons, astrocytes, oligodendrocytes and microglia is exceedingly difficult to be modeled *in vitro*. Regardless what isolation protocol is used (for additional methods see below), it is important to keep in mind that one must be cautious in correlating the *in vitro* data generated from cultured primary microglia with their physiological and pathological profile in living animals. Issues related to the advantages and disadvantages offered by cell cultures have been previously addressed and apply to any cell type.

There are additional published methods to isolate primary microglia. Frank and Maier [216] reported a density gradient centrifugation method of homogenized hippocampal tissue in a 0/50/70% Percoll (Amersham Biosciences, Uppsala, Sweden) gradient that yields enriched rat primary microglia. The primary microglial cells are located at the 50/70% Percoll interface. The disadvantages of this protocol include long centrifugation (45 minutes) at 20°C as well as the homogenization of brain tissue before the spin down. The homogenization procedure may cause excessive cell damage and the subsequent long spin down time may further decrease the

microglial yield, thus selecting for a specific (potentially hardy) microglial phenotype. Hassan and Douglas introduced another protocol to isolate human [217], mouse [218] and rabbit [219] primary microglia using orbital shaker. Briefly, flasks with the mixed glial culture are shaken in an orbital shaker for 16 h at 150 rpm at 37°C. The supernatant media are then centrifuged for 10 minutes at 1,200 r.p.m at 4°C. This method is short and saves labor, and also yields large amounts of primary microglia. Nevertheless, the sequalae of 16 h shaking on the functional and morphological properties of microglia needs to be considered and evaluated.

We do not recommend passaging of the mixed glial cell cultures. One may consider trypsinizing mixed glial cultures, splitting cells into more culture flasks and allowing them to grow until confluence (passage of cells). Although this will result in a greater glial cell yields, it should be considered that cell passaging may change their biochemical and immunological phenotypes (Cole and de Vellis, 1992). Therefore, we do not recommend this approach and advocate fresh isolations of microglia to obtain a constant supply of primary cells. .

Regardless what isolation protocol used, it is important to keep in mind that one must be cautious to correlate the in vitro data generated from cultured primary microglia with the physiological and pathological profile in the living animals.

ANTICIPATED RESULTS

The protocol described above results in the isolation of microglial cultures that exceed 95% purity [by immunohistochemical staining for the specific marker, OX42 (Fig 23)]. The primary microglia seeded and grown on Poly-L-lysine coated plastic surface do not grow in clusters, so

that fine structures on the cell membrane could be observed in detail (Fig 25A). Conversely, cultured primary microglia seeded on Collagen I grow in clusters (Fig 25B). Cell yields reach 1,000,000 microglial cells per brain with viability approximating 90%. Most isolated primary microglia (>90%) adhere to the coated cell culture plates 24 hours after the isolation. The fresh culture media can be changed 72 hours after initial isolation if necessary. Our experience dictates that 6,000,000- 8,000,000 cultured primary microglia provide ample RNA or protein for most real-time PCR or western blot procedure.

THE CONSIDERATIONS

The total time spent on the preparation of mixed glial culture is approximately 6 hours depending on the number of extractions performed and the number of rat pups used. The mixed glial cell culture is maintained in 225 cm^2 cell culture flasks on average for 2 weeks (dependent upon the endpoint of your experiment; obviously if you desire to study developmental changes, you may study the cells at earlier time points, keeping in mind that replicates should be at the same developmental stage and confluence). The twice weekly changing of media takes about 2 hours based on the number of flasks. It is recommended to feed the cells more frequently if the astrocytes adhere to the bottom very loosely. The isolation of primary microglia usually takes about 3 hours.

Fig 23

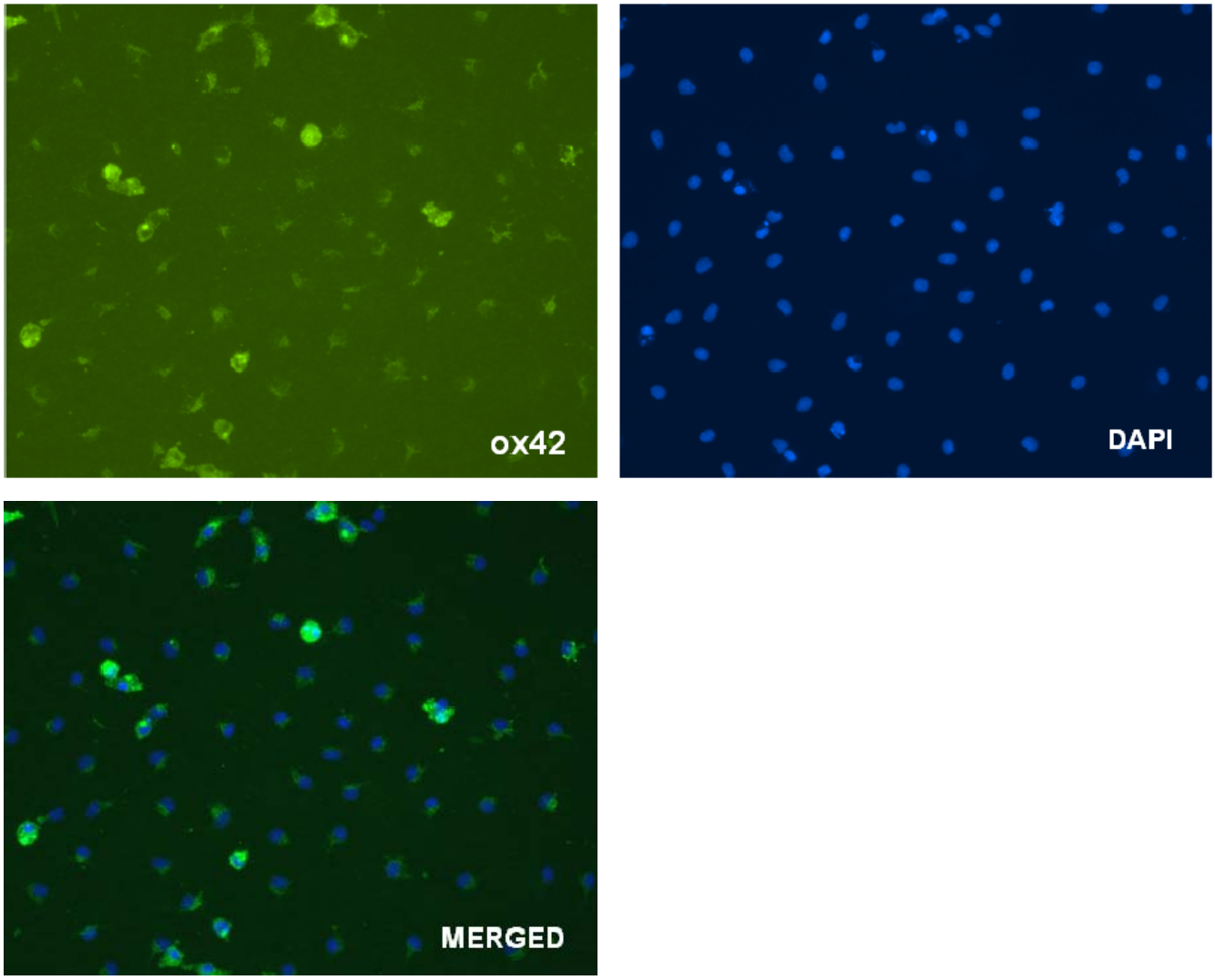

The purity of isolated primary microglia exceeds 95% as verified by immunohistochemistry staining for the microglia specific marker, OX 42. The nuclei are counterstained with 4',6-diamidino- 2- phenylindole (DAPI).

Fig 24

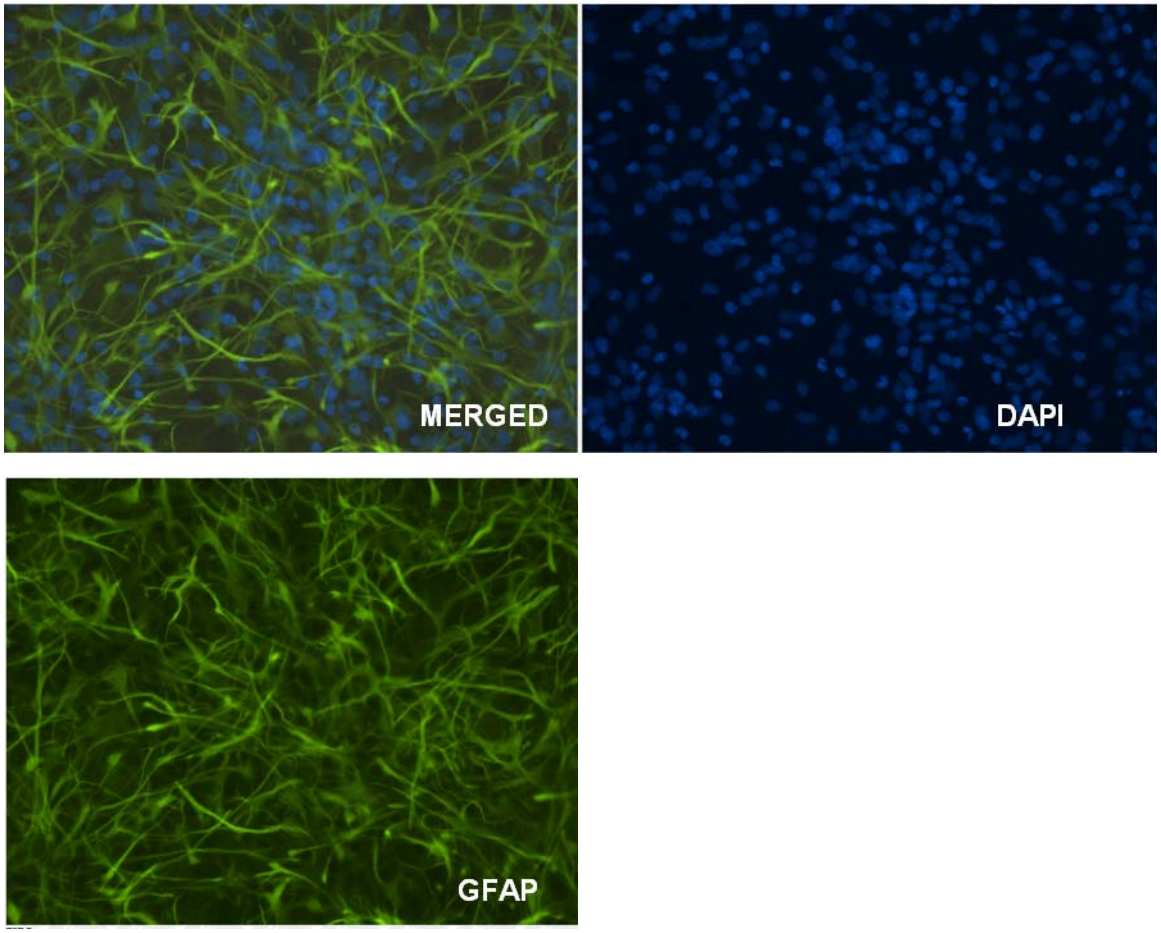

The purity of leftover astrocytes exceeds 95% as verified by immunohistochemistry staining for the astrocyte specific marker, GFAP. The nuclei are counterstained with DAPI.

Fig 25

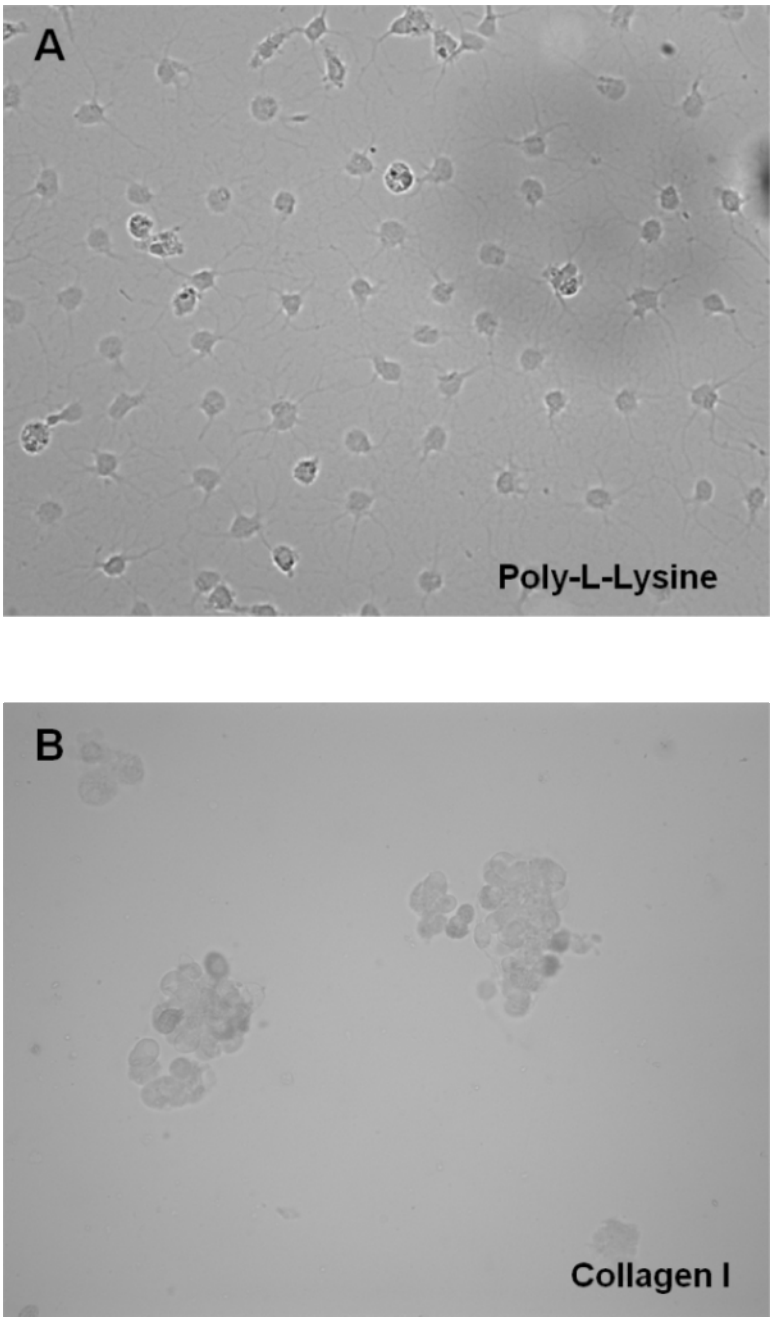

DIC images of cultures primary microglial cells. Fig. 25A shows the isolated primary microglial cells cultured on Poly-L-lysine coated plastic surface and Fig. 25B shows the cells cultured on Collagen I coated surface. Different coating materials produce different morphological attributes in these cells. In general, cells are widely spread when grown on poly-L-lysine (Fig. 25A) coated plastic surface with small spikes easily observed. Collagen I causes the microglia to grow in clusters (Fig. 25B).

B. Book chapter: Developmental Toxicity and Molecular Changes Induced by MeHg Exposure in Laboratory animals and humans.

This chapter has been published in

Chapter 34, Section 7,

Reproductive and Developmental Toxicology

Introduction

Human exposure to mercury (Hg) is mainly in the form of methylmercury (MeHg) predominantly from the consumption of fish [12-14]. Nearly all fish contain detectable amounts of MeHg (Clarkson et al, 1988). MeHg enrichment in the aquatic food chain is not uniform and is dependent upon water Hg content, bottom sediments, water pH and redox potential, the species, age and size of the particular fish. Furthermore, environmental conditions, such as anoxia, favor the growth of microorganisms and increase the methylation rate of Hg [15] and, by inference, its accumulation in fish. The mechanisms of Hg methylation in oceans and waterways are not fully understood.

The aims of this chapter are to outline the kinetics of organic mercury (MeHg) in humans and the toxic effects of MeHg on the developing fetal central nervous system (CNS) as well as on other organ systems. Herein, we also briefly review the differences in MeHg-induced brain damage between the fetus and the adult. The focus of the review is to highlight several of the proposed mechanisms of MeHg toxicity in the developing organism and discuss directions for future studies to address current gaps in the literature, enhance and expand our knowledge of

the underlying mechanisms of MeHg toxicity and its effects upon the environment, animals and humans.

Historical Background

Catastrophic epidemics due to environmental MeHg contamination in Japan [5, 6] and Sweden [16] have been previously reported. Exposure was also documented in Iraq, where locals consumed bread prepared from seeds treated with a fungicide containing MeHg [25], causing a large outbreak of human poisoning. Similar incidents have occurred in Pakistan, Guatemala and Ghana [220]. School children living in polluted areas have been found to exhibit diskinesia and intellectual disturbances [17]. The initial symptoms of classic congenital Minamata disease due to MeHg exposure were mental retardation, primitive reflexes, coordination disturbance, dysarthria, limb deformation, growth disorder, chorea-athetose and hypersalivation [18]. These symptoms occurred at Hg exposure levels exceeding the U.S. EPA RfD of 0.1 μg/kg body weight/day (an exposure without recognized adverse effects). As mentioned earlier [see also 2000 National Health and Nutrition Examination Survey (1999–2000 NHANES)], given that 8% of U.S. women of child-bearing age have blood Hg concentrations exceeding 5.8 μg/L (level equivalent to the current RfD), the total impact of exposure to Hg upon human populations is of considerable significance and may have tremendous societal consequences, affecting more than 300,000 newborns annually in the U.S. alone. It is reasonable to suggest, considering the magnitude of potential susceptible populations as well as the long latency period for the development of Hg-induced symptoms, that the true number of those affected is even greater than this conservative estimate.

Toxicokinetics in humans

The kinetics of MeHg in the human body is summarized in figure 1. MeHg derived from food or occupational exposure is efficiently absorbed (90%) and has a long retention time (half-life of ~70 days). After ingestion, the distribution to the blood compartment is complete within 30 hours, and the blood level accounts for about 7% of the ingested dose [19]. Circulating MeHg accumulates predominantly in red cells where it binds to cysteinyl residues (-SH) on the hemoglobin beta-chain [20], and is then slowly distributed reaching an equilibrium with other tissues at ~4 days [19].

In the brain, MeHg undergoes slow demethylation and is converted to inorganic mercury (IHg) [102]. About 10% mercury is retained in the brain Following a long-term exposure to MeHg accumulated inorganic mercury is deposited in the cortex of the calcarine sulcus of the female *Macaca fascicularis* [102], similar to prolonged subclinical exposure in humans. Mercury is not universally distributed and is deposited in certain central nervous system (CNS) cell types. Tissue staining following six months of exposure to MeHg reveals the largest IHg deposits in astrocytes and microglia. The total mercury accumulation in neurons are significantly lower than those present in the glial cells and increase with length of exposure; virtually all neurons are labeled following 18 months of exposure. In contrast, endothelial cells and pericytes do not contain notable mercury deposits, and deposits in oligodendrocytes are rarely observed. These data are consistent with the hypothesis that the neurotoxicity of MeHg is mediated, at least in part, by glial cells and that glial-neuron interactions play important roles in the process. Notably, staining of mercury deposits in IHg-exposed animals is lower compared to MeHg-exposed

animals, supporting the observation that it is the organic form of mercury that more readily crosses the blood-brain barrier (BBB) [102].

MeHg is incorporated into the hair during its formation. The MeHg concentration in blood and hair reflects the body burden, with a blood/hair concentration in humans approximating 1/250 under steady-state conditions (Skerfving, 1974). The net mercury excretion rate in humans is approximately 1% of the body content at non-symptomatic body burden level [22]. Most of the MeHg is eliminated through the liver into the bile and through the kidney into the urine. But most MeHg undergoes enterohepatic circulation by reabsorbtion from the bile in the gut. Slower urine excretion of MeHg in female versus male rats has been reported to result in higher toxicity [23]. Diet can affect MeHg excretion rate, since certain dietary components can interfere with MeHg reabsorption in the lower part of the intestines, thus breaking up the enterohepatic circulation [24].

Approximately 5% of the total MeHg in the maternal blood is found in breast milk [25], but the risk of MeHg exposure to infants through breast feeding declines rapidly during lactation, which is due to the rapid decrease in mercury transferred through breast milk postpartum and the fast growth of infants after birth [26]. MeHg crosses the placenta and accumulates in the fetus at concentrations higher than in the mother. For example, neonatal cord blood MeHg is more than twice as high as the level in maternal blood at delivery, but infant blood MeHg levels decrease significantly during the first 13 weeks of the infant's life, and, at three months, maternal MeHg concentrations are higher than those of the infant, opposite to the situation at parturition [26].

The rapid decline in infant MeHg concentrations postpartum can be explained by lower mercury transfer through breast milk and rapid infant growth after birth [26].

Hg is covalently bound to the carbon moiety in MeHg (CH_3-Hg^+). The carbon-Hg bond is chemically stable because of the low affinity of Hg for oxygen. MeHg does not exist as a free, unbound cation in biological systems (except an infinitesimal amount as governed by the law of mass action) [29], and the organic form is highly soluble in organic solvents and lipids. MeHg has a remarkably high affinity for the anionic form of –SH groups (log K, where k is the affinity constant and is on the order of 15–23) [29]. Despite the high thermodynamic stability of the MeHg-SH bond, very rapid exchange of MeHg between –SH groups is known to occur [31]. In cells, MeHg can form a complex with the –SH-containing amino acid cysteine [30]. The MeHg-S-Cys complex closely mimics the structure of the neutral amino acid, methionine, and is therefore a substrate of the L type large neutral amino acid transporter system (LAT1) [32]. This mimicry is responsible for MeHg uptake into cells. MeHg crosses the placenta via a similar neutral amino acid carrier, accumulating in fetal blood in a time- and dose-dependent manner [33].

Over-expression of LAT1 in CHO-k1 cells has been shown to be associated with enhanced uptake of [^{14}C]-MeHg when the cells are treated with $_L$-cysteine, but not with the $_D$-cysteine conjugate. In the presence of excess $_L$-methionine, a substrate for LAT1, $_L$-cysteine-conjugated [^{14}C]-MeHg uptake was significantly attenuated. Knock-down of LAT1 decreases the uptake of $_L$-cysteine-conjugated MeHg and attenuates the effects of MeHg on lactate dehydrogenase (LDH) leakage and CHO-k1 cell viability [32]. Notably, different neutral amino acids have

different suppression effects. For example, the suppression by methionine is not as remarkable as that produced by phenylalanine. This phenomenon could be due to the transient rapid cysteine surge after methionine administration, but not after phenylalanine administration. This newly synthesized cysteine in maternal blood accelerates the mercury uptake across the placenta.

Mechanisms of MeHg Neurotoxicity

As mentioned previously, MeHg has been found to bind to protein –SH groups of amino acids, such as cysteine, which is also present in glutathione (GSH) [221]. This affinity for the sulfur and sulfhydryl groups (–SH) is a major factor underlying the biochemical and toxic properties of MeHg and its interference with optimal cell function. A large body of research aimed at deciphering the cellular and molecular mechanisms of MeHg-induced neurotoxicity points to several critical features, namely: 1) inhibition of macromolecule synthesis (DNA, RNA and protein); 2) microtubule disruption; 3) increase in intracellular Ca^{2+} with disturbance of neurotransmitter function; and 4) oxidative stress. Nonetheless, MeHg's primary site of action and the genetic bases of its neurotoxicity have yet to be identified. A brief review outlining the most critical features of the mechanisms involved in MeHg-induced neurotoxicity follows.

MeHg reacts with DNA and RNA, resulting in changes in the secondary structure of these molecules [222]. Since the 1990s, epidemiological studies have suggested increased genotoxicity in human populations through dietary and occupational exposure [223]. MeHg inhibits DNA repair mechanisms, thereby leading to genotoxicity. For example, MeHg directly binds to the "zinc finger" core of DNA repair enzymes, affecting their activity. The "zinc finger" proteins contain an atom of zinc and four cysteines and/or histidines. Thus, the high affinity of mercury to

sulfhydryl groups on cysteines may deform the structural integrity and activity of these enzymes [79]. MeHg could also give rise to disturbances in protein synthesis [82, 93, 224, 225]. On the other hand increased protein synthesis due to reactive astrogliosis, has been reported after *in vivo* exposure to MeHg [226].

The inhibition of the polymerization of tubulin by MeHg is among the major mechanisms of developmental MeHg toxicity [80]. Microtubular fragmentation has been reported in cultured primary rat cerebellar granular neurons at a MeHg concentration of 0.5–1 μM [81]. Additionally, it has been reported that 4 μM mercury salt, independently of the anion, is capable of inhibiting the polymerization of isolated tubulin in a dose-dependent manner. Further, 0.1 μM mercury salt is sufficient to decrease kinesin-driven motility and to produce a significant increase of micronuclei in V9 hamster lung fibroblasts [227]. Since microtubules participate in cell division, their fragmentation by MeHg results in antimitotic effects, as well as the inhibition of neuronal migration and the degeneration of neuritis [82], all of which are inherent to developmental MeHg exposure outcomes.

MeHg depolarizes the presynaptic membrane, increasing Na^{2+} and decreasing K^{+} ion concentration. This, in turn, causes disruption of Ca^{2+} homeostasis leading to increased intracellular Ca^{2+} concentration [85, 86]. Blockers of voltage-dependent Ca^{2+} channels prevent the appearance of neurological signs [228]. Increased Ca^{2+} concentrations disrupt neurotransmitter signaling. Increased release of dopamine, glutamate, γ-amino butyric acid (GABA), glycine, choline [87] and acetylcholine [88] have been associated with MeHg exposure. Inhibition of the uptake of excitatory amino acids, such as glutamate and aspartate, has

also been implicated as a major mechanism of MeHg-induced neurotoxicity [89, 90]. Antagonists of the *N*-methyl-D-aspartic acid receptor have been reported to inhibit the toxic effects of MeHg [229].

MeHg also alters the cellular energy metabolism. Chen [230] reported that highly enriched Hg concentrations were found in mitochondrial fractions from Hg- exposed porcine cells. Yin [107] reported that MeHg causes a concentration-dependent reduction in the inner mitochondrial membrane potential ($\Delta\Psi m$) of primary cultured astrocytes. MeHg stimulates the ubiquinol: cytochrome C reductase complex (complex III) on the mitochondrial membrane [91], while inhibiting glutathione peroxidase (GPx) [92], which leads to lipid peroxidation. Fox [231] and Verity [93] further reported that MeHg inhibited state 3, but increases state 4 respiration, inhibiting tri-carboxylic-acid (TCA) cycle activity and decreasing ATP utilization. In brain tissues, MeHg affects respiratory control in synaptosomes both *in vitro* and *in vivo* [93, 231]. Effects on mitochondrial respiration in the brain have also been reported [93, 94], causing the inhibition of glycolysis and tri-carboxylic-acid cycle activity and a decrease in adenosine triphosphate utilization. Since the CNS is strictly dependent upon glucose for its energy production, high oxygen utilization and excitability renders it especially susceptible to toxins.

Disruption of redox cellular homeostasis by excess reactive oxygen species (ROS) formation leading to cumulative oxidative stress represents an important feature of MeHg neurotoxicity. MeHg is known to induce oxidative stress [232] both *in vitro* and *in vivo* [95-97, 150, 233]. The production of ROS by MeHg exacerbates toxicity by facilitating cell death via apoptotic pathways. Inhibition of glutathione peroxidase (GPx) by MeHg further potentiates lipid

peroxidation. Conversely, several studies have demonstrated partial amelioration of MeHg toxicity in the presence of antioxidants [150, 158, 234, 235]. A major source of MeHg-increased ROS generation is the mitochondrial electron transport chain. The damaged mitochondrion increases oxidative stress, leading to a decrease in defense mechanisms. It has also been reported that blockage of the mitochondrial transition pore by cyclosporin A in brain synaptosomes decreases MeHg-induced ROS production [236]. MeHg binds to GSH, which is one of the principal endogenous antioxidants, and this binding is responsible for the excretion of MeHg. Thus, decreased GSH levels parallel the increased oxidative stress caused by MeHg [237-239]. Upregulation of GSH is neuroprotective against MeHg-induced neurotoxicity [240].

Toxicity

MeHg Toxicity in Developing Brains

The brain is the primary target site for MeHg [71], and MeHg effects on the developing CNS are more severe than those in the mature CNS [72, 73]. There is usually a latent period of weeks to months between exposure and the onset of symptoms [220]. In less severe cases, psychomotor retardation and increased incidence of seizures have been reported [241]. In general, MeHg poisoning results in focal damage in adults and widespread and diffuse damage in the fetal and neonatal brain [74], likely reflecting the dynamic nature of the developing CNS (cell division, migration, differentiation, synaptogenesis). For example, the brain areas most vulnerable to MeHg after adult exposure include the primary sensory and motor cortices, pre- and post-central gyri, the temporal transverse gyrus and the cerebellum (but not Purkinje cells) [75]. In contrast, upon congenital exposure to MeHg, damage is more widespread, resulting in cortical atrophy, thinning of the corpus collosum and white matter shrinkage. Hematoxylin and eosin stain has

established diffuse spongiosus in the deeper layers as well as gliosis with loss of neurons in the upper layers [75, 76].

Because the vulnerability to MeHg poisoning is age-related, with susceptibility decreasing with increasing age, the symptoms of mercury poisoning and mercury deposits are quite different depending on the age at the time of exposure [75]. Davis and colleagues followed an entire family chronically exposed to MeHg. An infant exposed to MeHg *in utero* was born mute, blind, and with severe mental retardation, quadriparesis, choreoathetosis and seizures. An eight-year-old child in the same family had very similar symptoms. Both died 21 years post MeHg exposure. In contrast, a twenty-year-old child in the same family had a loss of peripheral vision, poor hand coordination and mild cognitive deficits. The parents were reported to be completely asymptomatic [76]. These results are consistent with previous observations reported by Berlin [242].

It is likely that unique features of the fetal blood-brain barrier (BBB) contribute to the vulnerability of the fetal brain to MeHg toxicity. The fetal BBB is not fully developed until the middle of the first year of life, resulting in constant exposure to MeHg throughout gestation [243] and during early postnatal life. It is also likely that, given the immaturity of the CNS, MeHg is not as efficiently excreted from the CNS, as transporters associated with this process are less likely to be fully developed. Furthermore, the increased burden of MeHg in general likely reflects the absence of an efficient mechanism(s) for excretion of MeHg via the bile.

MeHg causes mitotic arrest in developing neurons after prenatal exposure, and the effects of MeHg on neuron proliferation depend on which type neurons were forming at the time of exposure [243]. It is well known that the generation of neurons continues throughout gestation and well into the first year of life. Typically, a set of neurons destined to be similar in function and morphology is generated in a short period, sometimes within a few days of gestation. In general, large motor neurons are produced first, followed by sensory neurons. Nuclear groups in the brain stem and diencephalon are formed early, but the complex layered structures like the cerebral cortex, cerebellum and hippocampus add more neurons over a long period of time [243]. Therefore, in infants, diffuse neuronal degeneration is detected consistently in these early-formed brain structures.

Further, MeHg causes incomplete or abnormal migration of neurons to the cerebellar and cerebral cortices as well as deranged cortical organization of the cerebrum with regard to heterotopic neurons. Moreover, the laminar cortical pattern of the cerebrum is disturbed, consisting of irregular groupings and deranged alignment of cortical layers. Although the molecular targets of MeHg giving rise to these outcomes are not fully understood, studies on MeHg's effects in the Drosophila model suggest an altered Notch receptor pathway [244]. The Notch receptor pathway is a highly conserved cell-cell signaling mechanism that controls cell fate decision, proliferation, migration and neurite outgrowth during neural development [244].

Notch receptor activation requires proteolysis by a cell surface disintegrin and metalloproteinase (ADAM), which is required for normal neural development. MeHg exposure promotes activation of ADAM resulting in a concentration- and time- dependent increase in Notch receptor activity

[244]. Notably, inorganic mercury is significantly less potent for inducing Notch activity as compared to MeHg, suggesting a mechanism specific to the organic form of mercury [244].

MeHg also inhibits several fetal brain enzymes. Watanabe and colleagues reported that prenatal MeHg exposure significantly inhibits selenoenzymes, such as glutathione peroxidase (GPx), in fetal mouse brains injected with 3mgHg/kg of MeHg on gestational day 12~14 [245]. As a result, glutathione (GSH) is decreased and thiobarbituric acid- reactive substances (TBARS) are increased. Furthermore, lipid peroxidation is increased in fetal brains [246].

In addition to its effects on brain structure and brain enzymes, MeHg exposure also affects synaptic transmission. The acute effects of mercury on the amphibian neuromuscular junction have been studied using the isolated sciatic nerve/sartorius muscle preparation. Results have indicated that mercury primarily affects presynaptic neurotransmitter release, but not postsynaptic processes, which include the activation of receptor-associated ionic channels and degradation of chemical transmitters [247, 248]. Mercury also disrupts the intracellular buffering of calcium, which further inhibits the calcium-dependent neurotransmitter release [247, 248]. Mercury first causes an increase in evoked acetylcholine release followed by a sudden and complete blockade [247, 248].

In all age groups, myelination is greatly inhibited by MeHg. Biopsy of the sural nerve was performed on three patients who died of severe Minamata disease, and the results revealed numerous unmyelinated and poorly myelinated nerve fibers [249]. The myelinated fibers were scattered irregularly in small numbers or in groups of peculiar features in the intraneural bundle.

In addition, abnormally thin or poorly formed myelin sheaths were observed. Regenerated axons were extremely small in size, and sometimes the small axons were lost entirely, leaving only the thin myelin sheaths [249]. MeHg was also reported to inhibit UDP galactose:ceramide galactosyltransferase (CGalT) and 2',3'-cyclic-nucleotide 3'-phosphodiesterase (CNP), enzymes involved in myelin formation [250]. Notably, MeHg has greater inhibitory effects on myelin formation than diethylmercury, which suggests that different forms of organic mercury produce different effects [251].

MeHg Toxicity on Other Organ Systems

The developing immune system is especially sensitive to the elemental forms of mercury. Occupational studies and animal studies have demonstrated that MeHg affects immune-cell ratios and cellular responses [252]. MeHg reduces natural killer (NK) cell activity [253] and alters the mitogen response [254] as well the function of B cell and T cell subtypes [254]. As a result, MeHg-treated animals are more susceptible to viruses and bacterial infections [255]. MeHg also induces the autoimmune response by producing antinucleolar antibodies [256] and anti- DNA antibodies [257].

Paternal exposure to mercury in humans does not appear to cause infertility or malformations [258], but a study of pregnancy outcomes among the wives of 152 men occupationally exposed to Hg showed an increased incidence of spontaneous abortion [259]. At urinary Hg concentration levels exceeding 50 μg/L in male workers, the spontaneous abortion risk in their wives was doubled [259]. In animal tests, MeHg treatment caused abnormal sperm and a low conception

rate in monkeys *[260]*. In a mouse model, MeHg was shown to cause tubular atrophy of the testes [261].

The developing kidney is more sensitive to inhaled than to organic mercury [262]. High mercury exposure results in mild transient proteinuria, gross proteinuria, hematuria, oliguria and acute renal failure. Kidney biopsy specimens from patients with nephrotic syndrome following exposure to metallic mercury demonstrated proximal tubular and glomerular changes, such as necrosis of the tubule epithelium, swollen granular protoplasm and nonstainable nuclei in the kidneys, partially due to mercury accumulation [263, 264]. In rodents, MeHg has been shown to cause renal fibrosis [265], increase renal weight, decrease renal enzymes [266, 267] and result in renal hypertrophy [268]. Microscopic examinations reveal cytoplasmic masses in proximal tubules [269], degeneration of proximal tubules and interstitial fibrosis [270].

MeHg also affects other organ systems. It increases the risk for anemia and clotting disorders [271]. Furthermore, the cardiovascular system appears to be a target for MeHg toxicity in both human beings and animals, with adverse health effects including the following: 1) both elemental and organic forms of Hg alter blood-pressure regulation; 2) men with hair Hg concentration exceeding 2ppm have increased risk of acute myocardial infarction; and 3) prenatal exposure to MeHg is linked to heart-rate variability in children [252].

Risk Assessment

The risk and toxicity of MeHg have been analyzed by three epidemiological studies since the EPA's derivation of an RfD in 1995 [272]. These longitudinal, developmental studies were conducted in the Seychelles Islands, the Faroe Islands and in New Zealand (http://www.epa.gov/iris/subst/0073.htm). The subjects of the Seychelles longitudinal prospective study were 779 mother–infant pairs from a fish-eating population [273-276]. Infants were followed from birth to 5.5 years of age and assessed at various ages on a number of standardized neuropsychological endpoints. The independent variable was maternal-hair mercury levels. The Faroe Islands study was a longitudinal study of about 900 mother–infant pairs [277]. The main independent variable was cord-blood mercury; maternal-hair mercury was also measured. Children were evaluated at 7 years of age, based on a variety of tasks designed to assess function in specific behavioral domains. The New Zealand study was a prospective case control study of 38 children born to women with hair mercury levels greater than 6 ppm during pregnancy matched with children whose mothers had lower hair mercury levels [278, 279]. At 6 years of age, 237 children were assessed on a number of neuropsychological endpoints similar to those used in the Seychelles study [279]. The Seychelles study yielded scant evidence of impairment related to *in utero* MeHg exposure, whereas the other two studies found dose-related effects on a number of neuropsychological endpoints. However, in a 9-year follow-up study of 643 children, the authors of the Seychelles study did not find an association between prenatal MeHg exposure and developmental outcomes [280]. An analysis by Davidson of the same population in a 10.7 year follow-up found a significant association between prenatal exposure to MeHg and impaired visuospatial ability [281]. Furthermore, a National Academy of Sciences (NAS) expert panel reviewed the studies and concluded that the weight of the evidence

supported adverse health effects due to MeHg exposure [272] and recommended that levels of mercury not exceed 5.0 μg/L in whole blood or 1.0 μg/g in hair, corresponding to a reference dose (RfD) of 0.1 μg/kg body weight/day.

Various agencies have developed guidelines for "safe" exposure to MeHg, including the EPA [282], the U.S. Agency for Toxic Substances and Disease Registry [71], the U.S. Food and Drug Administration and the World Health Organization. These exposure levels range from 0.1 μg/kg body weight/day (EPA) to 0.47 μg/kg body weight/day [283]. The range of recommendations is due to varying safety margins, differing emphasis placed on various sources of data, the particular missions of the respective agencies and the unique population that each guideline is intended to protect. All guidelines, however, fall within the same order of magnitude. Although these guidelines may be used as screening tools in risk assessments to evaluate the "safety" of Hg exposures, they are not meant to be distinctive lines above which toxicity will definitely occur. However, as exposure levels increase in multiples of these guidelines, members of the public health community have become increasingly concerned that adverse health consequences may occur [282].

It needs to be emphasized that these levels of exposure to MeHg can be readily attained with only a few meals of fish per week, depending on the source and type of fish. In populations dependent on fish as their source of protein (e.g., in the Faroe Islands), increased hair Hg levels (up to 4.27 ppm) during pregnancy have been shown to be associated with impaired psychomotor test performance of children at 7 years of age [277]. Further, this type of diet led to an average cord-blood MeHg level of 22.9μg/L and was correlated with neurophysiological and

neuropsychological deficits. In a follow-up study in the Faroe Islands, it was reported similar correlations persisted in 14-year-old children [284]. In Japan, a strong association between the prevalence of mental retardation and Hg concentration in the umbilical cord was reported both in Minamata [285] and Niigata [286]. In another study from New Zealand [287] maternal hair Hg levels exceeding 6 ppm (range 5-20 ppm) correlated with a deficit in the Denver developmental screening test as well as a neurological screening test in children at 4 years of age. However, an epidemiological study in the province of Quebec, Canada [288] indicated no consistent relationship between maternal hair MeHg levels of 24 ppm during pregnancy and developmental outcomes in the female offspring. Also, in the Seychelles study [273, 287, 289] no adverse effects were detected at a maternal MeHg hair level of 6.8 ppm. The apparent differences in outcomes between the Faroe Islands and Seychelles studies are likely due to numerous factors, extensively reviewed by the National Academy of Science (NAS) [272]. The NAS emphasized that the weight of the evidence supported adverse health effects from MeHg [272] and recommended that levels of Hg not exceed 5.0 μg/L in whole blood or 1.0 μg/g in hair, corresponding to a reference dose (RfD) of 0.1 μg/kg body weight/day.

Treatment

The first step of treatment is to remove patients from the source of exposure. Decontamination requires removal of clothes, flushing eyes and exposed mucosa with saline solution, and washing skin with soap and water. If mercury is swallowed, activated charcoal is used to limit further mercury absorption from GI system. Patients are given adequate fluids and electrolytes to expedite the excretion of mercury through urine. In the severe cases, dialysis could be used.

Immediate chelation therapy is the standard of care for patient showing any symptoms of severe mercury poisoning or the patient history suggesting a large total mercury load [290].

Drug choice in chelation therapy depends on the form of mercury and patient age. In adult patients, acute inorganic mercury poisoning can be treated with Dimercaptosuccinic acid (DMSA), 2,3-dimercapto-1-propanesulfonic acid (DMPS), D-penicillamine (DPCN) or dimercaprol (BAL). Of these, only DMSA is currently approved by the FDA for the treatment of children exposed to mercury. However, previous studies found no clear clinical benefit from DMSA treatment in mercury vapor poisoning [291]. DMSA given orally has fewer side effects and has been reported to be superior to BAL, DPCN and DMPS [292]. Glutathione and Alpha-lipoic acid could also be used in mercury poisoning treatment, but they may increase mercury concentrations in the kidney and the brain, although the underlying mechanism is still unknown [293]. Notably, chelation therapy can be hazardous. Baxter [294] reported an incorrect form of EDTA used for chelation therapy caused cardiac arrest in a five-year-old autistic boy due to irreversible hypocalcemia.

Concluding Remarks and Future Directions

MeHg is a well-documented neurotoxicant. Studies in children suffering from tragic MeHg poisoning outbreaks in Japan and Iraq have revealed the pronounced susceptibility of the developing brain to MeHg. As a consequence, a plethora of studies have drawn attention to the consequences of prenatal exposure. Previous animal experiments also have shown similar neuromorphological and neurobehavioral alterations induced by MeHg after either acute or chronic exposure. Particular attention was directed to comparative toxicity assessments across

species and to the degree of concordance between human and animal data. In general, these studies have established that prenatal MeHg exposure in both humans and laboratory animals leads to diffuse brain damage including reduced brain size, damage to the cortex and basal ganglia, loss of cells, ventricular dilation, ectopic cells, disorganized brain layers and gliosis. The main difference between the human and the monkey in neuropathology is the relative insensitivity of the monkey's cerebellum to MeHg, which represents a major target in humans. Clinical symptoms of prenatal MeHg exposure include blindness, auditory defects, somatosensory impairment, difficulty in learning and delays in social development and in the attainment of cognitive milestones.

Guidelines for exposure to MeHg range from 0.1ug/kg body weight/day (EPA) to 0.47ug/kg body weight/day (WHO). The differences in the guidelines between various regulatory agencies are largely due to the uncertainties intrinsic to human epidemiological studies, including unmeasured confounders and effect modifiers, which could compromise the exposure outcomes. Thus, additional research addressing interspecies comparisons is necessary to determine a more specific standard for critical dose levels of MeHg. An accurate interspecies comparison should take several key factors into account, including the species-related differences in the kinetics of MeHg distribution and its concentration in target organs. Basu and colleagues studied the inhibitory effects of MeHg on the mACh receptor in the cerebral cortex and further cross-compared the species sensitivity between the human, rat, mouse, mink and river otter. Species sensitivities, irrespective of Hg type and brain region, can be ranked from most to least sensitive as follows: river otter>rat>mink>mouse>humans [295]. Thus, a well-designed comparative study

could provide data on interspecies differences and a framework for interpreting results generated from human, murine and wildlife studies.

As a potent environmental pollutant, MeHg reacts with DNA, RNA and proteins. Studies on the potential for toxicogenomic effects of MeHg are sparse, and future studies should focus on the identification of single nucleotide polymorphisms (SNPs) in various genes that will elicit novel information regarding the role of gene and environment interactions and a particular individual's susceptibility to MeHg. Due to the considerable disadvantages inherent in both human epidemiological studies and animal experiments, toxicologists face the major challenge of developing and validating other, more targeted and controlled model systems. For example, using Caenorhabditis elegans (*C. elegans*) as the model system in toxicological research is very promising due to this species' simple and well-defined nervous system, its ready visualization through the use of green fluorescent protein (GFP) and its rapid life cycle [296]. Further improving the C. elegans model and developing *in vitro* models will prove of particular import because future toxicological studies will be greatly expanded to cover a much wider range of environments and numbers of species. Additionally, the development of high throughput methods in proteomics, genomics and bioinformatics will lead to better understanding the developmental toxicity of MeHg by the accumulation of vast amounts of valuable toxicological information.

REFERENCES

1. Hamilton, J.A., et al., *Brain uptake and utilization of fatty acids, lipids and lipoproteins: application to neurological disorders.* J Mol Neurosci, 2007. **33**(1): p. 2-11.
2. Ritter, M.R., et al., *Myeloid progenitors differentiate into microglia and promote vascular repair in a model of ischemic retinopathy.* J Clin Invest, 2006. **116**(12): p. 3266-76.
3. Higueras, P., et al., *The Almaden district (Spain): anatomy of one of the world's largest Hg-contaminated sites.* Sci Total Environ, 2006. **356**(1-3): p. 112-24.
4. Zevenhoven, R. and P. Kilpinen, *Control of Pollutants in Flue Gases and Fuel Gases.* TKK, Espoo 2001, 2001.
5. Igata, A., *Epidemiological and clinical features of Minamata disease.* Environ Res, 1993. **63**(1): p. 157-69.
6. Tsubaki, T., et al., *Outbreak of intoxication by organic compounds in Niigata Prefecture. An epidemiological and clinical study.* Jpn J Med Sci Biol, 1967. **6**: p. 132-3. .
7. Tsubaki, T., *[Mercury poisoning].* Nippon Rinsho, 1967. **25**(8): p. 1644-6.
8. Tsuchiya, K., *Causation of Ouch-Ouch Disease (Itai-Itai Byo)--an introductory review. II. Epidemiology and evaluation.* Keio J Med, 1969. **18**(4): p. 195-211.
9. Tsuchiya, K., *Causation of Ouch-Ouch Disease (Itai-Itai Byo)--an introductory review. I. Nature of the disease.* Keio J Med, 1969. **18**(4): p. 181-94.
10. Karri, S.K., R.B. Saper, and S.N. Kales, *Lead encephalopathy due to traditional medicines.* Curr Drug Saf, 2008. **3**(1): p. 54-9.
11. Marshall, W.J. and S.K. Bangert, *Therapeutic drug monitoring and chemical aspects of toxicology* Chlinical Chemistry, 6th edition, 2008.
12. Clarkson, T.W., *The toxicology of mercury.* Crit Rev Clin Lab Sci, 1997. **34**(4): p. 369-403.
13. Kamps, L.R., R. Carr, and H. Miller, *Total mercury-monomethylmercury content of several species of fish.* Bull Environ Contam Toxicol, 1972. **8**(5): p. 273-9.
14. Spry, D.J. and J.G. Wiener, *Metal bioavailability and toxicity to fish in low-alkalinity lakes: A critical review.* Environ Pollut, 1991. **71**(2-4): p. 243-304.
15. Boudou, A., et al., *Synergic effect of gold mining and damming on mercury contamination in fish.* Environ Sci Technol, 2005. **39**(8): p. 2448-54.
16. Westoo, G., *Determination of methylmercury compounds in foodstuffs. I. Methylmercury compounds in fish, identification and determination.* Acta Chem Scand, 1966. **20**(8): p. 2131-7.
17. Harada, M., *[Neuropsychiatric Disturbances Due to Organic Mercury Poisoning during the Prenatal Period.].* Seishin Shinkeigaku Zasshi, 1964. **66**: p. 429-68.
18. Harada, M., *Minamata disease: methylmercury poisoning in Japan caused by environmental pollution.* Crit Rev Toxicol, 1995. **25**(1): p. 1-24.
19. Kershaw, T.G., T.W. Clarkson, and P.H. Dhahir, *The relationship between blood levels and dose of methylmercury in man.* Arch Environ Health, 1980. **35**(1): p. 28-36.
20. Doi, R., *Individual difference of methylmercury metabolism in animals and its significance in methylmercury toxicity.* . Advances in mercury toxicology. (T Suzuki, N Imura and T W Clarkson, Eds.), pp. 77-98. Plenum Press, New York, London., 1991.

21. Skerfving S, H.K., Mangs C, Lindsten J, Ryman N *Methylmercury-induced chromosome damage in man.* Environ Res 7, 83-98, 1974.
22. Swedish Expert Group, *Report on Mercury.* Nord Hyg Tidskr, 1971. **4**: p. 1-357.
23. Hirayama, K. and A. Yasutake, *Sex and age differences in mercury distribution and excretion in methylmercury-administered mice.* J Toxicol Environ Health, 1986. **18**(1): p. 49-60.
24. Landry, T.D., R.A. Doherty, and A.H. Gates, *Effects of three diets on mercury excretion after methylmercury administration.* Bull Environ Contam Toxicol, 1979. **22**(1-2): p. 151-8.
25. Bakir, F., et al., *Methylmercury poisoning in Iraq.* Science, 1973. **181**(96): p. 230-41.
26. Sakamoto, M., et al., *Declining risk of methylmercury exposure to infants during lactation.* Environ Res, 2002. **90**(3): p. 185-9.
27. Hester, P.Y., et al., *The excretory system of young chickens experiencing mercury toxicity--effects on kidney development, morphology, and function.* Arch Environ Contam Toxicol, 1978. **7**(3): p. 257-71.
28. Trachtenberg, F., L. Barregard, and S. McKinlay, *The influence of urinary flow rate on mercury excretion in children.* J Trace Elem Med Biol. **24**(1): p. 31-5.
29. Hughes, W.L., *A physicochemical rationale for the biological activity of mercury and its compounds.* Ann N Y Acad Sci, 1957. **65**(5): p. 454-60.
30. Bridges, C.C. and R.K. Zalups, *Homocysteine, system b0,+ and the renal epithelial transport and toxicity of inorganic mercury.* Am J Pathol, 2004. **165**(4): p. 1385-94.
31. Rabenstein, D.L. and M.T. Fairhurst, *Nuclear magnetic resonance studies of the solution chemistry of metal complexes. XI. The binding of methylmercury by sulfhydryl-containing amino acids and by glutathione.* J Am Chem Soc, 1975. **97**(8): p. 2086-92.
32. Yin, Z., et al., *The methylmercury-L-cysteine conjugate is a substrate for the L-type large neutral amino acid transporter.* J Neurochem, 2008. **107**(4): p. 1083-90.
33. Kajiwara, Y., et al., *Methylmercury transport across the placenta via neutral amino acid carrier.* Arch Toxicol, 1996. **70**(5): p. 310-4.
34. Bechtholt-Gompf, A.J., et al., *Blockade of astrocytic glutamate uptake in rats induces signs of anhedonia and impaired spatial memory.* Neuropsychopharmacology. **35**(10): p. 2049-59.
35. Beenhakker, M.P. and J.R. Huguenard, *Astrocytes as gatekeepers of GABAB receptor function.* J Neurosci. **30**(45): p. 15262-76.
36. Walz, W., *Role of astrocytes in the clearance of excess extracellular potassium.* Neurochem Int, 2000. **36**(4-5): p. 291-300.
37. Tschirgi, R.D., *Blood-brain barrier: fact or fancy?* Fed Proc, 1962. **21**: p. 665-71.
38. Tschirgi, R.D. and J.L. Taylor, *Slowly changing bioelectric potentials associated with the blood-brain barrier.* Am J Physiol, 1958. **195**(1): p. 7-22.
39. Kimelberg, H.K., *Active accumulation and exchange transport of chloride in astroglial cells in culture.* Biochim Biophys Acta, 1981. **646**(1): p. 179-84.
40. Dissing-Olesen, L., et al., *Axonal lesion-induced microglial proliferation and microglial cluster formation in the mouse.* Neuroscience, 2007. **149**(1): p. 112-22.
41. Aloisi, F., *Immune function of microglia.* Glia, 2001. **36**(2): p. 165-79.
42. Zhang, P., A. Hatter, and B. Liu, *Manganese chloride stimulates rat microglia to release hydrogen peroxide.* Toxicol Lett, 2007. **173**(2): p. 88-100.

43. Ryu, J., et al., *Thrombin induces NO release from cultured rat microglia via protein kinase C, mitogen-activated protein kinase, and NF-kappa B.* J Biol Chem, 2000. **275**(39): p. 29955-9.
44. Takeuchi, H., et al., *Blockade of microglial glutamate release protects against ischemic brain injury.* Exp Neurol, 2008. **214**(1): p. 144-6.
45. Gilgun-Sherki, Y., et al., *Riluzole suppresses experimental autoimmune encephalomyelitis: implications for the treatment of multiple sclerosis.* Brain Res, 2003. **989**(2): p. 196-204.
46. Streit, W.J., *Microglia and Alzheimer's disease pathogenesis.* J Neurosci Res, 2004. **77**(1): p. 1-8.
47. El Khoury, J., et al., *Microglia, scavenger receptors, and the pathogenesis of Alzheimer's disease.* Neurobiol Aging, 1998. **19**(1 Suppl): p. S81-4.
48. Eikelenboom, P. and R. Veerhuis, *The role of complement and activated microglia in the pathogenesis of Alzheimer's disease.* Neurobiol Aging, 1996. **17**(5): p. 673-80.
49. Le, W., et al., *Microglial activation and dopaminergic cell injury: an in vitro model relevant to Parkinson's disease.* J Neurosci, 2001. **21**(21): p. 8447-55.
50. Yadav, A. and R.G. Collman, *CNS inflammation and macrophage/microglial biology associated with HIV-1 infection.* J Neuroimmune Pharmacol, 2009. **4**(4): p. 430-47.
51. Napoli, I. and H. Neumann, *Protective effects of microglia in multiple sclerosis.* Exp Neurol. **225**(1): p. 24-8.
52. Eto, K., et al., *A fetal type of Minamata disease. An autopsy case report with special reference to the nervous system.* Mol Chem Neuropathol, 1992. **16**(1-2): p. 171-86.
53. Eto, K., M. Marumoto, and M. Takeya, *The pathology of methylmercury poisoning (Minamata disease).* Neuropathology.
54. Kitamura, S., *[Epidemiology of Minamata disease--epidemiological approach to the organomercury poisoning].* Saishin Igaku, 1971. **26**(10): p. 1966-72.
55. Takeuchi, T., et al., *The outbreak of Minamata disease (methyl mercury poisoning) in cats on Northwestern Ontario reserves.* Environ Res, 1977. **13**(2): p. 215-28.
56. Mattsson, J.L., et al., *Early effects of methylmercury on the visual evoked response of the dog.* Neurotoxicology, 1981. **2**(3): p. 499-514.
57. Dietrich, M.O., et al., *Motor impairment induced by oral exposure to methylmercury in adult mice.* Environ Toxicol Pharmacol, 2005. **19**(1): p. 169-75.
58. Inouye, M., K. Murao, and Y. Kajiwara, *Behavioral and neuropathological effects of prenatal methylmercury exposure in mice.* Neurobehav Toxicol Teratol, 1985. **7**(3): p. 227-32.
59. Farina, M., et al., *Protective effects of Polygala paniculata extract against methylmercury-induced neurotoxicity in mice.* J Pharm Pharmacol, 2005. **57**(11): p. 1503-8.
60. Rocha, J.B., et al., *Effects of methylmercury exposure during the second stage of rapid postnatal brain growth on negative geotaxis and on delta-aminolevulinate dehydratase of suckling rats.* Braz J Med Biol Res, 1993. **26**(10): p. 1077-83.
61. Rice, D.C., *Sensory and cognitive effects of developmental methylmercury exposure in monkeys, and a comparison to effects in rodents.* Neurotoxicology, 1996. **17**(1): p. 139-54.
62. Samson, J.C., et al., *Delayed effects of embryonic exposure of zebrafish (Danio rerio) to methylmercury (MeHg).* Aquat Toxicol, 2001. **51**(4): p. 369-76.

63. Burbacher, T.M., et al., *Prenatal methylmercury exposure affects spatial vision in adult monkeys.* Toxicol Appl Pharmacol, 2005. **208**(1): p. 21-8.
64. Ferraro, L., et al., *Developmental exposure to methylmercury elicits early cell death in the cerebral cortex and long-term memory deficits in the rat.* Int J Dev Neurosci, 2009. **27**(2): p. 165-74.
65. Onishchenko, N., et al., *Developmental exposure to methylmercury alters learning and induces depression-like behavior in male mice.* Toxicol Sci, 2007. **97**(2): p. 428-37.
66. Castoldi, A.F., et al., *Human developmental neurotoxicity of methylmercury: impact of variables and risk modifiers.* Regul Toxicol Pharmacol, 2008. **51**(2): p. 201-14.
67. Mansour, M.M., et al., *Maternal-fetal transfer of organic and inorganic mercury via placenta and milk.* Environ Res, 1973. **6**(4): p. 479-84.
68. Olson, F.C. and E.J. Massaro, *Pharmacodynamics of methyl mercury in the murine maternal/embryo:fetal unit.* Toxicol Appl Pharmacol, 1977. **39**(2): p. 263-73.
69. Watanabe, C., et al., *In utero exposure to methylmercury and Se deficiency converge on the neurobehavioral outcome in mice.* Neurotoxicol Teratol, 1999. **21**(1): p. 83-8.
70. Myers, G.J. and P.W. Davidson, *Does methylmercury have a role in causing developmental disabilities in children?* Environ Health Perspect, 2000. **108 Suppl 3**: p. 413-20.
71. Agency for Toxic Substances and Disease Registry, *Toxicological profile for mercury. Atlanta, GA: Agency for Toxic Substances and Disease Registry.* 1999.
72. Atchison, W.D., *Is chemical neurotransmission altered specifically during methylmercury-induced cerebellar dysfunction?* Trends Pharmacol Sci, 2005. **26**(11): p. 549-57.
73. Hursh, J.B., S.P. Sichak, and T.W. Clarkson, *In vitro oxidation of mercury by the blood.* Pharmacol Toxicol, 1988. **63**(4): p. 266-73.
74. Lapham, L.W., et al., *An analysis of autopsy brain tissue from infants prenatally exposed to methymercury.* Neurotoxicology, 1995. **16**(4): p. 689-704.
75. Taber, K.H. and R.A. Hurley, *Mercury exposure: effects across the lifespan.* J Neuropsychiatry Clin Neurosci, 2008. **20**(4): p. iv-389.
76. Davis, L.E., et al., *Methylmercury poisoning: long-term clinical, radiological, toxicological, and pathological studies of an affected family.* Ann Neurol, 1994. **35**(6): p. 680-8.
77. Belletti, S., et al., *Time course assessment of methylmercury effects on C6 glioma cells: submicromolar concentrations induce oxidative DNA damage and apoptosis.* J Neurosci Res, 2002. **70**(5): p. 703-11.
78. Chang, L.W., A.H. Martin, and H.A. Hartmann, *Quantitative autoradiographic study on the RNA synthesis in the neurons after mercury intoxication.* Exp Neurol, 1972. **37**(1): p. 62-7.
79. Asmuss, M., L.H. Mullenders, and A. Hartwig, *Interference by toxic metal compounds with isolated zinc finger DNA repair proteins.* Toxicol Lett, 2000. **112-113**: p. 227-31.
80. Sager, P.R., R.A. Doherty, and P.M. Rodier, *Effects of methylmercury on developing mouse cerebellar cortex.* Exp Neurol, 1982. **77**(1): p. 179-93.
81. Castoldi, A.F., et al., *Early acute necrosis, delayed apoptosis and cytoskeletal breakdown in cultured cerebellar granule neurons exposed to methylmercury.* J Neurosci Res, 2000. **59**(6): p. 775-87.

82. Choi, B.H., K.H. Cho, and L.W. Lapham, *Effects of methylmercury on DNA synthesis of human fetal astrocytes: a radioautographic study.* Brain Res, 1980. **202**(1): p. 238-42.
83. Leong, C.C., N.I. Syed, and F.L. Lorscheider, *Retrograde degeneration of neurite membrane structural integrity of nerve growth cones following in vitro exposure to mercury.* Neuroreport, 2001. **12**(4): p. 733-7.
84. Vendrell, I., et al., *Methylmercury disrupts the balance between phosphorylated and non-phosphorylated cofilin in primary cultures of mice cerebellar granule cells. A proteomic study.* Toxicol Appl Pharmacol. **242**(1): p. 109-18.
85. Komulainen, H. and S.C. Bondy, *Increased free intrasynaptosomal Ca2+ by neurotoxic organometals: distinctive mechanisms.* Toxicol Appl Pharmacol, 1987. **88**(1): p. 77-86.
86. Oyama, Y., et al., *Methylmercury-induced augmentation of oxidative metabolism in cerebellar neurons dissociated from the rats: its dependence on intracellular Ca2+.* Brain Res, 1994. **660**(1): p. 154-7.
87. Bondy, S.C., et al., *The effects of organic and inorganic lead and mercury on neurotransmitter high-affinity transport and release mechanisms.* Environ Res, 1979. **19**(1): p. 102-11.
88. Juang, M.S., *An electrophysiological study of the action of methylmercuric chloride and mercuric chloride on the sciatic nerve-sartorius muscle preparation of the frog.* Toxicol Appl Pharmacol, 1976. **37**(2): p. 339-48.
89. Aschner, M., et al., *Methylmercury alters glutamate transport in astrocytes.* Neurochem Int, 2000. **37**(2-3): p. 199-206.
90. Aschner, M., et al., *Methylmercury-induced alterations in excitatory amino acid transport in rat primary astrocyte cultures.* Brain Res, 1993. **602**(2): p. 181-6.
91. Yee, S. and B.H. Choi, *Oxidative stress in neurotoxic effects of methylmercury poisoning.* Neurotoxicology, 1996. **17**(1): p. 17-26.
92. Franco, J.L., et al., *Methylmercury neurotoxicity is associated with inhibition of the antioxidant enzyme glutathione peroxidase.* Free Radic Biol Med, 2009. **47**(4): p. 449-57.
93. Verity, M.A., W.J. Brown, and M. Cheung, *Organic mercurial encephalopathy: in vivo and in vitro effects of methyl mercury on synaptosomal respiration.* J Neurochem, 1975. **25**(6): p. 759-66.
94. Von Burg R, L.A., Smith C *Oxygen consumption of rat tissue slices exposed to methylmercury in vitro.* Neurosci Lett 14, 309-314. , 1979.
95. Ali, S.F., C.P. LeBel, and S.C. Bondy, *Reactive oxygen species formation as a biomarker of methylmercury and trimethyltin neurotoxicity.* Neurotoxicology, 1992. **13**(3): p. 637-48.
96. LeBel, C.P., S.F. Ali, and S.C. Bondy, *Deferoxamine inhibits methyl mercury-induced increases in reactive oxygen species formation in rat brain.* Toxicol Appl Pharmacol, 1992. **112**(1): p. 161-5.
97. Yee, S. and B.H. Choi, *Methylmercury poisoning induces oxidative stress in the mouse brain.* Exp Mol Pathol, 1994. **60**(3): p. 188-96.
98. Li, T.Y., et al., *[Impact of antioxidant vitamins and heavy metal levels at birth on neurodevelopment of children assessed at two years of age].* Zhonghua Er Ke Za Zhi. **49**(6): p. 439-44.
99. Shichiri, M., et al., *Protection of cerebellar granule cells by tocopherols and tocotrienols against methylmercury toxicity.* Brain Res, 2007. **1182**: p. 106-15.

100. Zhang, P., et al., *In vitro protective effects of pyrroloquinoline quinone on methylmercury-induced neurotoxicity.* Environ Toxicol Pharmacol, 2009. **27**(1): p. 103-10.
101. Charleston, J.S., et al., *Increases in the number of reactive glia in the visual cortex of Macaca fascicularis following subclinical long-term methyl mercury exposure.* Toxicol Appl Pharmacol, 1994. **129**(2): p. 196-206.
102. Charleston, J.S., et al., *Autometallographic determination of inorganic mercury distribution in the cortex of the calcarine sulcus of the monkey Macaca fascicularis following long-term subclinical exposure to methylmercury and mercuric chloride.* Toxicol Appl Pharmacol, 1995. **132**(2): p. 325-33.
103. Vernadakis, A., *Neuron-glia interrelations.* Int Rev Neurobiol, 1988. **30**: p. 149-224.
104. Schwabe, T., et al., *GPCR signaling is required for blood-brain barrier formation in drosophila.* Cell, 2005. **123**(1): p. 133-44.
105. Allen, N.J. and B.A. Barres, *Signaling between glia and neurons: focus on synaptic plasticity.* Curr Opin Neurobiol, 2005. **15**(5): p. 542-8.
106. Shanker, G., et al., *Methylmercury enhances arachidonic acid release and cytosolic phospholipase A2 expression in primary cultures of neonatal astrocytes.* Brain Res Mol Brain Res, 2002. **106**(1-2): p. 1-11.
107. Yin, Z., et al., *Methylmercury induces oxidative injury, alterations in permeability and glutamine transport in cultured astrocytes.* Brain Res, 2007. **1131**(1): p. 1-10.
108. Allen, J.W., et al., *The consequences of methylmercury exposure on interactive functions between astrocytes and neurons.* Neurotoxicology, 2002. **23**(6): p. 755-9.
109. Vitarella, D., H.K. Kimelberg, and M. Aschner, *Inhibition of regulatory volume decrease in swollen rat primary astrocyte cultures by methylmercury is due to increased amiloride-sensitive Na+ uptake.* Brain Res, 1996. **732**(1-2): p. 169-78.
110. Yao, C.P., et al., *Foreign metallothionein-I expression by transient transfection in MT-I and MT-II null astrocytes confers increased protection against acute methylmercury cytotoxicity.* Brain Res, 2000. **855**(1): p. 32-8.
111. Yao, C.P., et al., *Transfection and overexpression of metallothionein-I in neonatal rat primary astrocyte cultures and in astrocytoma cells increases their resistance to methylmercury-induced cytotoxicity.* Brain Res, 1999. **818**(2): p. 414-20.
112. Schousboe, A., et al., *Regulatory role of astrocytes for neuronal biosynthesis and homeostasis of glutamate and GABA.* Prog Brain Res, 1992. **94**: p. 199-211.
113. Ransohoff, R.M. and V.H. Perry, *Microglial physiology: unique stimuli, specialized responses.* Annu Rev Immunol, 2009. **27**: p. 119-45.
114. Shie, F.S., et al., *Modulation of microglial innate immunity in Alzheimer's disease by activation of peroxisome proliferator-activated receptor gamma.* Curr Med Chem, 2009. **16**(6): p. 643-51.
115. Rogers, J., et al., *Neuroinflammation in Alzheimer's disease and Parkinson's disease: are microglia pathogenic in either disorder?* Int Rev Neurobiol, 2007. **82**: p. 235-46.
116. Dheen, S.T., C. Kaur, and E.A. Ling, *Microglial activation and its implications in the brain diseases.* Curr Med Chem, 2007. **14**(11): p. 1189-97.
117. Monnet-Tschudi, F., et al., *Effects of trimethyltin (TMT) on glial and neuronal cells in aggregate cultures: dependence on the developmental stage.* Neurotoxicology, 1995. **16**(1): p. 97-104.

118. Monnet-Tschudi, F., et al., *Microglial responsiveness as a sensitive marker for trimethyltin (TMT) neurotoxicity.* Brain Res, 1995. **690**(1): p. 8-14.
119. Maier, W.E., et al., *Trimethyltin increases interleukin (IL)-1 alpha, IL-6 and tumor necrosis factor alpha mRNA levels in rat hippocampus.* J Neuroimmunol, 1995. **59**(1-2): p. 65-75.
120. Kuhlmann, A.C. and T.R. Guilarte, *Cellular and subcellular localization of peripheral benzodiazepine receptors after trimethyltin neurotoxicity.* J Neurochem, 2000. **74**(4): p. 1694-704.
121. Tamm, C., et al., *High susceptibility of neural stem cells to methylmercury toxicity: effects on cell survival and neuronal differentiation.* J Neurochem, 2006. **97**(1): p. 69-78.
122. Shanker, G., et al., *Methylmercury inhibits cysteine uptake in cultured primary astrocytes, but not in neurons.* Brain Res, 2001. **914**(1-2): p. 159-65.
123. Hur, K.Y., et al., *Protective effects of magnesium lithospermate B against diabetic atherosclerosis via Nrf2-ARE-NQO1 transcriptional pathway.* Atherosclerosis. **211**(1): p. 69-76.
124. Garbin, U., et al., *Cigarette smoking blocks the protective expression of Nrf2/ARE pathway in peripheral mononuclear cells of young heavy smokers favouring inflammation.* PLoS One, 2009. **4**(12): p. e8225.
125. Jeong, G.S., et al., *Protective effect of sauchinone by upregulating heme oxygenase-1 via the P38 MAPK and Nrf2/ARE pathways in HepG2 cells.* Planta Med. **76**(1): p. 41-7.
126. Qiang, W., et al., *Activation of transcription factor Nrf-2 and its downstream targets in response to moloney murine leukemia virus ts1-induced thiol depletion and oxidative stress in astrocytes.* J Virol, 2004. **78**(21): p. 11926-38.
127. Koh, K., et al., *tBHQ inhibits LPS-induced microglial activation via Nrf2-mediated suppression of p38 phosphorylation.* Biochem Biophys Res Commun, 2009. **380**(3): p. 449-53.
128. Kraft, A.D., et al., *Neuronal sensitivity to kainic acid is dependent on the Nrf2-mediated actions of the antioxidant response element.* J Neurochem, 2006. **98**(6): p. 1852-65.
129. Kensler, T.W. and N. Wakabayashi, *Nrf2: Friend or Foe for Chemoprevention?* Carcinogenesis, 2009.
130. Kahn, N.W., et al., *Proteasomal dysfunction activates the transcription factor SKN-1 and produces a selective oxidative-stress response in Caenorhabditis elegans.* Biochem J, 2008. **409**(1): p. 205-13.
131. McMahon, M., et al., *Redox-regulated turnover of Nrf2 is determined by at least two separate protein domains, the redox-sensitive Neh2 degron and the redox-insensitive Neh6 degron.* J Biol Chem, 2004. **279**(30): p. 31556-67.
132. McMahon, M., et al., *Keap1-dependent proteasomal degradation of transcription factor Nrf2 contributes to the negative regulation of antioxidant response element-driven gene expression.* J Biol Chem, 2003. **278**(24): p. 21592-600.
133. Li, W. and A.N. Kong, *Molecular mechanisms of Nrf2-mediated antioxidant response.* Mol Carcinog, 2009. **48**(2): p. 91-104.
134. Itoh, K., et al., *Keap1 regulates both cytoplasmic-nuclear shuttling and degradation of Nrf2 in response to electrophiles.* Genes Cells, 2003. **8**(4): p. 379-91.
135. Nguyen, T., et al., *Increased protein stability as a mechanism that enhances Nrf2-mediated transcriptional activation of the antioxidant response element. Degradation of Nrf2 by the 26 S proteasome.* J Biol Chem, 2003. **278**(7): p. 4536-41.

136. Itoh, K., et al., *Keap1 represses nuclear activation of antioxidant responsive elements by Nrf2 through binding to the amino-terminal Neh2 domain.* Genes Dev, 1999. **13**(1): p. 76-86.
137. Prestera, T. and P. Talalay, *Electrophile and antioxidant regulation of enzymes that detoxify carcinogens.* Proc Natl Acad Sci U S A, 1995. **92**(19): p. 8965-9.
138. Prestera, T., et al., *Chemical and molecular regulation of enzymes that detoxify carcinogens.* Proc Natl Acad Sci U S A, 1993. **90**(7): p. 2965-9.
139. Ramos-Gomez, M., et al., *Sensitivity to carcinogenesis is increased and chemoprotective efficacy of enzyme inducers is lost in nrf2 transcription factor-deficient mice.* Proc Natl Acad Sci U S A, 2001. **98**(6): p. 3410-5.
140. Enomoto, A., et al., *High sensitivity of Nrf2 knockout mice to acetaminophen hepatotoxicity associated with decreased expression of ARE-regulated drug metabolizing enzymes and antioxidant genes.* Toxicol Sci, 2001. **59**(1): p. 169-77.
141. Das, J., et al., *Acetaminophen induced acute liver failure via oxidative stress and JNK activation: protective role of taurine by the suppression of cytochrome P450 2E1.* Free Radic Res. **44**(3): p. 340-55.
142. Chan, K., X.D. Han, and Y.W. Kan, *An important function of Nrf2 in combating oxidative stress: detoxification of acetaminophen.* Proc Natl Acad Sci U S A, 2001. **98**(8): p. 4611-6.
143. Eskes, C., et al., *Microglial reaction induced by noncytotoxic methylmercury treatment leads to neuroprotection via interactions with astrocytes and IL-6 release.* Glia, 2002. **37**(1): p. 43-52.
144. Garg, T.K. and J.Y. Chang, *Methylmercury causes oxidative stress and cytotoxicity in microglia: attenuation by 15-deoxy-delta 12, 14-prostaglandin J2.* J Neuroimmunol, 2006. **171**(1-2): p. 17-28.
145. Levesque, P.C. and W.D. Atchison, *Disruption of brain mitochondrial calcium sequestration by methylmercury.* J Pharmacol Exp Ther, 1991. **256**(1): p. 236-42.
146. Kauppinen, R.A., H. Komulainen, and H. Taipale, *Cellular mechanisms underlying the increase in cytosolic free calcium concentration induced by methylmercury in cerebrocortical synaptosomes from guinea pig.* J Pharmacol Exp Ther, 1989. **248**(3): p. 1248-54.
147. Mutkus, L., et al., *Mercuric chloride inhibits the in vitro uptake of glutamate in GLAST- and GLT-1-transfected mutant CHO-K1 cells.* Biol Trace Elem Res, 2006. **109**(3): p. 267-80.
148. Monnet-Tschudi, F., *Induction of apoptosis by mercury compounds depends on maturation and is not associated with microglial activation.* J Neurosci Res, 1998. **53**(3): p. 361-7.
149. Dreiem, A. and R.F. Seegal, *Methylmercury-induced changes in mitochondrial function in striatal synaptosomes are calcium-dependent and ROS-independent.* Neurotoxicology, 2007. **28**(4): p. 720-6.
150. Shanker, G. and M. Aschner, *Methylmercury-induced reactive oxygen species formation in neonatal cerebral astrocytic cultures is attenuated by antioxidants.* Brain Res Mol Brain Res, 2003. **110**(1): p. 85-91.
151. Akagi, H., et al., *Methylmercury dose estimation from umbilical cord concentrations in patients with Minamata disease.* Environ Res, 1998. **77**(2): p. 98-103.

152. Ni, M. and M. Aschner, *Neonatal Rat Primary Microglia: Isolocation, Culturing and Selected Applications.* . Current Protocol in Toxicology 2010(12.17): p. 16.
153. Wang, L., et al., *Methylmercury toxicity and Nrf2-dependent detoxification in astrocytes.* Toxicol Sci, 2009. **107**(1): p. 135-43.
154. Reenila, I., et al., *Increase of catechol-O-methyltransferase activity in rat brain microglia after intrastriatal infusion of fluorocitrate, a glial toxin.* Neurosci Lett, 1997. **230**(3): p. 155-8.
155. Chang, J.Y., *Methylmercury causes glial IL-6 release.* Neurosci Lett, 2007. **416**(3): p. 217-20.
156. Long, T.C., et al., *Nanosize titanium dioxide stimulates reactive oxygen species in brain microglia and damages neurons in vitro.* Environ Health Perspect, 2007. **115**(11): p. 1631-7.
157. Mundy, W.R. and T.M. Freudenrich, *Sensitivity of immature neurons in culture to metal-induced changes in reactive oxygen species and intracellular free calcium.* Neurotoxicology, 2000. **21**(6): p. 1135-44.
158. Sanfeliu, C., J. Sebastia, and S.U. Ki, *Methylmercury neurotoxicity in cultures of human neurons, astrocytes, neuroblastoma cells.* Neurotoxicology, 2001. **22**(3): p. 317-27.
159. Mullaney, K.J., et al., *The role of -SH groups in methylmercuric chloride-induced D-aspartate and rubidium release from rat primary astrocyte cultures.* Brain Res, 1994. **641**(1): p. 1-9.
160. Mullaney, K.J., et al., *Stimulation of D-aspartate efflux by mercuric chloride from rat primary astrocyte cultures.* Brain Res Dev Brain Res, 1993. **75**(2): p. 261-8.
161. Konig, J., et al., *Conjugate export pumps of the multidrug resistance protein (MRP) family: localization, substrate specificity, and MRP2-mediated drug resistance.* Biochim Biophys Acta, 1999. **1461**(2): p. 377-94.
162. Miura, K., et al., *Establishment and characterization of methylmercury-resistant PC12 cell line.* Environ Health Perspect, 1994. **102 Suppl 3**: p. 313-5.
163. Miura, K. and T.W. Clarkson, *Reduced methylmercury accumulation in a methylmercury-resistant rat pheochromocytoma PC12 cell line.* Toxicol Appl Pharmacol, 1993. **118**(1): p. 39-45.
164. Garman, R.H., B. Weiss, and H.L. Evans, *Alkylmercurial encephalopathy in the monkey (Saimiri sciureus and Macaca arctoides): a histopathologic and autoradiographic study.* Acta Neuropathol, 1975. **32**(1): p. 61-74.
165. Gehrmann, J., Y. Matsumoto, and G.W. Kreutzberg, *Microglia: intrinsic immuneffector cell of the brain.* Brain Res Brain Res Rev, 1995. **20**(3): p. 269-87.
166. Toyama, T., et al., *Cytoprotective role of Nrf2/Keap1 system in methylmercury toxicity.* Biochem Biophys Res Commun, 2007. **363**(3): p. 645-50.
167. Yang, M. and C.R. Chitambar, *Role of oxidative stress in the induction of metallothionein-2A and heme oxygenase-1 gene expression by the antineoplastic agent gallium nitrate in human lymphoma cells.* Free Radic Biol Med, 2008. **45**(6): p. 763-72.
168. Leonard, M.O., et al., *Reoxygenation-specific activation of the antioxidant transcription factor Nrf2 mediates cytoprotective gene expression in ischemia-reperfusion injury.* FASEB J, 2006. **20**(14): p. 2624-6.
169. Yamada, M. and H. Hatanaka, *Interleukin-6 protects cultured rat hippocampal neurons against glutamate-induced cell death.* Brain Res, 1994. **643**(1-2): p. 173-80.

170. Akaneya, Y., M. Takahashi, and H. Hatanaka, *Interleukin-1 beta enhances survival and interleukin-6 protects against MPP+ neurotoxicity in cultures of fetal rat dopaminergic neurons.* Exp Neurol, 1995. **136**(1): p. 44-52.
171. Thimmulappa, R.K., et al., *Nrf2-dependent protection from LPS induced inflammatory response and mortality by CDDO-Imidazolide.* Biochem Biophys Res Commun, 2006. **351**(4): p. 883-9.
172. Eskes, C., et al., *Involvement of microglia-neuron interactions in the tumor necrosis factor-alpha release, microglial activation, and neurodegeneration induced by trimethyltin.* J Neurosci Res, 2003. **71**(4): p. 583-90.
173. Thomas, W.E., *Brain macrophages: evaluation of microglia and their functions.* Brain Res Brain Res Rev, 1992. **17**(1): p. 61-74.
174. Jensen, S. and A. Jernelov, *Biological methylation of mercury in aquatic organisms.* Nature, 1969. **223**(5207): p. 753-4.
175. EPA, *Mercury Study Report to Congress, Office of Air Quality Planning & Standards and Office of Research and Development.* Health Effects of Mercury and Mercury Compounds, 1997. **V**: p. EPA-452/R-97-007.
176. Kuntz, S.W., et al., *Methylmercury risk and awareness among American Indian women of childbearing age living on an inland northwest reservation.* Environ Res, 2009. **109**(6): p. 753-9.
177. Dorea, J.G., *Persistent, bioaccumulative and toxic substances in fish: human health considerations.* Sci Total Environ, 2008. **400**(1-3): p. 93-114.
178. Irukayama, K., et al., *[Consideration of the Toxicity of Methylmercuric Compounds and the Causative Agent of Minamata Disease.].* Nisshin Igaku Jpn J Med Prog, 1963. **50**: p. 491-505.
179. Yuan, Y. and W.D. Atchison, *Methylmercury-induced increase of intracellular Ca2+ increases spontaneous synaptic current frequency in rat cerebellar slices.* Mol Pharmacol, 2007. **71**(4): p. 1109-21.
180. Verkhratsky, A., *Physiology of neuronal-glial networking.* Neurochem Int, 2010
181. Heneka, M.T., J.J. Rodriguez, and A. Verkhratsky, *Neuroglia in neurodegeneration.* Brain Res Rev, 2010. **63**(1-2): p. 189-211.
182. Verkhratsky, A. and A. Butt, *Glial Neurobiology* 2007: p. 230.
183. Alarcon, R., et al., *Expression of scavenger receptors in glial cells. Comparing the adhesion of astrocytes and microglia from neonatal rats to surface-bound beta-amyloid.* J Biol Chem, 2005. **280**(34): p. 30406-15.
184. Goritz, C., et al., *Glia-induced neuronal differentiation by transcriptional regulation.* Glia, 2007. **55**(11): p. 1108-22.
185. Griffiths, M.R., P. Gasque, and J.W. Neal, *The multiple roles of the innate immune system in the regulation of apoptosis and inflammation in the brain.* J Neuropathol Exp Neurol, 2009. **68**(3): p. 217-26.
186. Bechmann, I., et al., *Immune surveillance of mouse brain perivascular spaces by blood-borne macrophages.* Eur J Neurosci, 2001. **14**(10): p. 1651-8.
187. Ni, M., et al., *Methylmercury Induces Acute Oxidative Stress, Altering Nrf2 Protein Level in Primary Microglial Cells.* Toxicol Sci. , 2010. **Epub April 26**
188. Sakamoto, M., et al., *Possible involvement of cathepsin B released by microglia in methylmercury-induced cerebellar pathological changes in the adult rat.* Neurosci Lett, 2008. **442**(3): p. 292-6.

189. Nishioku, T., et al., *Involvement of caspase 3-like protease in methylmercury-induced apoptosis of primary cultured rat cerebral microglia.* Brain Res, 2000. **871**(1): p. 160-4.
190. Kim, Y.S. and T.H. Joh, *Microglia, major player in the brain inflammation: their roles in the pathogenesis of Parkinson's disease.* Exp Mol Med, 2006. **38**(4): p. 333-47.
191. Chen, W., et al., *Direct interaction between Nrf2 and p21(Cip1/WAF1) upregulates the Nrf2-mediated antioxidant response.* Mol Cell, 2009. **34**(6): p. 663-73.
192. Ni, M. and M. Aschner, *Neonatal Rat Primary Microglia: Isolocation, Culturing and Selected Applications.* . Current Protocol in Toxicology, 2010(12.17): p. 16.
193. Heuff, G., et al., *Isolation of cytotoxic Kupffer cells by a modified enzymatic assay: a methodological study.* J Immunol Methods, 1993. **159**(1-2): p. 115-23.
194. van de Loosdrecht, A.A., et al., *Apoptosis in tumor necrosis factor-alpha-dependent, monocyte-mediated leukemic cell death: a functional, morphologic, and flow-cytometric analysis.* Exp Hematol, 1993. **21**(13): p. 1628-39.
195. Hernandez, J.M., et al., *Novel kidney cancer immunotherapy based on the granulocyte-macrophage colony-stimulating factor and carbonic anhydrase IX fusion gene.* Clin Cancer Res, 2003. **9**(5): p. 1906-16.
196. Wang, H. and J.A. Joseph, *Quantifying cellular oxidative stress by dichlorofluorescein assay using microplate reader.* Free Radic Biol Med, 1999. **27**(5-6): p. 612-6.
197. Hwang, C., A.J. Sinskey, and H.F. Lodish, *Oxidized redox state of glutathione in the endoplasmic reticulum.* Science, 1992. **257**(5076): p. 1496-502.
198. LaDu, M.J., et al., *Apolipoprotein E receptors mediate the effects of beta-amyloid on astrocyte cultures.* J Biol Chem, 2000. **275**(43): p. 33974-80.
199. Das, G.C., et al., *Enhanced gamma-glutamylcysteine synthetase activity decreases drug-induced oxidative stress levels and cytotoxicity.* Mol Carcinog, 2006. **45**(9): p. 635-47.
200. Yin, Z., et al., *Comparison of alterations in amino acids content in cultured astrocytes or neurons exposed to methylmercury separately or in co-culture.* Neurochem Int, 2009. **55**(1-3): p. 136-42.
201. Farina, M., et al., *Probucol Increases Glutathione Peroxidase-1 Activity and Displays Long-Lasting Protection Against Methylmercury Toxicity in Cerebellar Granule Cells.* Toxicol Sci, 2009.
202. Wang, Z., et al., *Activation of astrocytes by advanced glycation end products: cytokines induction and nitric oxide release.* Acta Pharmacol Sin, 2002. **23**(11): p. 974-80.
203. Ni, M., et al., *Comparative study on the response of rat primary astrocytes and microglia to methylmercury toxicity.* Glia. **59**(5): p. 810-20.
204. He, X. and Q. Ma, *NRF2 cysteine residues are critical for oxidant/electrophile-sensing, Kelch-like ECH-associated protein-1-dependent ubiquitination-proteasomal degradation, and transcription activation.* Mol Pharmacol, 2009. **76**(6): p. 1265-78.
205. Heggland, I., P. Kaur, and T. Syversen, *Uptake and efflux of methylmercury in vitro: comparison of transport mechanisms in C6, B35 and RBE4 cells.* Toxicol In Vitro, 2009. **23**(6): p. 1020-7.
206. Barger, S.W. and A.S. Basile, *Activation of microglia by secreted amyloid precursor protein evokes release of glutamate by cystine exchange and attenuates synaptic function.* J Neurochem, 2001. **76**(3): p. 846-54.
207. Aschner, M. and J.W. Allen, *Astrocytes in methylmercury, ammonia, methionine sulfoximine and alcohol-induced neurotoxicity.* Neurotoxicology, 2000. **21**(4): p. 573-9.

208. Yin, Z., et al., *Mitochondrial-dependent manganese neurotoxicity in rat primary astrocyte cultures.* Brain Res, 2008. **1203**: p. 1-11.
209. Castellano, B., et al., *A double staining technique for simultaneous demonstration of astrocytes and microglia in brain sections and astroglial cell cultures.* J Histochem Cytochem, 1991. **39**(5): p. 561-8.
210. McCarthy, K.D. and J. de Vellis, *Preparation of separate astroglial and oligodendroglial cell cultures from rat cerebral tissue.* J Cell Biol, 1980. **85**(3): p. 890-902.
211. Yang, I., et al., *The role of microglia in central nervous system immunity and glioma immunology.* J Clin Neurosci, 2009.
212. Park, L.C., H. Zhang, and G.E. Gibson, *Co-culture with astrocytes or microglia protects metabolically impaired neurons.* Mech Ageing Dev, 2001. **123**(1): p. 21-7.
213. Wang, Y., et al., *A critical role of activin A in maturation of mouse peritoneal macrophages in vitro and in vivo.* Cell Mol Immunol, 2009. **6**(5): p. 387-92.
214. Ye, S.M. and R.W. Johnson, *Increased interleukin-6 expression by microglia from brain of aged mice.* J Neuroimmunol, 1999. **93**(1-2): p. 139-48.
215. Pocock, J.M. and H. Kettenmann, *Neurotransmitter receptors on microglia.* Trends Neurosci, 2007. **30**(10): p. 527-35.
216. Frank, M.G., et al., *Rapid isolation of highly enriched and quiescent microglia from adult rat hippocampus: immunophenotypic and functional characteristics.* J Neurosci Methods, 2006. **151**(2): p. 121-30.
217. Hassan, N.F., et al., *Isolation and characterization of human fetal brain-derived microglia in in vitro culture.* Neuroscience, 1991. **41**(1): p. 149-58.
218. Hassan, N.F., et al., *Isolation and flow cytometric characterization of newborn mouse brain-derived microglia maintained in vitro.* J Leukoc Biol, 1991. **50**(1): p. 86-92.
219. Hassan, N.F., et al., *Isolation and characterization of newborn rabbit brain-derived microglia.* Clin Immunol Immunopathol, 1991. **59**(3): p. 426-35.
220. Clarkson, T.W., L. Magos, and G.J. Myers, *The toxicology of mercury--current exposures and clinical manifestations.* N Engl J Med, 2003. **349**(18): p. 1731-7.
221. Clarkson, T.W., *Molecular and ionic mimicry of toxic metals.* Annu Rev Pharmacol Toxicol, 1993. **33**: p. 545-71.
222. Gruenwedel, D.W. and M.K. Cruikshank, *Effect of methylmercury (II) on the synthesis of deoxyribonucleic acid, ribonucleic acid and protein in HeLa S3 cells.* Biochem Pharmacol, 1979. **28**(5): p. 651-5.
223. Crespo-Lopez, M.E., et al., *Mercury and human genotoxicity: critical considerations and possible molecular mechanisms.* Pharmacol Res, 2009. **60**(4): p. 212-20.
224. Chang, L.W., P.A. Desnoyers, and H.A. Hartmann, *Quantitative cytochemical studies of RNA in experimental mercury poisoning. Changes in RNA content.* J Neuropathol Exp Neurol, 1972. **31**(3): p. 489-501.
225. Farris, F.F. and J.C. Smith, *In vivo incorporation of 14-C-leucine into brain protein of methylmercury treated rats.* Bull Environ Contam Toxicol, 1975. **13**(4): p. 451-5.
226. Brubaker, P.E., et al., *DNA, RNA, and protein synthesis in brain, liver, and kidneys of asymptomatic methylmercury treated rats.* Exp Mol Pathol, 1973. **18**(3): p. 263-80.
227. Thier, R., et al., *Interaction of metal salts with cytoskeletal motor protein systems.* Toxicol Lett, 2003. **140-141**: p. 75-81.
228. Sakamoto, M., N. Ikegami, and A. Nakano, *Protective effects of Ca2+ channel blockers against methyl mercury toxicity.* Pharmacol Toxicol, 1996. **78**(3): p. 193-9.

229. Park, S.T., et al., *Methylmercury-induced neurotoxicity in cerebral neuron culture is blocked by antioxidants and NMDA receptor antagonists.* Neurotoxicology, 1996. **17**(1): p. 37-45.
230. Chen, C., et al., *Accumulation of mercury, selenium and their binding proteins in porcine kidney and liver from mercury-exposed areas with the investigation of their redox responses.* Sci Total Environ, 2006. **366**(2-3): p. 627-37.
231. Fox, J.H., K. Patel-Mandlik, and M.M. Cohen, *Comparative effects of organic and inorganic mercury on brain slice respiration and metabolism.* J Neurochem, 1975. **24**(4): p. 757-62.
232. Sarafian, T.A., *Methylmercury-induced generation of free radicals: biological implications.* Met Ions Biol Syst, 1999. **36**: p. 415-44.
233. Fujimoto, Y., et al., *Enhancement of methyl mercury-induced lipid peroxidation by the addition of ascorbic acid.* Res Commun Chem Pathol Pharmacol, 1985. **49**(2): p. 267-75.
234. Gasso, S., et al., *Antioxidant compounds and Ca(2+) pathway blockers differentially protect against methylmercury and mercuric chloride neurotoxicity.* J Neurosci Res, 2001. **66**(1): p. 135-45.
235. Roos, D.H., et al., *Guanosine and synthetic organoselenium compounds modulate methylmercury-induced oxidative stress in rat brain cortical slices: involvement of oxidative stress and glutamatergic system.* Toxicol In Vitro, 2009. **23**(2): p. 302-7.
236. Myhre, O. and F. Fonnum, *The effect of aliphatic, naphthenic, and aromatic hydrocarbons on production of reactive oxygen species and reactive nitrogen species in rat brain synaptosome fraction: the involvement of calcium, nitric oxide synthase, mitochondria, and phospholipase A.* Biochem Pharmacol, 2001. **62**(1): p. 119-28.
237. Sternlicht, M., et al., *A novel strategy for the investigation of clonality in precancerous disease states and early stages of tumor progression.* Biochem Biophys Res Commun, 1994. **199**(2): p. 511-8.
238. Vijayalakshmi, K. and P.P. Sood, *Ameliorative capacities of vitamins and monothiols post therapy in the restoration of methylmercury altered glutathione metabolism.* Cell Mol Biol (Noisy-le-grand), 1994. **40**(2): p. 211-24.
239. Li, S., S.A. Thompson, and J.S. Woods, *Localization of gamma-glutamylcysteine synthetase mRNA expression in mouse brain following methylmercury treatment using reverse transcription in situ PCR amplification.* Toxicol Appl Pharmacol, 1996. **140**(1): p. 180-7.
240. Choi, B.H., S. Yee, and M. Robles, *The effects of glutathione glycoside in methyl mercury poisoning.* Toxicol Appl Pharmacol, 1996. **141**(2): p. 357-64.
241. Marsh, D.O., et al., *Fetal methylmercury poisoning: clinical and toxicological data on 29 cases.* Ann Neurol, 1980. **7**(4): p. 348-53.
242. Berlin, M. and S. Ullberg, *Accumulation and retention of mercury in the mouse. I. An autoradiographic study after a single intravenous injection of mercuric chloride.* Arch Environ Health, 1963. **6**: p. 589-601.
243. Rodier, P.M., *Developing brain as a target of toxicity.* Environ Health Perspect, 1995. **103 Suppl 6**: p. 73-6.
244. Bland, C. and M.D. Rand, *Methylmercury induces activation of Notch signaling.* Neurotoxicology, 2006. **27**(6): p. 982-91.
245. Watanabe, C., et al., *In utero methylmercury exposure differentially affects the activities of selenoenzymes in the fetal mouse brain.* Environ Res, 1999. **80**(3): p. 208-14.

246. Watanabe, C., et al., *The effect of prenatal methylmercury exposure on the GSH level and lipid peroxidation in the fetal brain and placenta of mice.* Tohoku J Exp Med, 1999. **187**(2): p. 121-6.
247. Atchison, W.D., *Effects of neurotoxicants on synaptic transmission: lessons learned from electrophysiological studies.* Neurotoxicol Teratol, 1988. **10**(5): p. 393-416.
248. Cooper, G.P. and R.S. Manalis, *Influence of heavy metals on synaptic transmission: a review.* Neurotoxicology, 1983. **4**(4): p. 69-83.
249. Takeuchi, T., et al., *Ultrastructural changes of human sural nerves in the neuropathy induced by intrauterine methylmercury poisoning (so-called fetal Minamata disease).* Virchows Arch B Cell Pathol, 1978. **27**(2): p. 137-54.
250. Grundt, I.K. and N.M. Neskovic, *UDPgalactose:ceramide galactosyltransferase and 2',3'-cyclic-nucleotide 3'-phosphodiesterase activities in rat brain after long-term exposure to methylmercury or triethyllead.* Exp Neurol, 1985. **88**(3): p. 580-9.
251. Grundt, I.K., E. Stensland, and T.L. Syverson, *Changes in fatty acid composition of myelin cerebrosides after treatment of the developing rat with methylmercury chloride and diethylmercury.* J Lipid Res, 1980. **21**(2): p. 162-8.
252. Committee on the Toxicological Effects of Methylmercury, B.o.E.S.a.T., National Research Council *Toxicological Effects of Methylmercury.* 2000.
253. Ilback, N.G., J. Sundberg, and A. Oskarsson, *Methyl mercury exposure via placenta and milk impairs natural killer (NK) cell function in newborn rats.* Toxicol Lett, 1991. **58**(2): p. 149-58.
254. Wild, L.G., et al., *Immune system alteration in the rat after indirect exposure to methyl mercury chloride or methyl mercury sulfide.* Environ Res, 1997. **74**(1): p. 34-42.
255. Ilback, N.G., et al., *Effects of methyl mercury on cytokines, inflammation and virus clearance in a common infection (coxsackie B3 myocarditis).* Toxicol Lett, 1996. **89**(1): p. 19-28.
256. Hultman, P. and H. Hansson-Georgiadis, *Methyl mercury-induced autoimmunity in mice.* Toxicol Appl Pharmacol, 1999. **154**(3): p. 203-11.
257. Cardenas, A., et al., *Markers of early renal changes induced by industrial pollutants. I. Application to workers exposed to mercury vapour.* Br J Ind Med, 1993. **50**(1): p. 17-27.
258. Alcser, K.H., et al., *Occupational mercury exposure and male reproductive health.* Am J Ind Med, 1989. **15**(5): p. 517-29.
259. Cordier, S., et al., *Paternal exposure to mercury and spontaneous abortions.* Br J Ind Med, 1991. **48**(6): p. 375-81.
260. Mohamed, M.K., T.M. Burbacher, and N.K. Mottet, *Effects of methyl mercury on testicular functions in Macaca fascicularis monkeys.* Pharmacol Toxicol, 1987. **60**(1): p. 29-36.
261. Hirano, M., et al., *Further carcinogenicity study on methylmercury chloride in ICR mice.* Nippon Juigaku Zasshi, 1986. **48**(1): p. 127-35.
262. Samuels, E.R., et al., *A case of accidental inorganic mercury poisoning.* J Anal Toxicol, 1982. **6**(3): p. 120-2.
263. Kazantzis, G., et al., *Albuminuria and the nephrotic syndrome following exposure to mercury and its compounds.* Q J Med, 1962. **31**: p. 403-18.
264. Hook, O., K.D. Lundgren, and A. Swensson, *On alkyl mercury poisoning; with a description of two cases.* Acta Med Scand, 1954. **150**(2): p. 131-7.

265. Magos, L. and W.H. Butler, *Cumulative effects of methylmercury dicyandiamide given orally to rats.* Food Cosmet Toxicol, 1972. **10**(4): p. 513-7.
266. Verschuuren, H.G., et al., *Toxicity of methylmercury chloride in rats I. Short-term study.* Toxicology, 1976. **6**(1): p. 85-96.
267. Verschuuren, H.G., et al., *Toxicity of methylmercury chloride in rats. III. Long-term toxicity study.* Toxicology, 1976. **6**(1): p. 107-23.
268. Slotkin, T.A., et al., *Biochemical and functional alterations in renal and cardiac development resulting from neonatal methylmercury treatment.* Toxicology, 1985. **36**(2-3): p. 231-41.
269. Fowler, B.A., *The morphologic effects of dieldrin and methyl mercuric chloride on pars recta segments of rat kidney proximal tubules.* Am J Pathol, 1972. **69**(1): p. 163-78.
270. Mitsumori, K., et al., *Chronic toxicity and carcinogenicity of methylmercury chloride in B6C3F1 mice.* Fundam Appl Toxicol, 1990. **14**(1): p. 179-90.
271. Munro, D.J. and W.D. Gummer, *Mercury accumulation in biota of Thunder Creek, Saskatchewan.* Bull Environ Contam Toxicol, 1980. **25**(6): p. 884-90.
272. National Academy of Science, *Committee on the Toxicological Effects of Methylmercury, Board on Environmental Studies and Toxicology, National Research Council. Toxicological Effect of Methylmercury, National Academies Press, Washington, DC,.* 2000.
273. Davidson, P.W., et al., *Effects of prenatal and postnatal methylmercury exposure from fish consumption on neurodevelopment: outcomes at 66 months of age in the Seychelles Child Development Study.* JAMA, 1998. **280**(8): p. 701-7.
274. Davidson, P.W., et al., *Longitudinal neurodevelopmental study of Seychellois children following in utero exposure to methylmercury from maternal fish ingestion: outcomes at 19 and 29 months.* Neurotoxicology, 1995. **16**(4): p. 677-88.
275. Myers, G.J., et al., *Summary of the Seychelles child development study on the relationship of fetal methylmercury exposure to neurodevelopment.* Neurotoxicology, 1995. **16**(4): p. 711-16.
276. Myers, G.J., et al., *Effects of prenatal methylmercury exposure from a high fish diet on developmental milestones in the Seychelles Child Development Study.* Neurotoxicology, 1997. **18**(3): p. 819-29.
277. Grandjean, P., et al., *Cognitive deficit in 7-year-old children with prenatal exposure to methylmercury.* Neurotoxicol Teratol, 1997. **19**(6): p. 417-28.
278. Kjellstrom, T., et al., *Kjellstrom T, Kennedy P, Wallis S, Mantell C. Physical and mental development of children with prenatal exposure to mercury from fish. .* Stage 1. Preliminary tests at age 4, Solna, Sweden., 1986: p. 3080.
279. Kjellstrom, T., P. Kennedy, and S. Wallis, *Physical and mental development of children with prenatal exposure to mercury from fish. Stage 2. Interviews and psychological tests at age 6, Solna, Sweden.* National Swedish Environmental Board Report, 1989: p. 3642.
280. van Wijngaarden, E., et al., *Interpreting epidemiological evidence in the presence of multiple endpoints: an alternative analytic approach using the 9-year follow-up of the Seychelles child development study.* Int Arch Occup Environ Health, 2009. **82**(8): p. 1031-41.
281. Davidson, P.W., et al., *Association between prenatal exposure to methylmercury and visuospatial ability at 10.7 years in the seychelles child development study.* Neurotoxicology, 2008. **29**(3): p. 453-9.

282. Mahaffey, K.R., *Methylmercury: a new look at the risks.* Public Health Rep, 1999. **114**(5): p. 396-9, 402-13.
283. WHO, *Mercury, in air quality guidelines* 2000.
284. Debes, F., et al., *Impact of prenatal methylmercury exposure on neurobehavioral function at age 14 years.* Neurotoxicol Teratol, 2006. **28**(5): p. 536-47.
285. Harada, M., *Congenital Minamata disease: intrauterine methylmercury poisoning.* Teratology, 1978. **18**(2): p. 285-8.
286. Tsubaki, T. and K. Irukayma, *Methylmercury poisoning in Minamata and Niigata, Japan.* Minamata Disease (T Tsubaki and K Irukayma, Eds.) Kodansha ltd. Tokyo, Elsevier, Amsterdam., 1977.
287. Kjellstrom, T. and P. Kennedy, *The association between developmental retardation in children and their prenatal exposure to methylmercury due to maternal fish consumption, SNV-PM.* . National Environmental Protection Board Report, Solna, Sweden, 1985.
288. Keown-Eyssen, G., J. Ruedy, and A. Neims, *Methylmercury exposure in northern Quebec II. Neurologic findings in children.* Am J Epidemiol 118, 470-479. , 1983.
289. Myers, G.J., et al., *Prenatal methylmercury exposure from ocean fish consumption in the Seychelles child development study.* Lancet, 2003. **361**(9370): p. 1686-92.
290. Clifton, J.C., 2nd, *Mercury exposure and public health.* Pediatr Clin North Am, 2007. **54**(2): p. 237-69, viii.
291. Risher, J.F. and S.N. Amler, *Mercury exposure: evaluation and intervention the inappropriate use of chelating agents in the diagnosis and treatment of putative mercury poisoning.* Neurotoxicology, 2005. **26**(4): p. 691-9.
292. Long, H., L. Nelson, and J. Tintinalli, *Metals and metalloids.* Emergency Medicine: A Comprehensive Study Guide, 6th ed, 2004.
293. Rooney, J.P., *The role of thiols, dithiols, nutritional factors and interacting ligands in the toxicology of mercury.* Toxicology, 2007. **234**(3): p. 145-56.
294. Baxter, A.J. and E.P. Krenzelok, *Pediatric fatality secondary to EDTA chelation.* Clin Toxicol (Phila), 2008. **46**(10): p. 1083-4.
295. Basu, N., et al., *An interspecies comparison of mercury inhibition on muscarinic acetylcholine receptor binding in the cerebral cortex and cerebellum.* Toxicol Appl Pharmacol, 2005. **205**(1): p. 71-6.
296. Helmcke, K.J., et al., *Characterization of the effects of methylmercury on Caenorhabditis elegans.* Toxicol Appl Pharmacol, 2009.